学位論文

# Systems biology analysis of temporal pattern transfer in signal transduction mechanisms

シグナル伝達機構における時間パターン伝播の

システム生物学的解析

**平成 23 年 12 月　博士(理学)申請**

東京大学大学院理学系研究科

生物化学専攻

**豊島 有**

# Systems biology analysis of temporal pattern transfer in signal transduction mechanisms

by

**Yu Toyoshima**

December 2011

A thesis submitted to Graduate School of Sciences, the University of Tokyo,
in partial fulfillment of the requirement for the degree of Doctor of Philosophy,
in Department of Biophysics and Biochemistry

Supervisor: Prof. Shinya Kuroda

# Abstract

Cells use signal transduction to respond the external stimuli and exert biological functions. Cells should detect strength of a stimulus and accordingly regulate responses. By recent advancement of molecular biology, qualitative knowledge of the components of the signal transduction systems has been growing. However, the quantitative input-output relationships of cell response and their regulation mechanisms remain elusive. Especially, how efficiency of signal transfer and sensitivity of a signaling pathway to strength of an activator or an inhibitor are controlled is a fundamental unsolved question.

In our previous work about Akt pathway, we found counterintuitive results that peak amplitudes of receptor and downstream signals are decoupled; a weak sustained receptor signal, rather than a strong transient signal, strongly induced downstream response. By experiments and simulations, we found that the low-pass filter characteristics of the Akt pathway can explain the decoupling effect. This indicates that, depending on temporal patterns, transfer efficiency of the peak amplitude is variable, and consequently the sensitivity of peak amplitude is also variable.

Here, we examined the signal transfer efficiency of the peak amplitude in a simple signaling pathway that can be approximated by a consecutive first-order reaction, which exhibits low-pass filter characteristics. We theoretically found that signal transfer efficiency attenuates when the time constant of the negative regulation of the downstream molecule is longer than the duration of transient peak of the upstream molecule. We experimentally found that the quantitative property of the attenuation of the signal transfer efficiency was conserved among species of signaling pathways including Akt and ERK pathways, growth factors and cell lines.

Because of this property, the effective dose of the activator for the downstream

molecule becomes smaller than that for the upstream molecule, indicating an increased sensitivity of the downstream molecule to the activator. This increase became larger when the negative regulation became weaker. Similarly, the effective dose of an inhibitor for the downstream molecule becomes larger than that for the upstream molecule, indicating a decreased sensitivity of the downstream molecule to the inhibitor. This decrease became larger when the negative regulation became weaker. We experimentally verified the sensitivity decrease to an inhibitor using the lapatinib (an EGF receptor inhibitor)-dependent inhibition of Akt and S6 phosphorylation.

These results demonstrate that attenuation of signal transfer efficiency through negative regulation is a novel conserved property of the signaling pathway. These results also suggest that cells can control their sensitivity to an activator and inhibitor by changing the expression levels of negative regulators, such as phosphatase or protease.

# Table of contents

# List of figures

# List of Tables

# 1. INTRODUCTIONS

## 1.1. Background

Cells have signal transduction mechanisms so that they can respond to the external stimuli. The cells are considered to have specific signal transduction pathways for respective stimuli. The stimulus activates the corresponding receptors and its downstream signaling molecules. The signal is transferred to the genome and downstream effecters, and changes the behaviors of the cell such as transcription and metabolic system. By recent advancement of molecular biology, qualitative knowledge about these signaling molecules and genes is growing. However, the quantitative input-output relationships between stimuli and cell response, and their regulation mechanisms remain elusive.

In order to appropriate response, the cells should distinguish respective stimuli and detect the strength of the stimulus. These processes may seem to be qualitative, but actually they are quantitative process. A good example is the cell fate determination in PC12 cells (Ebisuya et al., 2005; Marshall, 1995). PC12 cells show epidermal growth factor (EGF)-dependent cell growth and nerve growth factor (NGF)-dependent neuronal differentiation, and the extracellular signal-regulated kinase (ERK) pathway is known to be sufficient for these cellular responses. Because both stimuli activate ERK, the cells cannot distinguish between EGF and NGF stimulations based on whether ERK is activated or not. More quantitatively, it is known that EGF induces rapid transient activation of ERK, and NGF induces rapid transient and slow sustained activation of ERK. Therefore, the PC12 cells can distinguish the stimuli by using the difference of the temporal pattern of ERK activation. Then, how do the cells put the information of the stimuli into the temporal pattern (“encode”), and how do the cells extract the information from the temporal pattern (“decode”)? To solve such quantitative, dynamic and system-level questions, systems biology analysis and quantitative

measurement should be applied.

Previously, my supervisor and his research team analyzed the encoding mechanisms by combination of experiments and simulations (Sasagawa et al., 2005). They found that the network motifs called incoherent feed forward loop (IFFL) and feed forward (FF) induce the transient and sustained activation of ERK, respectively, in EGF and NGF dependent signal transduction pathways in PC12 cells. They also found that the difference of the temporal pattern of ERK activation comes from quantitative differences of the affinity of EGF and NGF receptors to their downstream molecule. The decoding mechanisms have not yet been analyzed well. The functions of the network motifs are extensively investigated (Alon, 2006a; Kholodenko, 2006; Kholodenko et al., 2010; Shoval and Alon, 2010), and it is known that negative feedback loop (NFBL) and incoherent feed forward loop (IFFL) can respond specifically to transient input, and feed forward (FF) can respond specifically to sustained input. Therefore, these network motifs can serve as the decoding machinery at the downstream of ERK. Actually, it is reported that there is NFBL around c-Fos, one of the downstream genes of ERK (Nakakuki et al., 2010).

The temporal information coding mechanisms seems to be used in other cases (Behar and Hoffmann, 2010). For example, in the case of $Ca^{2+}$-dependent (Dolmetsch et al., 1997; Dolmetsch et al., 1998; Tomida et al., 2003) and TNF-dependent (Ashall et al., 2009; Hoffmann et al., 2002) regulation of NF-κB transcription factors, temporal patterns of the stimuli seem to regulate the expression of multiple genes differently through the temporal patterns of the oscillation of nuclear localization of NF-κB. In the case of “temporal patterns of insulin”-dependent regulation of metabolic response in mammals (O'Rahilly et al., 1988; Paolisso et al., 1991), insulin is secreted in a pulsatile fashion in healthy humans but not in patients with diabetes, and 13-minutes oscillation of insulin has greater effect on the glucose

metabolism than continuous insulin. In the case of the NaCl-dependent chemotactic behavior in a nematode *C. elegans* (Iino and Yoshida, 2009), the nematode seems to be able to detect the special gradient of NaCl in the direction of locomotion and the direction of perpendicular to its own locomotion simultaneously. The two types of information of the special gradient seem to be encoded in the temporal patterns of activity of a single neuron. Thus, the temporal patterns of signaling activity seem to play important roles in many signal transduction systems.

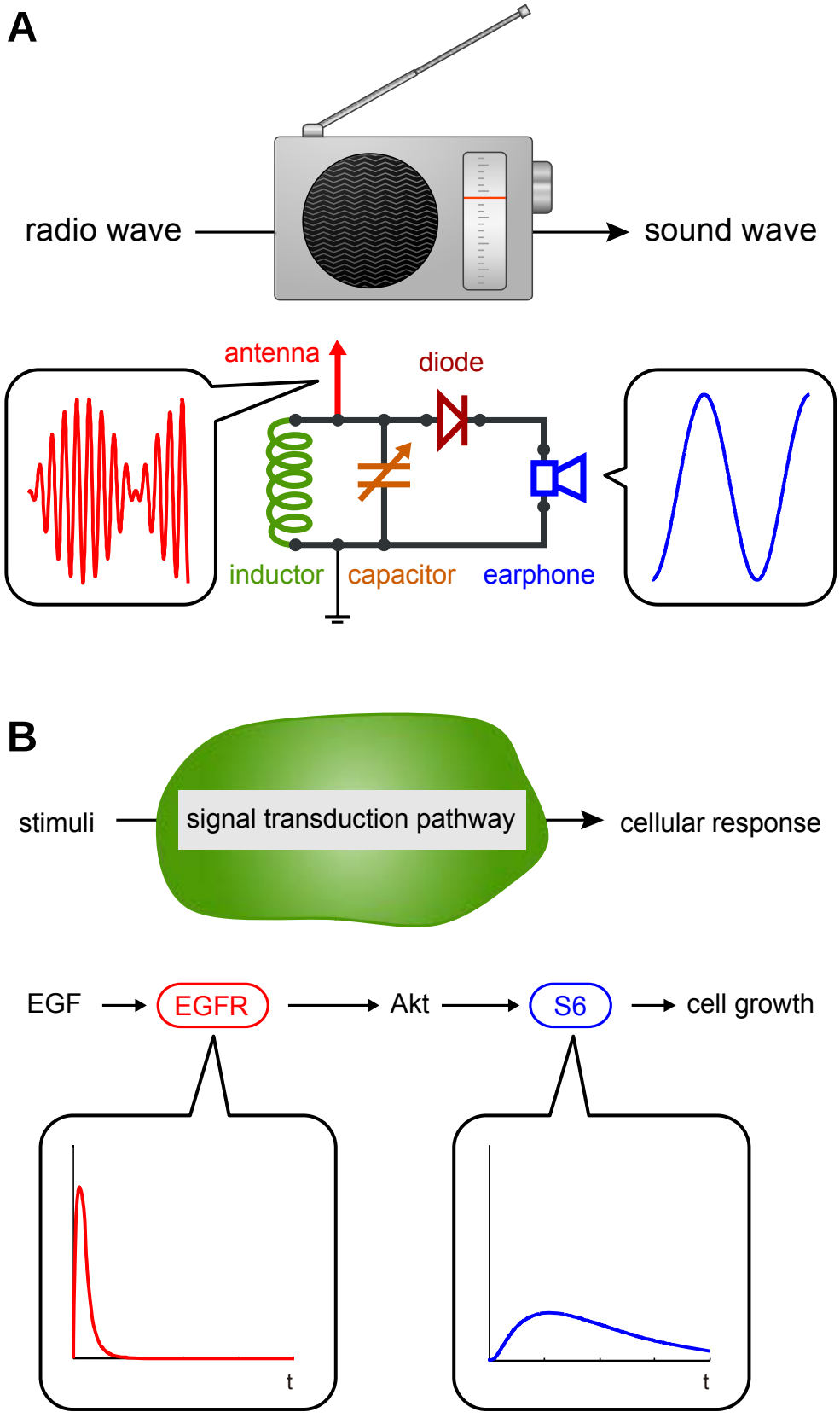


**Figure 1: Signal processing in radio (A) and cell (B)**

Then, how the temporal information coding mechanisms should be analyzed? From the view point of systems biology, I would like to explain it with the example of radio (Bray, 1995; Lathi, 1998; Lazebnik, 2002). The simple radio consists of the antenna, the tuned circuit consisting of the coil and capacitor, the diode, and earphone (Figure 1). The antenna converts the radio wave into the electric signal. The tuned circuit filters specific frequency component in the electric signal. The diode cuts off the lower half of the electric signal. The earphone detects the envelope of the signal and converts the electric signal into sound wave. This is how the electric signal is processed and how the radio works (i.e. operating principle). If we do not know the principle, how we analyze it? For example, if we removed the diode from the radio, the radio would not work and we would find that the diode is necessary for the radio. Thus, it is important to identify the component of the system and the network between components. However, we cannot find how the electric signal is processed in the radio in this way because removing the component breaks signal processing system. Then, it is necessary to measure the electric signal quantitatively in the intact system under many patterns of input. From propagations of temporal patterns of electric signals, we will find how the component processes the signals, and consequently we will find how the radio works.

This strategy can be applied to the biological systems. For example, by knocking out a gene, we would find that the molecule is necessary for the signaling pathway. But we cannot find how the molecule processing the signal because the signal processing system is broken by knocking out the gene. Furthermore, knocking out the gene not only removes the component but also disconnects the circuit, and observation may be biased because we can observe the cells which can survive under such abnormal states (i.e. compensation or adaptation may occurred in the remained cells). Then, it is necessary to measure the temporal patterns of signaling activity quantitatively in the intact signaling pathway under many patterns of input. From propagations of the temporal patterns, we will find how the molecule

(or the network motif including the molecule) processes the signals, and consequently we will find operating principle of the biological dynamic systems. Additionally, from this comparison between the radio and the cell, one may find that signaling molecules themselves are only components for transferring and processing the signals as well as the electric parts in the radio, and that the information inducing the cellular responses are encoded into the temporal patterns of the activities of the signaling molecules.

## 1.2. Our previous study

Based on the background described above, Dr. Fujita and I investigated the signaling dynamics and its regulation mechanisms in Akt signal transduction pathway in PC12 cells previously (Fujita et al., 2010). The activity of Akt [also known as protein kinase B (PKB)] is stimulated by various growth factors and this serine-threonine kinase plays evolutionarily conserved roles in many cellular functions, such as protein synthesis and cell growth (Manning and Cantley, 2007). We quantitatively measured EGF-dependent phosphorylation (i.e. activation) of EGF receptor (EGFR), Akt, and the ribosomal protein S6 (a molecule downstream of Akt) under various stimulation patterns (Figure 2). We found the decoupling phenomenon between receptor and its downstream signals; weak sustained phosphorylation of EGFR, rather than strong transient one, strongly induced S6 phosphorylation. We made and analyzed a simulation model of the pathway and found that the Akt pathway can be approximated by a consecutive first-order reaction, and the low frequency pass filter characteristics of the reaction induce this decoupling phenomenon (Figure 3).

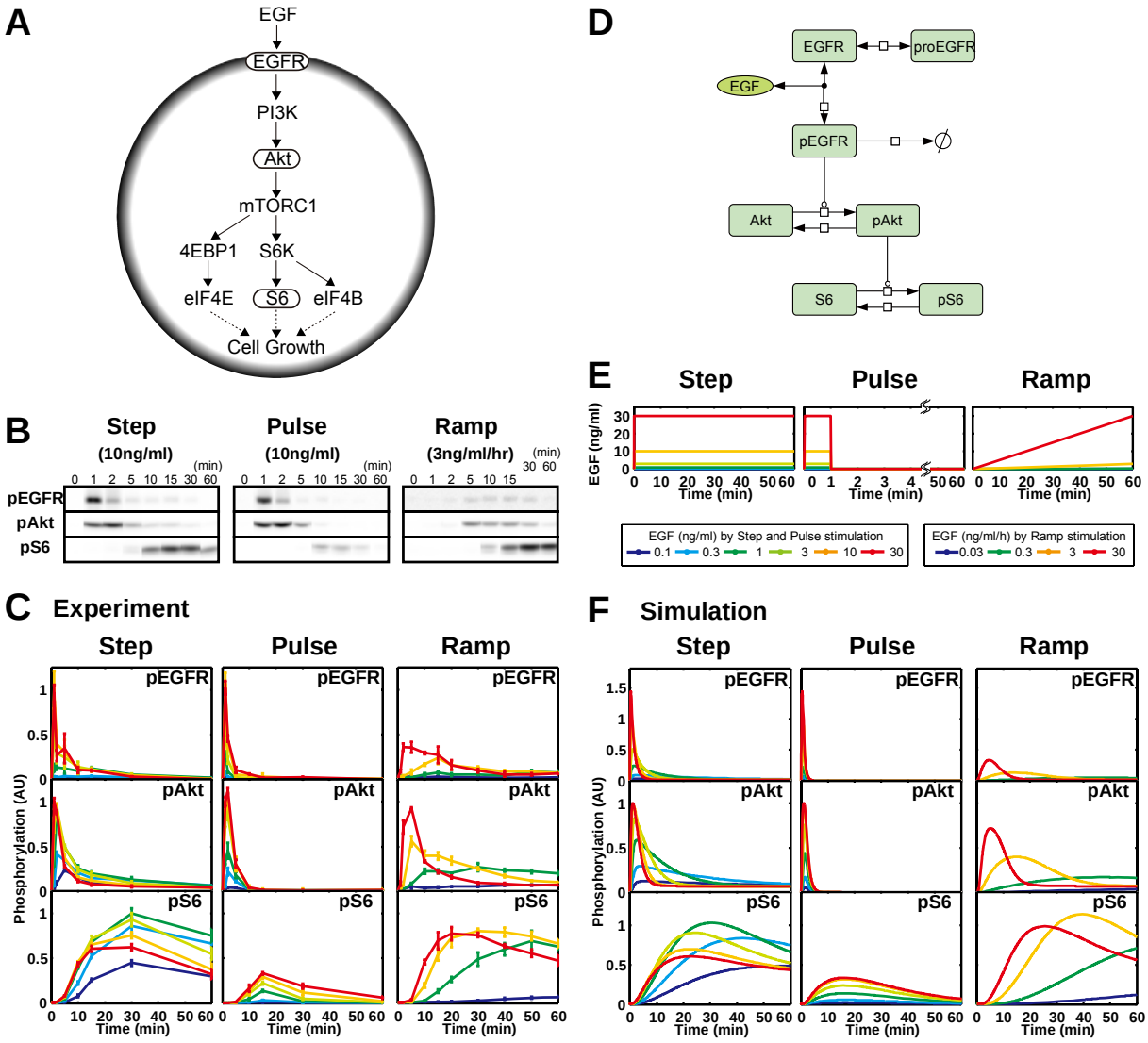


**Figure 2: EGF-dependent dynamics of the Akt pathway.**

(**A**) In the Akt pathway, binding of growth factors to their receptors leads to phosphorylation and activation of downstream molecules including Akt and S6. (**B**) Phosphorylation of EGFR, Akt and S6 were measured by quantitative western blotting in PC12 cells in response to various patterns of EGF stimulation shown in **E**. (**C**) The time courses of pEGFR and pAkt by the step and pulse stimulations were similar, whereas that of pS6 was apparently different. Ramp stimulation did not induce strong transient peaks of pEGFR and pAkt, but pS6 was more strongly induced than by pulse stimulation (decoupling). Weak sustained signals rather than strong transient signals seem to be transferred downstream efficiently, indicating that the signal transfer efficiency differs depending on the shapes of the time course. (**D**) A simple simulation model of the Akt pathway was developed and the parameters were estimated based on the result of step experiment. (**F**) The estimated model reproduced the features of the result of step experiment and was validated by the results of pulse and ramp experiments, indicating that the model can capture the essential systems-level dynamics of the Akt pathway.

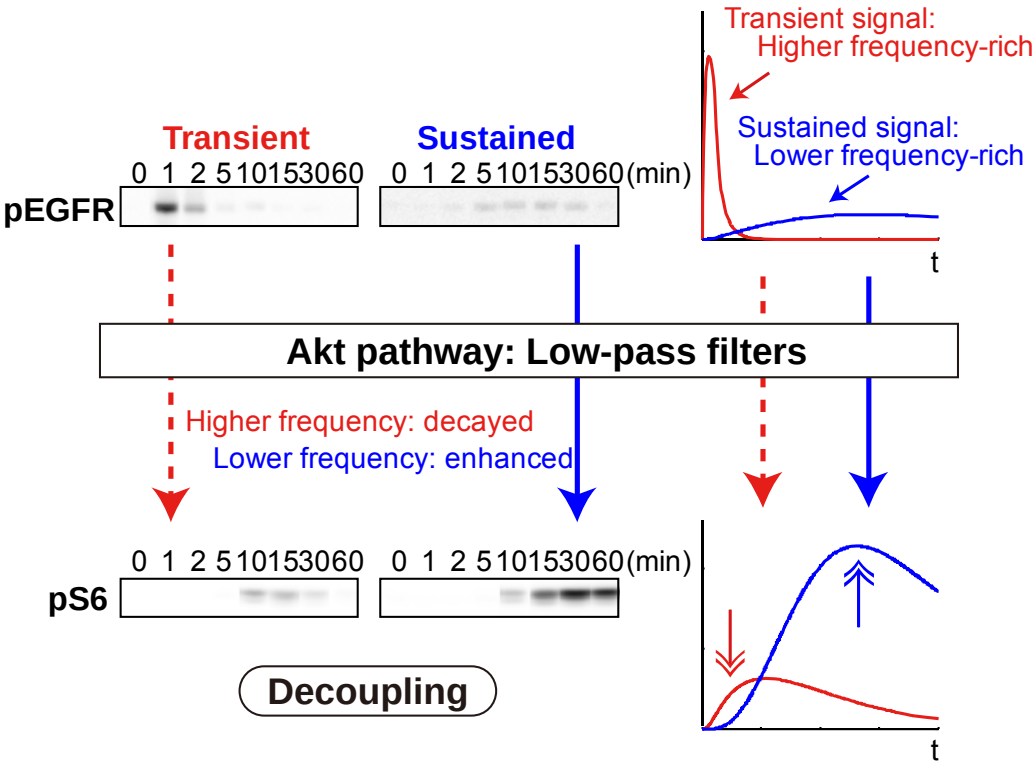


**Figure 3: Decoupling of the relationship of the peak amplitudes between pEGFR and pS6 by the low-pass filter characteristic of the Akt pathway**.

The peak amplitudes of EGFR and S6 phosphorylation were decoupled in PC12 cells; a weak sustained EGFR phosphorylation, rather than a strong transient phosphorylation, strongly induced S6 phosphorylation. The transient and sustained EGFR phosphorylation consisted of higher and lower frequency waves, respectively. Because the Akt pathway exhibited a low-pass filter characteristic, the higher frequency waves were not efficiently transferred downstream, relative to the lower frequency waves. Thus, the Akt pathway serves as a low-pass filter, enabling the decoupling of EGFR phosphorylation and downstream effector phosphorylation.

Phosphorylation of S6, one of the components of ribosome, correlates with ribosome biogenesis and protein synthesis (Meyuhas, 2008), processes that consume the majority of a growing cell's energy (Schmidt, 1999) and that take about 30 minutes (Alon, 2006b). If the signal continued for less than 30 minutes, then ribosome biogenesis and protein synthesis would not be completed and the energy would be wasted. Because of the low frequency pass filter characteristics, the Akt pathway would only transmit upstream signals with a sufficient duration for the completion of the processes and would filter out signals with a shorter duration.

Furthermore, we predicted and validated that an EGFR inhibitor converted strong transient Akt phosphorylation into weak sustained Akt phosphorylation, and, because of the low frequency pass filter characteristics of the Akt pathway, this led to stronger S6 phosphorylation than occurred in the absence of the inhibitor (Figure 4).

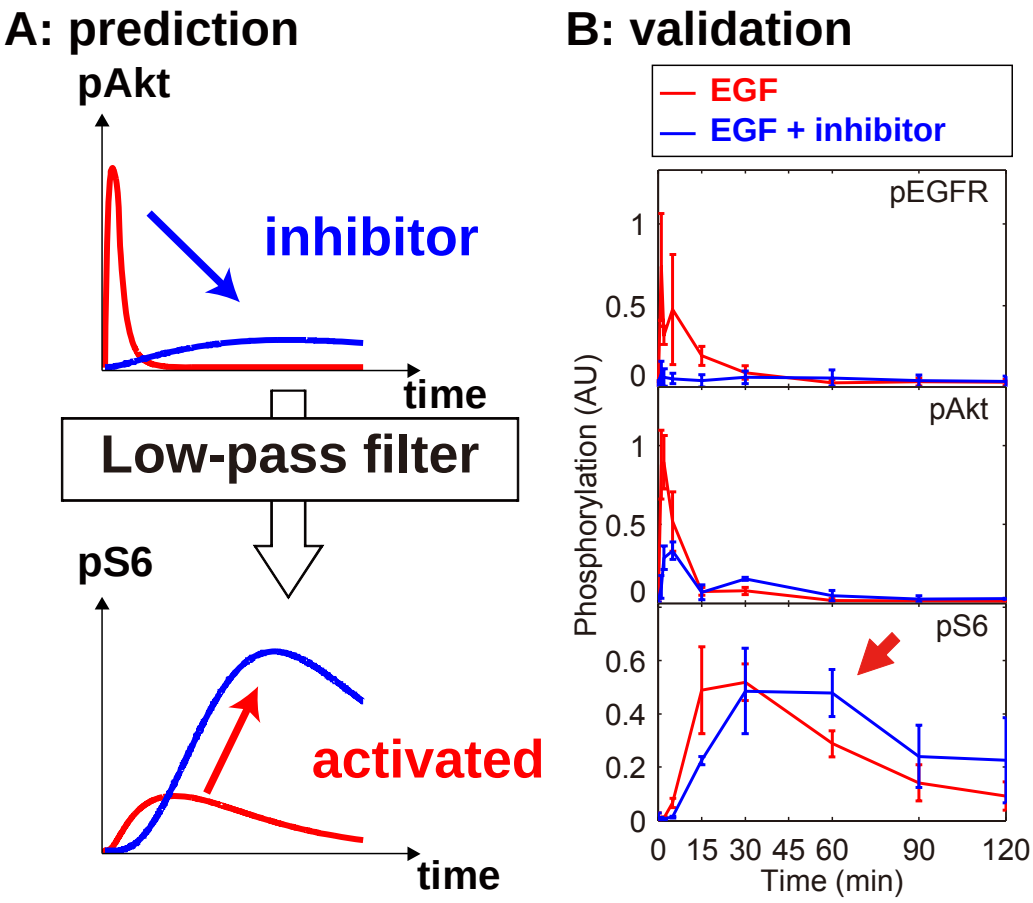


**Figure 4: Low-pass filter characteristic of the Akt pathway can convert an EGFR inhibitor into an activator of S6 phosphorylation.**

(**A**) The fact that a weak sustained time course of pEGFR induced pS6 more strongly than a strong transient time course raises the possibility that an inhibitor may convert a strong transient time course of an upstream molecule into a weak sustained time course, thus the inhibitor could be a downstream activator. (**B**) Experimental validation of the prediction. After treatment of lapatinib, an EGFR inhibitor, for 16 h, the PC12 cells were stimulated with 30 ng/mL of EGF and the phosphorylation of the indicated proteins was measured. Lapatinib inhibited the transient activation of the upstream molecules, but prolonged and enhanced the activities of the downstream molecules.

As well as EGF, NGF also activates the Akt pathway (Figure 5A). Then we also examine the response of the Akt pathway against NGF stimulation. We measured NGF-dependent phosphorylation of TrkA (a part of the receptor complex for NGF), Akt, and S6 (Figure 5B). We found that the dose response of pS6 for NGF at 30 minutes was monotonically increasing sigmoidal shape, whereas that for EGF was convex shape (Figure 5C). In other words, there is optimal dose of EGF, and the EGF stimulation of higher concentration induces lower response of S6. This means that, as in the case of ERK pathway, EGF and NGF induce different responses at the downstream molecules although the growth factors share the same Akt signaling pathway.

In order to uncover the mechanisms underlying the difference of the dose responses, we made a model which can reproduce the experimental results (Figure 5D). The parameters of the model were estimated based on the experimental results by using a numerical optimization method. The established model can reproduce the experimental results, especially EGF-dependent convex dose response and NGF-dependent monotonic dose response of pS6 (Figure 5E and F). This indicates that we may find the mechanisms of the difference of the dose response by analyzing the model.

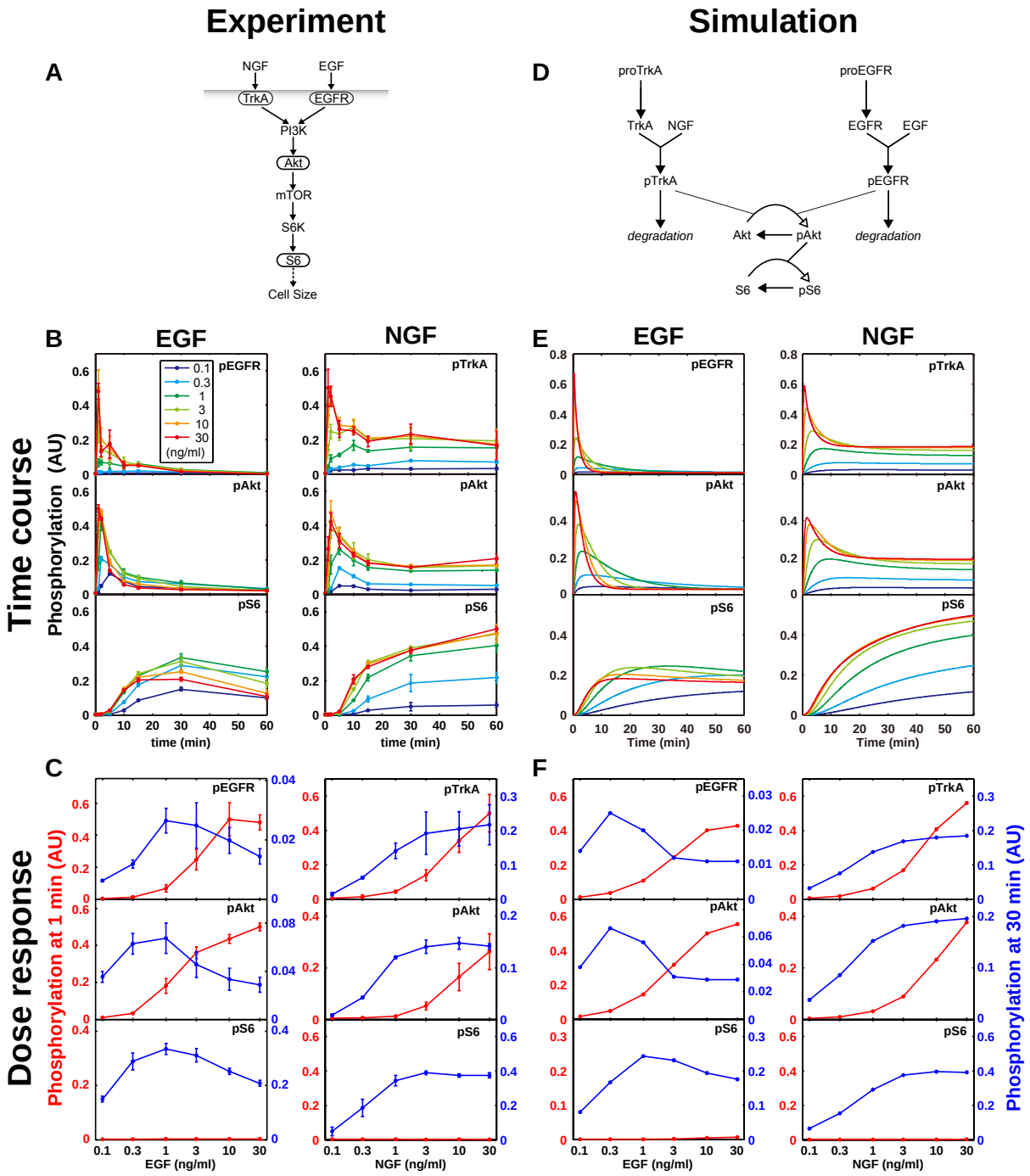


**Figure 5: Convex and monotonic dose response in experiment and simulation.**

(**A**) EGF and NGF dependent Akt pathway. (**B**) Experimental time courses of signaling molecules against indicated concentrations of EGF or NGF (inset). (**C**) Experimental dose responses of signaling molecules at 1 minutes (red) and 30 minutes (blue) in **B**. Please note that the vertical axes are scaled. (**D**) A schematic of simulation model of EGF and NGF dependent Akt pathway. Parameters of the model were estimated based on the time courses in **B**. (**E**) Time courses of signaling molecules in the estimated model. (**F**) Dose responses of signaling molecules in **E**.

Because the model shares the downstream pathways of the receptors, we focused the dynamics around the receptors in the model. The structures and the equations of the model around the respective receptors are same (Figure 6A and B), but the values of the parameters for the respective receptors are different. This indicates that the differences of the parameters are responsible for the differences of the dose responses. Then we obtained the analytical solution of the activated receptor $P$ and found that the receptor dynamics $P(t)$ can be divided into two terms; $P_r(t)$ and $P_d(t)$ (Figure 6C; for mathematical description, see Supplementary Text 7.1.12). The term $P_r(t)$ was scaled by the initial amount of the inactive receptor ($r$) but not by the turnover rate ($d$). The term $P_r(t)$ induced weak sustained activation at the later time point whose dose response is convex (Figure 6D, left, blue), along with strong transient activation at the faster time point whose dose response is monotonic (Figure 6D, left, red). We named this dynamics as depletion dynamics because this convex dose response came from the depletion of the inactive receptor. On the other hand, the term $P_d(t)$ was scaled by the turnover rate ($d$) but not by the initial amount of the receptor ($r$). The term $P_d(t)$ induced only strong sustained activation whose dose response is monotonic (Figure 6D, right). We named this dynamics as turnover dynamics.

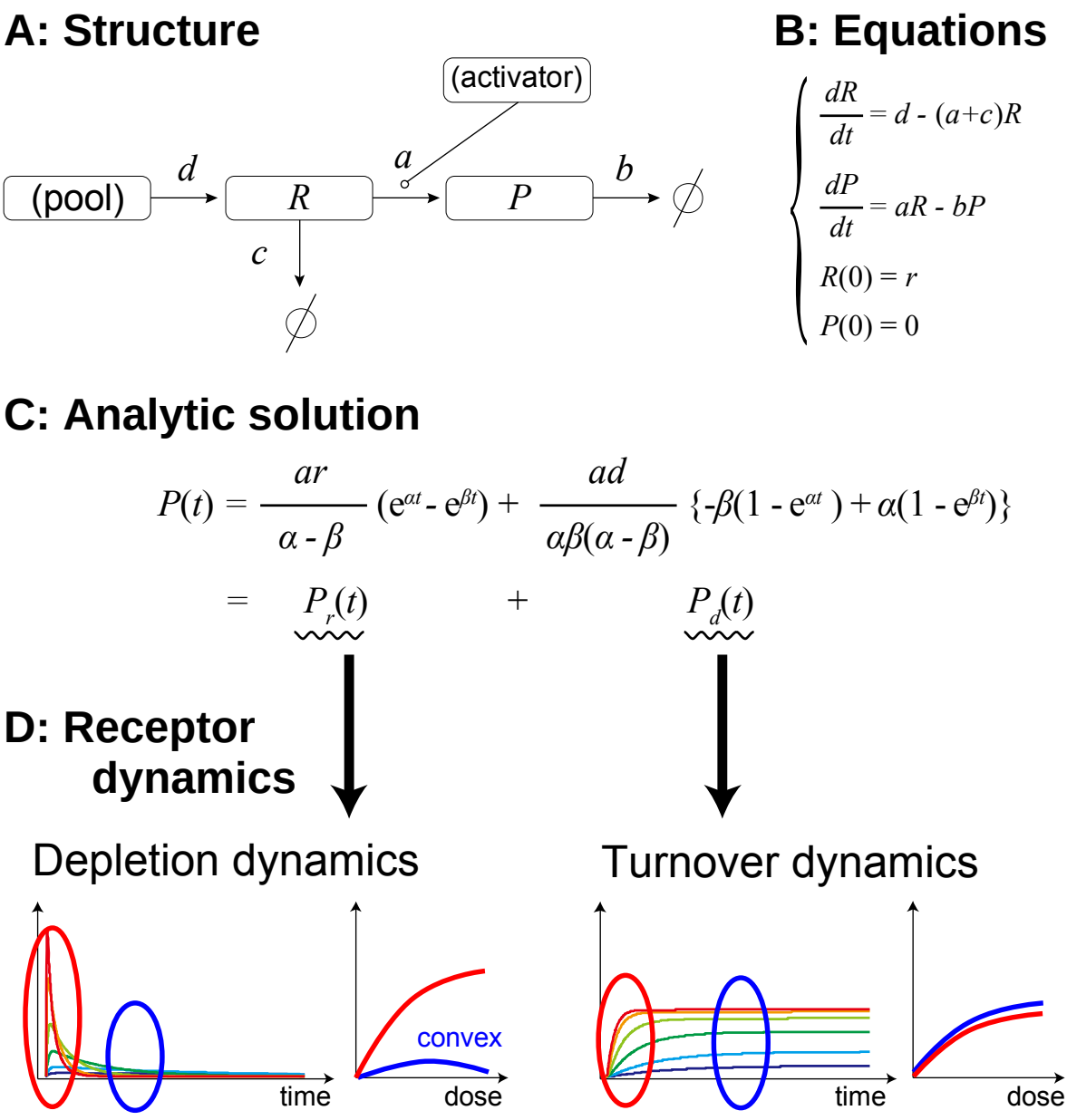


**Figure 6: A model of receptor dynamics.**

(**A**) A schematic of the structure of the model around the receptors. (**B**) Ordinal differential equations of **A**. (**C**) The analytical solution of activated receptor $P$, where $\alpha$ = -$b$, and $\beta$ = -($a$+$c$). The solution $P(t)$ is a sum of the two terms, $P_r(t)$ and $P_d(t)$. (**D**) The term $P_r(t)$ depends on $r$, and introduce the monotonic dose response at the faster time point (red circle) and the convex dose response at the later time point (blue circle) through the depletion dynamics. The term $P_d(t)$ depends on $d$ and introduce the monotonic dose response all the time point through turnover dynamics. For mathematical description, see Supplementary Text 7.1.12.

The time courses of the upstream molecule depend on the balance of the strength of the depletion dynamics and turnover dynamics (Figure 7). For EGF stimulation, pEGFR showed the convex dose response at the later time point because the time courses of pEGFR were mainly composed by the depletion dynamics. The low frequency characteristics of the Akt pathway extract and transfer the slower component, whose dose response is convex, and then the downstream molecule showed the convex dose response (Figure 8, left). On the other hand, for NGF stimulation, pTrkA always showed the monotonic dose response. The time courses of pTrkA were composed by both the depletion dynamics and turnover dynamics, and the convex dose response from depletion dynamics at the later time point is masked by the monotonic dose response from the turnover dynamics because the strength of the former response is weaker than that of the latter response (Figure 7). Then the downstream molecule showed the monotonic dose response (Figure 8, right).

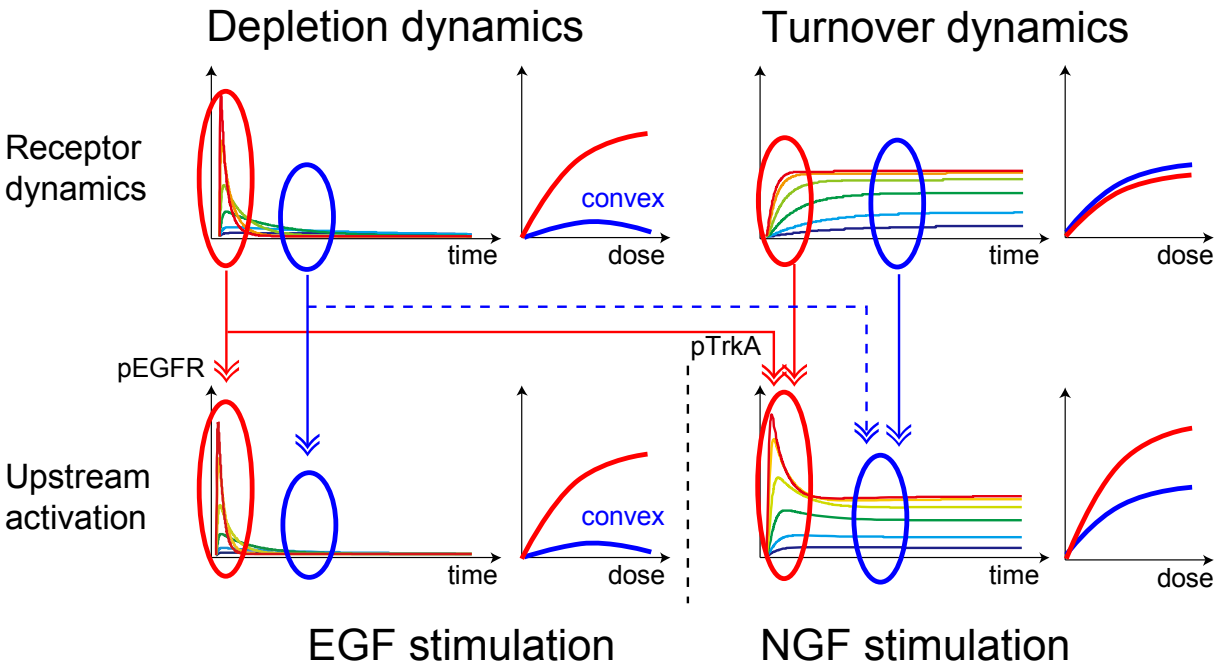


**Figure 7: Depletion and turnover dynamics induce the dynamics of upstream molecules.** For EGF stimulation, the time courses of upstream activation (pEGFR) are composed by only the depletion dynamics. The depletion dynamics induce the strong monotonic dose response at the faster time point (red) and the weak convex dose response at the later time point (blue). For NGF stimulation, the time courses of upstream activation (pTrkA) are composed by both depletion dynamics and turnover dynamics. The strength of convex dose response from the depletion dynamics is weaker than that of the monotonic dose response from the turnover dynamics at the later time point (blue). Therefore, the convex dose response is masked (blue dashed line), resulting in the monotonic dose response at both the faster time point (red) and the later time point (blue).

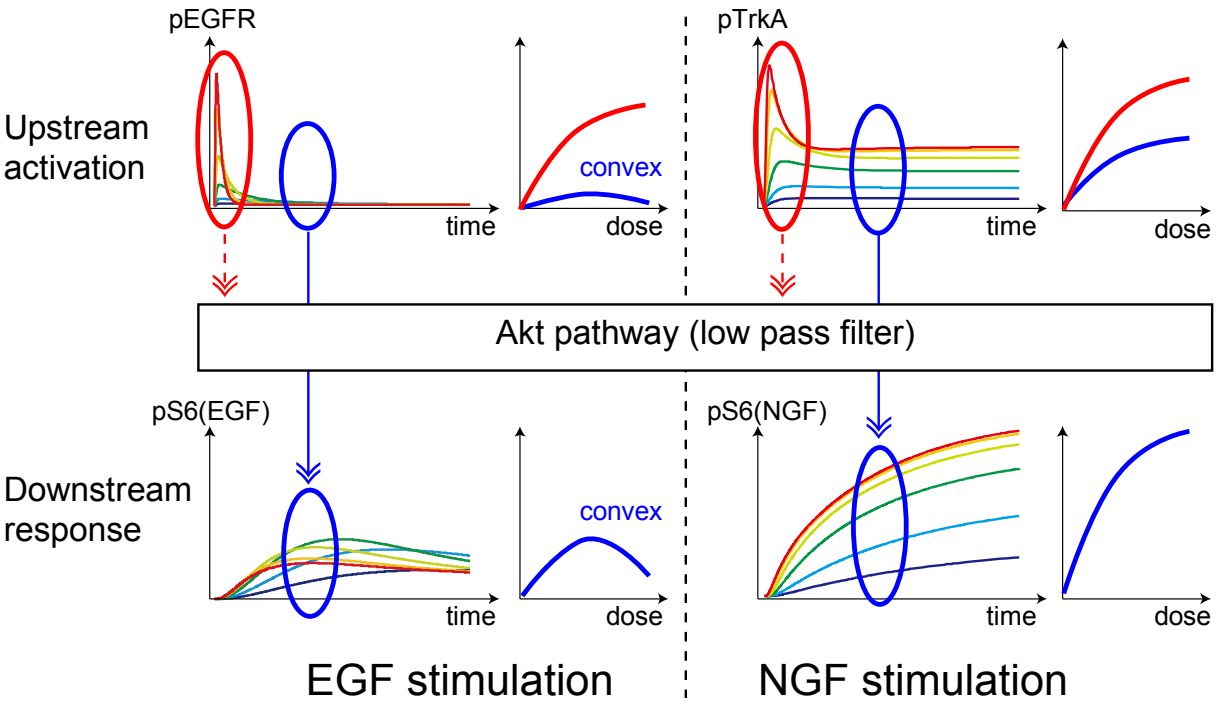


**Figure 8: Extraction and transfer of the convex dose response components by low-pass filter.**

For EGF stimulation, the strength of the convex dose response at the later time point (blue) is weaker than that of the monotonic dose response at the faster time point (red) in the upstream molecule. The low frequency pass characteristics of the Akt pathway extracts and transfer the slower component of the upstream time course to the downstream molecule. Then the downstream molecule shows convex dose response. For NGF stimulation, the upstream time courses always show monotonic dose response, and then the downstream time courses always show monotonic dose response.

Thus, the difference of the dose responses at downstream molecule against EGF and NGF can be explained by the qualitative dynamics around the receptors for respective growth factors. The turnover dynamics can represent many detailed biological processes which can act the supplying of the inactive receptor and therefore the source of the inactive receptor can be a pool of newly synthesized receptors and recycled receptors from the compartment of the phosphorylated and internalized receptor. Our finding that EGFR is less dependent on turnover dynamics is consistent the report that phosphorylated EGFR is ubiquitinated and degraded by proteasome, which resulting in the weak recycling reaction (Di Fiore and Gill, 1999). EGF has been also reported to trigger a convex dose response in various cellular processes, such as DNA synthesis in corneal fibroblasts (Woost et al., 1985), corneal wound healing (Mathers et al., 1989), and proliferation in endometrial carcinoma (Korc et al., 1987). Our finding of the receptor dynamics and the low frequency pass filter in the Akt pathway may explain these in vivo responses. Such mechanisms of the quantitative phenomenon would not be uncovered only by knocking out or other qualitative methods, as I mentioned above (the example of the radio, in INTRODUCTIONS 1.1). This study proved the importance and effectiveness of the strategy that quantitative measurement and analysis of the temporal patterns in intact systems.

The low frequency pass filter characteristics of the pathway play a role in signal processing in Akt pathway. Similar analyses of signaling cascades have been used to investigate osmotic adaptation in the Hog1 mitogen-activated protein kinase pathway of budding yeast (Hersen et al., 2008; Mettetal et al., 2008), calcium signaling (De Koninck and Schulman, 1998; Dolmetsch et al., 1997; Dolmetsch et al., 1998; Tomida et al., 2003), and other studies (Bennett et al., 2008; Detwiler et al., 2000; Samoilov et al., 2002). Especially, low frequency pass filter characteristics (and also band pass filter characteristics) are

experimentally found in some of the above studies. These findings suggest that such frequency filter are common characteristics in living organisms and play a role in many other biological circuits than the Akt pathway.

Although the consecutive first-order reaction found in the Akt pathway is one of the simplest chemical reactions, the reaction can induce the counter-intuitive decoupling phenomena, and the dynamics of the reaction remains elusive. Information of signal strength and its propagation, such as convex dose response and decoupling phenomena, are very important for analyzing the mechanisms of signal processing. Therefore, I extended our previous studies and extensively investigated the propagation of the temporal patterns and its regulation mechanisms in the hypothetical signal transduction pathway consisting of a consecutive first-order reaction.

## 1.3. Introduction of this study

The sensitivities of upstream and downstream molecules to an activator or inhibitor can differ, and variations in sensitivity among cell lines are also observed. Such sensitivity is often measured by the peak amplitude (Behar et al., 2007a; Goentoro et al., 2009; Moyer et al., 1997; Solca et al., 2004; Wakeling et al., 2002), equilibrium amplitude (Behar et al., 2007b; Moasser et al., 2001; O'Shaughnessy et al., 2011; Rusnak et al., 2001), duration (Behar et al., 2008; Dolmetsch et al., 1997; Heinrich et al., 2002), and integration (area under a curve) (Becker et al., 2010; Janes, 2005; Muzzey et al., 2009) of the activity of a signaling molecule. Several possible mechanisms for controlling the sensitivity of the equilibrium amplitude have been proposed, such as substrate depletion in a biochemical reaction (Huang and Ferrell, 1996; Kholodenko et al., 1997; Koshland et al., 1982) and characteristics of network motifs (Behar et al., 2007b, 2008; Entus et al., 2007; Yu et al., 2008). However, although the peak amplitude is often used as an index of signaling activity, the mechanism responsible for controlling the sensitivity of the peak amplitude remains to be elucidated.

On the other hand, we previously found that weak, sustained epidermal growth factor receptor (EGFR) phosphorylation, rather than strong, transient phosphorylation, strongly induced the phosphorylation of S6, a downstream molecule in the Akt pathway, indicating that the relationship of the peak signal amplitudes of Akt and S6 were decoupled in PC12 cells in response to EGF stimulation (Figure 3) (Fujita et al., 2010). Interestingly, a consecutive first-order reaction, which represents a simple signaling pathway, can reproduce this decoupling effect (Fujita et al., 2010). The decoupling effect depends on the attenuation of the signal transfer efficiency of the peak amplitudes between upstream and downstream molecules, and the signal transfer efficiency depends on both the temporal patterns of the signals and the characteristics of the consecutive first-order reaction (Figure 9A; see below). Therefore, the

mechanism leading to attenuation of the signal transfer efficiency remains to be elucidated.

In this study, we first examined the conditions for attenuation of signal transfer efficiency in a consecutive first-order reaction and found that attenuation of signal transfer efficiency depended on the relationship between the half-life time of decay of the upstream molecule and the time constant of negative regulation. We experimentally found that considerable numbers of signaling pathways, including Akt and ERK pathways, in various cell lines can be reasonably approximated by a consecutive first-order reaction although actual molecular networks should consist of multiple complex biochemical reactions and that the property of attenuation of signal transfer efficiency was conserved among such pathways. These findings led us to observe that attenuation of signal transfer efficiency controls the sensitivities to an activator or an inhibitor and that the alteration of sensitivity can be controlled through negative regulation. We experimentally verified the control of sensitivity to an inhibitor in the Akt pathway. Our study demonstrates that attenuation of signal transfer efficiency through negative regulation is a conserved property of the signaling pathway and is one of the core mechanisms of sensitivity control to an activator and an inhibitor. This indicates that cells can control sensitivity to an activator or an inhibitor by changing the expression level of negative regulators.

# 2. Materials and methods

## 2.1. Cell culture and growth factor treatments

The cell cultures and growth factor stimulation were performed as follows. In common, the cells were maintained on 100-mm non-coated dishes in indicated medium at 37 degree Celsius in a saturating humidified atmosphere of 95% air and 5% $CO_2$.

The PC12 cells were provided by M. Nakafuku (Cincinnati Children's Hospital Medical Center, Cincinnati, OH) and cultured in Dulbecco modified Eagle medium (DMEM) (low-glucose, Sigma, #D6046) supplemented with 10% fetal bovine serum (FBS) and 5% horse serum. The PC12 cells ($8 \times 10^5$ cells) were seeded onto 60-mm poly-D-lysine–coated dishes. One day later, the PC12 cells were serum starved for 16 h and then stimulated with EGF or NGF as previously described (Fujita et al., 2010). In the inhibitor experiment, lapatinib (Toronto Research Chemicals, #L175800) was added from serum starvation and the cells were stimulated with EGF (30 ng/ml; Figure 22).

The HeLa cells were kindly provided by S. Sigismund (Fondazione Istituto FIRC di Oncologia Molecolare, Milan, Italy) (Sigismund et al., 2008) and cultured in minimum essential medium (MEM; Sigma, #M4655) supplemented with 10% FBS, 1mM sodium pyruvate, and 0.1mM MEM nonessential amino acids (Invitrogen, #11140-050). The HeLa cells ($2 \times 10^5$ cells) were seeded into 60-mm poly-D-lysine–coated dishes. One day later, the medium of the HeLa cells was renewed and after 16 h, the HeLa cells were stimulated with EGF (0, 1, or 100 ng/ml).

The Swiss-3T3 cells were obtained from Health Science Research Resources Bank (Osaka, Japan, #JCRB9019) and cultured in DMEM (low-glucose, Sigma #D6046) supplemented with 10% FBS. The Swiss-3T3 cells ($1.5 \times 10^5$ cells) were seeded into 35-mm

non-treated dishes. Two days later, the Swiss-3T3 cells were serum starved for 16 h and then stimulated with EGF (0.1, 1, 10, 100 ng/ml) (Shaw and Cohen, 1999).

The HUVECs and culture media (HuMedia-EG2) were purchased from a commercial source (Kurabo) (Maeda et al., 2006). HUVECs ($3 \times 10^5$ cells) at the sixth passage were seeded onto 35-mm collagen-coated dishes. One day later, HUVECs were serum starved for 16 h and then stimulated with EGF (0.1, 0.3, 1, 3, 10, 30, 100 ng/ml) (Zingg et al., 2004).

## 2.2. Immunoblotting

Immunoblotting and processing of signal intensities of immunoblots were performed as follows. Cell lysates were subjected to standard SDS-PAGE, and transferred to nitrocellulose membrane. The membranes were probed with following antibodies; PathScan Multiplex Western Cocktail I (antibodies against phosphorylated p90RSK [Ser380], phosphorylated Akt [Ser473], phosphorylated ERK1/2 [Thr202/Tyr204], phosphorylated S6 [Ser235/236], and total eIF4E, #5301), phosphorylated EGFR [Tyr1068] (#2234), phosphorylated TrkA [Tyr490] (#9141), phosphorylated TSC2 [Thr1462] (#3617), phosphorylated S6 kinase [Thr389] (#9205 or #9206), phosphorylated eIF4B [Ser422] (#3591), phosphorylated GSK3β [Ser9] (#9336), phosphorylated CREB [Ser133] (#9191), c-Fos (#2250), c-Jun (#9165), EGR1 (#4154), and p21Cip1 (#2947). All antibodies were purchased from Cell Signaling Technology. Immunoblotting was performed with horseradish peroxidase (HRP) conjugated secondary antibodies (GE Healthcare, UK). and Immobilon Western Chemiluminescent HRP Substrate (Millipore).

The signals of immunoblots were detected with a luminoimage analyzer (LAS-4000; Fujifilm). We quantified chemiluminescent signals with the analysis software TotalLab TL120 (Nonlinear Dynamics). We obtained the signal intensities of the respective molecules by quantifying immunoblot images. We normalized the signal intensities so that the peak intensity of each molecule was set at 1. We used a single gel and membrane for an independent experiment of a single molecule so that the intensities of the single molecule could be compared directly.

A part of the experimental data shown in Figure 15B and Figure 22 came from previously reported data (Fujita et al., 2010).

## 2.3. Simulation and parameter estimation

We performed the simulation and analysis using MATLAB (version R2010a, MathWorks) and SBTOOLBOX2 (Schmidt and Jirstrand, 2006), a third party toolbox for MATLAB. We estimated the parameters based on a previously reported protocol (Fujita et al., 2010). The detailed method used for the parameter estimation is described in the Supplementary Text 7.1.7.

## 2.4. Experimental validation of the attenuation property of signal transfer efficiency

We obtained 568 sets of time courses of 110 pathways from the experiments in four cell lines stimulated by two ligands (Supplementary Data). Each pathway consists of an upstream and a downstream molecule. When the cell lines or ligand or stimulation pattern (step, pulse, or ramp stimulation) are different, the same set of the upstream and downstream molecules is regarded as the different pathway. Each pathway involves time courses by multiple doses. We estimated the parameters of the activator model for each set of time courses obtained by experiments (see Supplementary Text 7.1.7 and Supplementary Data). *c* and *d* were estimated for each pathway because *c* and *d* were parameters for a pathway and should be conserved regardless of the doses of a stimulation, whereas *a* and *b* were estimated for each dose of stimulation because *a* and *b* were parameters for stimulation and could vary depending on the dose.

We selected pathways that satisfy conditions (i) and (ii) (described in DISCUSSION 4.2) as follows. The squared sum of the residuals (RSS) between experiment and simulation were calculated for each time course or all time courses in each pathway and then normalized by the squared sum of the experimental value. We excluded the pathways whose normalized RSS was larger than 0.1. We excluded the set of the time course whose normalized RSS was larger than 0.3. We also excluded the time course of the inhibitor experiments and the set of the time course whose half-life time ($t_{1/2}$) or peak amplitudes could not be obtained by experiment because of sustained response or non response to the stimuli. We selected the rest of the time courses as satisfying conditions (i) and (ii) and analyzed their experimental data for Figure 15B. The half-life time ($t_{1/2}$) was obtained by linear interpolation of the experimental time course of the upstream molecule. The signal transfer efficiency ($E$) was obtained from the ratio of the peak amplitudes of the experimental time courses and then normalized by the gain of the estimated activator model.

# 3. RESULTS

## 3.1. Attenuation of signal transfer efficiency of the peak amplitude

We made a simple model using a consecutive first-order reaction (Figure 9B; see Supplementary Text 7.1.1) and numerically analyzed the conditions for attenuation of signal transfer efficiency. This model is the simplified version of the model used in the previous study (see INTRODUCTIONS 1.2) and can reproduce the time courses of EGF experiment. The model can be described using the following ordinary differential equations:

$$\begin{cases} \dfrac{dX}{dt} &= -a \cdot X, \\ \dfrac{dY}{dt} &= a \cdot X - b \cdot Y, \\ \dfrac{dZ}{dt} &= c \cdot Y - d \cdot Z. \end{cases} \tag{1}$$

The initial conditions were given as follows:

$$\begin{cases} X(0) &= 1, \\ Y(0) &= 0, \\ Z(0) &= 0, \end{cases} \tag{2}$$

and the analytical solution of the equations is

$$\begin{cases} X(t) &= \mathrm{e}^{-at}, \\ Y(t) &= \dfrac{a}{b-a}\left(\mathrm{e}^{-at} - \mathrm{e}^{-bt}\right), \\ Z(t) &= \dfrac{-ac\mathrm{e}^{-at}}{(d-a)(a-b)} + \dfrac{-ac\mathrm{e}^{-bt}}{(a-b)(b-d)} + \dfrac{-ac\mathrm{e}^{-dt}}{(b-d)(d-a)}, \end{cases} \tag{3}$$

where $(a \neq b \neq d)$.

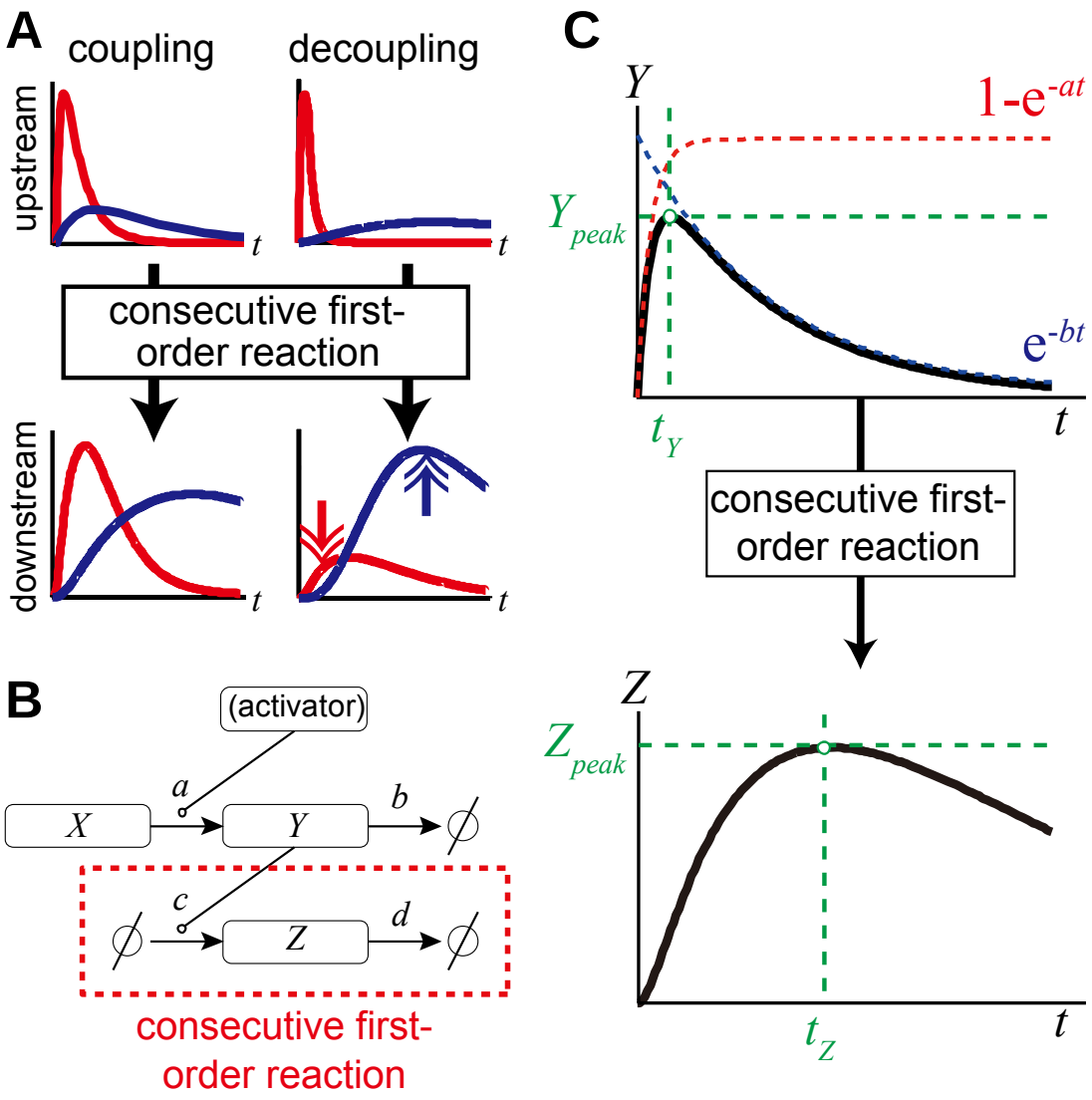


**Figure 9: Activator model.**

(**A**) Time courses of the activities of the upstream and downstream molecules under either coupling or decoupling conditions. (**B**) Activator model. The boxes and arrows represent the molecules and chemical reactions, respectively. A circle with a line through it represents a pool of substrates or degradation products. A circle connected to an arrow represents a catalytic contribution to the reaction. *a*, *b*, *c*, and *d* indicate the rate constants of the respective reactions. (**C**) Representative time courses of *Y* and *Z* (black lines). $Y_{peak}$ and $Z_{peak}$ are the peak amplitudes of the time courses of *Y* and *Z*, respectively. $t_Y$ and $t_Z$ are the peak times of the time courses of *Y* and *Z*, respectively. The colored dashed lines in the upper panel are the asymptotic lines of the time course of *Y*. The rate constants *a* and *b* also represent the rise and decay rates of the time course of *Y* when *a* is larger than *b*.

*Y* and *Z* were regarded as amounts of activated upstream and downstream molecules of a signaling pathway, respectively. In this study, we focused on the relationships between *Y* and *Z* and, therefore, the biologic counterpart of *X* was not specified. The model had four rate constants: *a*, *b*, *c*, and *d*. The constant *a* was the synthesis rate constant of *Y*, and the value of *a* simultaneously means the concentration of the activator. The constant *b* was the degradation rate constant of *Y*. The constant *c* was the synthesis rate constant of *Z*. The constant *d* was the degradation rate constant of *Z*. The degradation of *Z* can be regarded as a negative regulation of the pathway from *Y* to *Z*, and therefore, the value of *d* corresponds to the strength of negative regulation. Hereafter, this model is referred to as the activator model.

The time course of *Y* exhibited a single peak and was expressed as the sum of two exponential functions (Figure 9C). The rate constants *a* and *b* also represented the rise and decay rates of the time course of *Y*. The time course of *Z* also had a single peak. Hereafter, the peak amplitudes of *Y* and *Z* are referred to as $Y_{peak}$ and $Z_{peak}$, respectively, and the peak times of *Y* and *Z* are referred to as $t_Y$ and $t_Z$, respectively. We changed the time course of *Y* by changing *a* and *b* and examined the response of $Z_{peak}$. Note that the amplitude of *Z* was uniformly scaled by *k* (= *c*/*d*, see Supplementary Text 7.1.1 and 7.1.2), and therefore the ratio of $Z_{peak}$ to $Y_{peak}$ was also scaled by *k*. To remove the effect of *k*, the signal transfer efficiency *E* was defined as following normalized form:

$$E = \frac{1}{k} \cdot \frac{Z_{peak}}{Y_{peak}}. \tag{4}$$

Note that, as *d* increases, $Z_{peak}$ decreases and the ratio of $Z_{peak}$ to $Y_{peak}$ also decreases. But *E* increases because 1/*k* (= *d*/*c*) increases along with the increase of *d* and because the increase of 1/*k* overcomes the decrease of $Z_{peak}$.

We examined how the signal transfer efficiency $E$ is determined using numerical simulation (Figure 10). The $Z_{peak}$ indicated in red became lower than that indicated in blue despite the same $Y_{peak}$ (Figure 10A), indicating that the $Y$ signal shown in red was not transferred efficiently to $Z$ compared with the signal indicated in blue. We next examined the effects of parameters $a$ and $b$ on $Y_{peak}$ and $Z_{peak}$ (Figure 10B and C). $Y_{peak}$ was determined by the ratio of $a$ to $b$ ($a$/$b$) and increased as a function of $a$/$b$ (Figure 10D). Similarly, $Z_{peak}$ seemed to be determined by $a$/$b$ when both $a$ and $b$ were smaller than $d$ (Figure 10C). However, $Z_{peak}$ seemed to become independent of $a$/$b$ and instead was determined by $b$ when $a$ was larger than $d$. We confirmed that similar results were obtained for a wide range of $d$ values (Figure 11). We then obtained the signal transfer efficiency $E$ from $Z_{peak}$ and $Y_{peak}$ (Figure 10E). $E$ reached a maximum value of about 1 when $a$ or $b$ was smaller than $d$ and decreased to values less than 1 when $a$ or $b$ was larger than $d$. This finding indicates that the signal transfer efficiency $E$ was higher when either the synthesis or degradation rate constant of the upstream signal was smaller than the rate constant of negative regulation, whereas $E$ attenuated when both the synthesis and degradation rate constants of the upstream signal were larger than the rate constant of negative regulation.

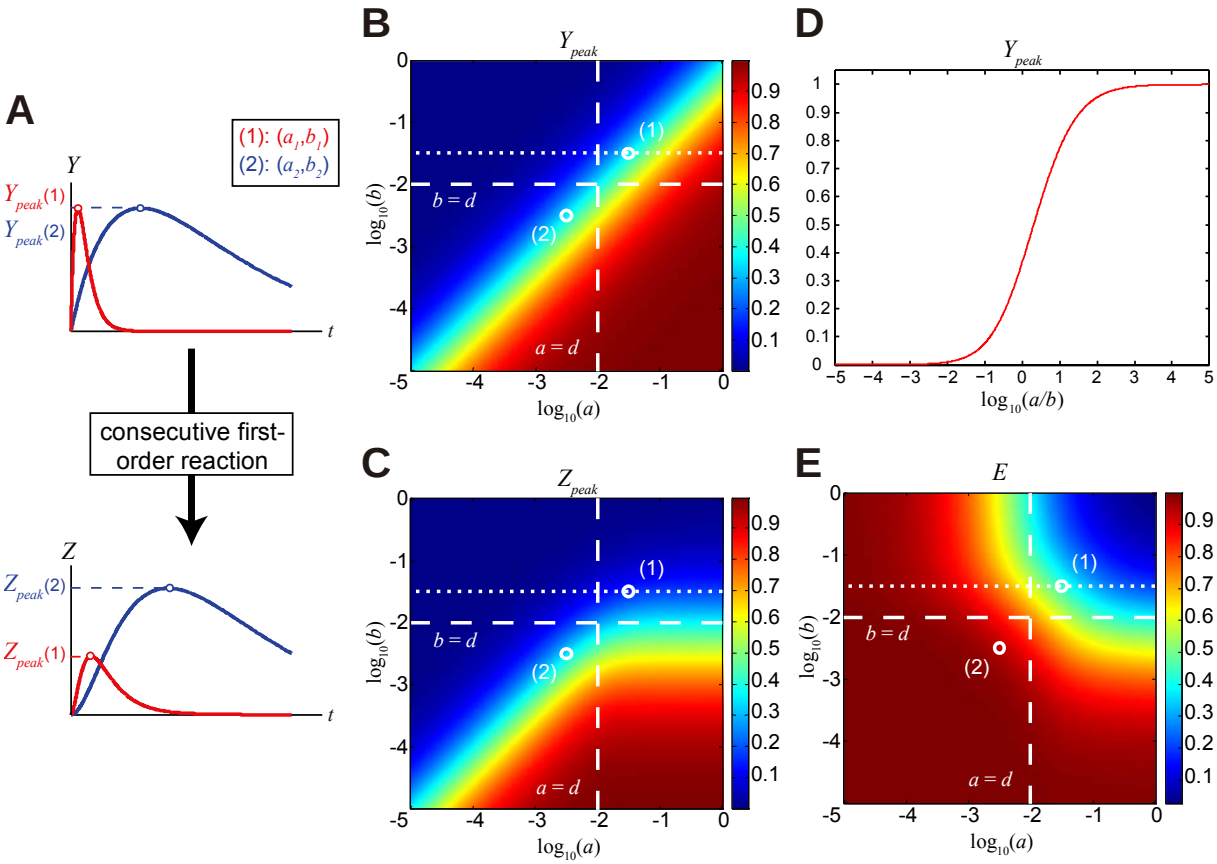


**Figure 10: Attenuation of signal transfer efficiency.**

(**A**) The degree of attenuation depends on the upstream time course. The time courses of $Y$, indicated in red and blue, have different parameters. (**B**) Dependence of $Y_{peak}$ on $a$ and $b$. The color scale indicates $Y_{peak}$. $c$ and $d$ were set at 0.01. The white circles correspond to the time courses shown in panel **A**. The white dashed lines indicate when $a$ or $b$ equals $d$. The white dotted lines corresponds to the lines in Figure 16D. (**C**) Dependence of $Z_{peak}$ on $a$ and $b$. (**D**) $Y_{peak}$ is an increasing function of $a/b$. The diagonal pattern of the contour line in panel **B** indicates that $Y_{peak}$ was determined by $a/b$. (**E**) Dependence of $E$ on $a$ and $b$.

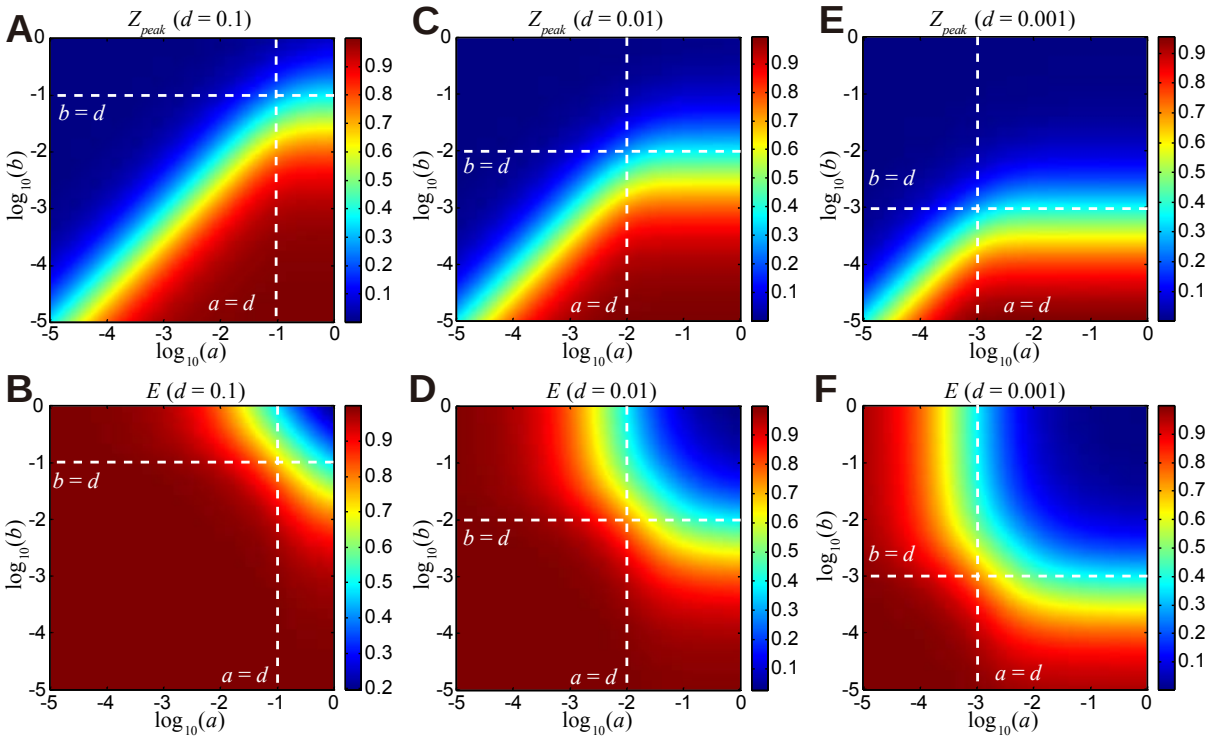


**Figure 11: Effect of parameter *d* on $Z_{peak}$ and *E*.**

(**A**, **C**, and **E**) $Z_{peak}$ against the indicated ranges of *a* and *b* when *d* was set at 0.1, 0.01, and 0.001, respectively. The value of *c* was the same as that of *d*. The white dashed lines indicate when *a* or *b* equals *d*. (**B**, **D**, and **F**) Signal transfer efficiency, *E*, against the indicated ranges of *a* and *b* when *d* was set at 0.1, 0.01, and 0.001, respectively. The value of *c* was the same as that of *d*. *d* affected $Z_{peak}$ and *E*, but did not affect the condition when $Z_{peak}$ became attenuated.

We also obtained analytical solutions for $Y_{peak}$ and $Z_{peak}$ (see Supplementary Text 7.1.3). An analytical solution for $Y_{peak}$ (and also for $t_Y$) can be easily obtained, but it is not easy to get an analytical solution for $Z_{peak}$. We divided the parameter space into three areas (areas I to III, as shown in Figure 12A) and approximated the analytical solution of $Z$ so that we could obtain the approximate analytical solution of $Z_{peak}$ and $t_Z$. $Z_{peak}$ in the approximate analytical solution (Figure 12B) was very similar to $Z_{peak}$ in the numerical solution (Figure 10C), except for some inaccurate approximations in a few areas (Figure 12C). We also estimated $E$ based on the approximation (Figure 13).

Based on the approximate analytical solutions, we obtained the conditions under which decoupling occurs using simple expressions (see Supplementary Text 7.1.5). This result indicates that the decoupling effect was caused by the strong attenuation in the signal transfer efficiency, $E$.

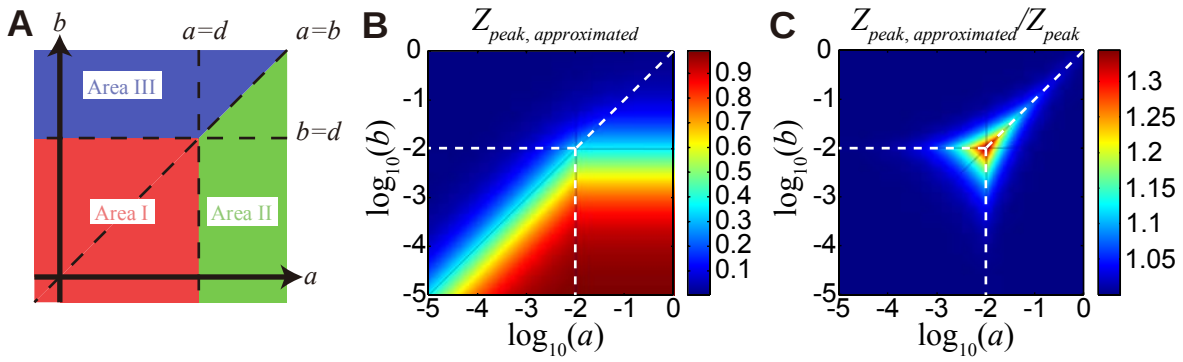


**Figure 12: Approximate analytic solution of $Z_{peak}$.**

(**A**) The parameter space was divided into three areas. We obtained an approximate analytic solution of $Z_{peak}$ for each area (see Supplementary Text 7.1.3). (**B**) Approximate analytical solution of $Z_{peak}$. The white dashed lines indicate the borders of the areas. (**C**) Ratio of the numerical and the approximate analytic solution of $Z_{peak}$. The approximate analytical solution of $Z_{peak}$ was very similar to the numerical solution of $Z_{peak}$. The approximation became inaccurate around the borders of the areas, but the difference between the numerical and analytical values was less than about 35%.

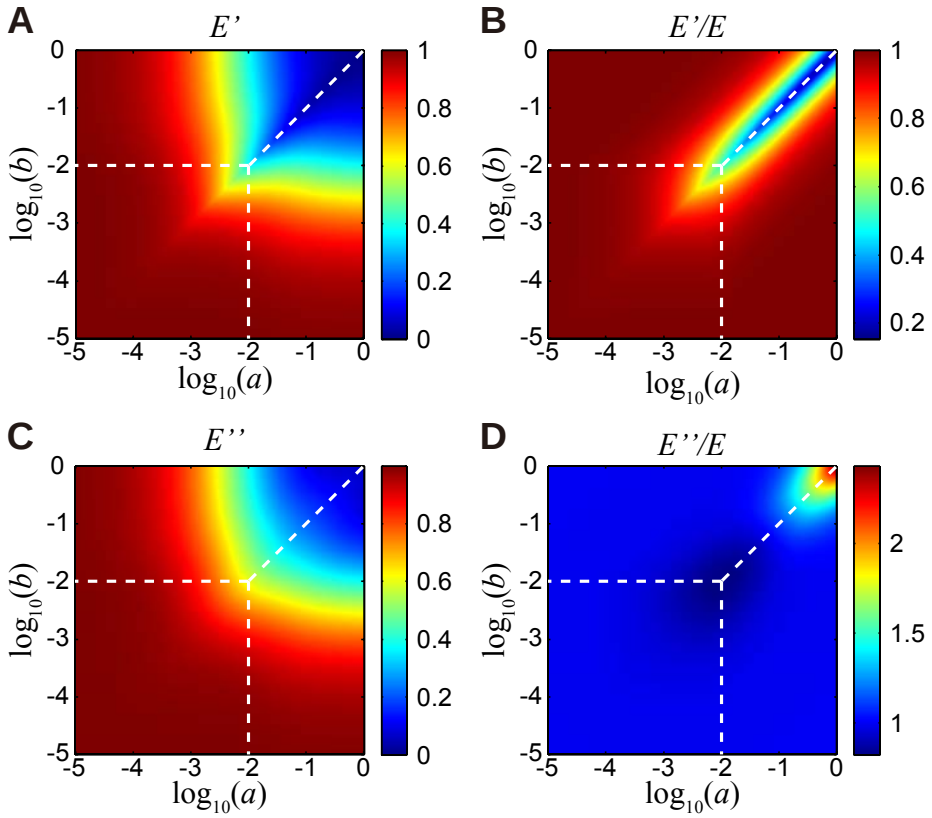


**Figure 13: Estimation of *E*.**

(**A**) Estimation of *E*. The efficiency, *E*, is not a simple ratio of the peak amplitudes of a single set of upstream and downstream time courses in different scales, but should be scaled by *k*. We identified a means of estimating *E* from a single set of upstream and downstream time courses. Based on the approximate analytical solution of *Z*, the efficiency, *E*, was expressed in terms of the difference in the peak times, $\Delta t$ (defined as $t_Z$ - $t_Y$), and the parameters *a* and *b* (see Supplementary Text 7.1.6). These values could be obtained from the experimental data of a single set of upstream and downstream time courses. We estimated *E* from the numerical value of $\Delta t$ and the parameters *a* and *b*. This value was denoted as *E'* and is shown in color. (**B**) Ratio of *E'* to the numerical value of *E*. *E'* was very similar to *E*, but the ratio became extremely low around the borders of areas II and III. (**C**) Estimation of *E* using an ad hoc substitution. We introduced an ad hoc substitution to estimate *E* (see Supplementary Text 7.1.6) and estimated the value of *E* based on the new expression. This value was denoted as *E''* and is shown in color. (**D**) Ratio of *E''* to the numerical value of *E*. *E''* was very similar to *E*, and the ratio was closer to 1 than the case for *E'*, indicating an improvement in the estimation. This finding indicates that the signal transfer efficiency *E* can be estimated from a single set of time courses of *Y* and *Z*.

## 3.2. Attenuation of signal transfer efficiency is a conserved property

We tried to validate the signal transfer efficiency in experiments. Therefore, we determined how to estimate $E$ in experiments (Figure 14 and Figure 15). We found that $E$ can be estimated by the half-life time ($t_{1/2}$) of the upstream signal and the time constant $\tau$ ($\tau = 1/d$) of negative regulation of a signaling pathway, both of which can be experimentally measured (Figure 14C and Figure 15A). $t_{1/2}$ roughly corresponds to the duration of the upstream signal. $E$ attenuated when $t_{1/2}$ became shorter and $E$ became 0.5 when $t_{1/2}$ was equal to $\tau$ (Figure 14C), indicating that attenuation of $E$ depends on the ratio of $t_{1/2}$ to $\tau$. This means that $E$ can be controlled by negative regulation. The theoretical line of estimation of $E$ against $t_{1/2}$ normalized by $\tau$ in the model (Figure 14C, black line) was obtained as

$$E = \frac{1}{1 + \left( \frac{t_{1/2}}{\tau} \cdot \frac{1}{1.17} \right)^{-0.932}} . \tag{5}$$

Approximately half of the maximal $E$ is given when $t_{1/2}$ becomes the same as $\tau$. If $t_{1/2}$ is shorter than $\tau$, $E$ becomes smaller than 0.5, whereas if $t_{1/2}$ is longer than $\tau$, $E$ becomes larger than 0.5 (Figure 15A). For example, consider a pathway where $\tau$ is 30 min. If $t_{1/2}$ is 10 min (shorter than $\tau$), $E$ becomes smaller (0.23). Conversely, if $t_{1/2}$ is 60 min (longer than $\tau$), $E$ becomes larger (0.62). This indicates that the signal transfer efficiency $E$ attenuates when $t_{1/2}$ is shorter than $\tau$.

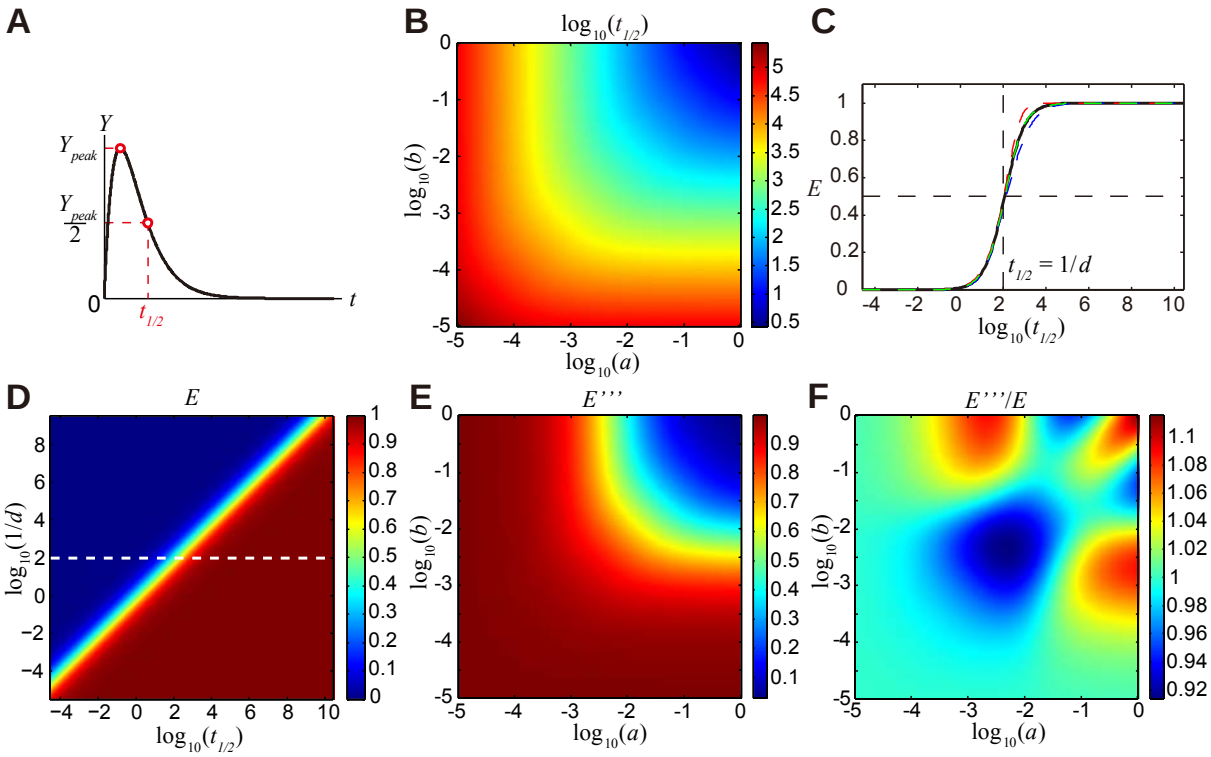


**Figure 14: The efficiency *E* can also be estimated from the half-life time, $t_{1/2}$.**

(**A**) The half-life time $t_{1/2}$ is the time at which the value of *Y* has decreased to half of the $Y_{peak}$. (**B**) $t_{1/2}$ for the indicated ranges of *a* and *b*. The color indicates $t_{1/2}$ on a logarithmic scale. The concentric pattern of $t_{1/2}$ was similar to that of the efficiency *E* (Figure 10E). (**C**) Relationship between *E* and $t_{1/2}$. All the data points were plotted in the small area bounded by the red and blue dashed lines. The green dashed line was the midpoint of the red and blue dashed lines. The black solid line shows a sigmoid curve fitted to the green broken line (equation (5)). These lines moved horizontally depending on the value of *d*, and the value of *E* was about 50% when the value of $t_{1/2}$ was the same as that of $1/d$. (**D**) Effect of $t_{1/2}$ and $1/d$ on *E*. The value of $t_{1/2}$ and $1/d$ are shown using a logarithmic scale. The white dashed line corresponds to the black solid line in **c**. The efficiency *E* became smaller when $t_{1/2}$ or *d* became smaller. The diagonal pattern of the contour line indicates that *E* can be estimated by the ratio of $t_{1/2}$ and $1/d$. (**E**) Estimation of the efficiency *E* from $t_{1/2}$. The estimated *E* (*E'''*) was obtained from the numerical value of $t_{1/2}$ and equation (5). (**F**) Ratio of *E'''* to the numerical value of *E*. The difference was as much as 10%, indicating that the efficiency *E* can be reasonably estimated using this method when *d* is already known. This method does not require the parameters *a, b,* nor the time course of *Z*.

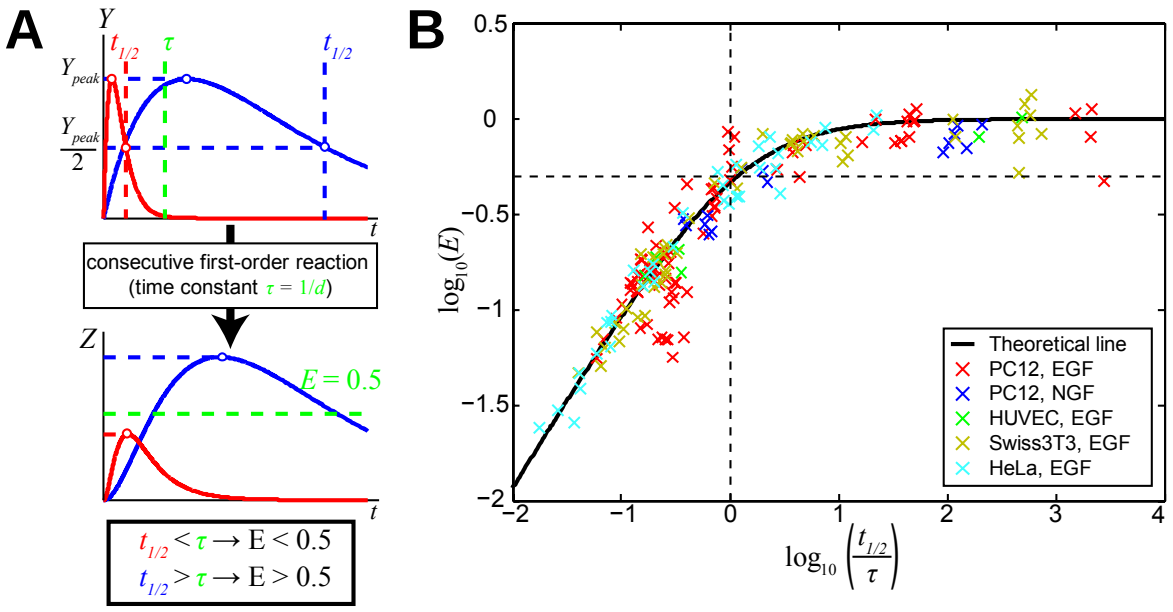


**Figure 15: Attenuation of the signal transfer efficiency is a conserved property.**

(**A**) The half-life time, $t_{1/2}$, is the time at which the value of $Y$ has decreased to half of the $Y_{peak}$. The time constant τ is the inverse of the rate constant, $d$, of the negative regulation of the consecutive first-order reaction. If $t_{1/2}$ is shorter than $\tau$, $E$ becomes smaller than 0.5, whereas if $t_{1/2}$ is longer than $\tau$, $E$ becomes larger than 0.5. (**B**) $E$ against $t_{1/2}$ normalized by $\tau$. The solid line indicates the theoretical line of the model, which is given by equation (5) (see Figure 14C). The crosses indicate $E$ obtained by experiment. The horizontal and vertical dashed lines indicate where $E = 0.5$ and where $t_{1/2} = \tau$, respectively.

To examine whether the attenuation of the signal transfer efficiency is a general property of a signaling pathway, we measured the time courses of various signaling pathways by changing doses of different ligands in various cell lines. Experimentally, *E* can be obtained under the conditions where the time course of upstream molecules can be approximated by the sum of two exponential curves and the pathway can be approximated by a consecutive first-order reaction (Figure 9C; see DISCUSSION 4.2). Among 568 sets of upstream and downstream time courses of signaling pathways, 169 sets satisfied the conditions (Supplementary Data; see also Materials and methods 2.4 and Supplementary Text 7.1.7) including pAkt to pS6 pathway (Figure 15B) (Fujita et al., 2010). It is quite surprising that, although actual molecular network should consist of multiple complex biochemical reactions, considerable numbers of sets of time courses between upstream and downstream molecules (169 sets of 568 sets) can be reasonably approximated by a simple linear reaction. This suggests that, with the time resolution of minutes, the selected signaling pathways apparently behave as a simple linear input–output relationship despite the more complex nonlinear reactions in reality. This also suggests that, even if detailed information about reaction steps or schemes is unknown in a certain signaling pathway, a consecutive first-order reaction can potentially approximate behaviors of considerable numbers of signaling pathways.

Among the 169 sets, we first examined whether attenuation of signal transfer efficiency was observed in EGF-dependent pathways in PC12 cells involving EGFR, Akt, ERK1, ERK2, S6 kinase, S6, eIF4B, RSK, and c-Fos (70 sets of time courses in 16 pathways; Figure 15B; Supplementary Data). For such pathways, *E* obtained by experiment appeared along the theoretical line in the model (Figure 15B, red points). This indicates that the *E,* indeed, depends on a ratio of $t_{1/2}$ to $\tau$ regardless of the pathway and that the attenuation property was conserved among the signaling pathways. We also asked whether or not this property is specific to EGF and can be seen in other ligands such as nerve growth factor (NGF). *E* of the

NGF-dependent signaling pathways in PC12 cells (6 sets of time courses in 2 pathways) similarly appeared along the theoretical line (Figure 15B, blue points; Supplementary Data). This indicates that the attenuation property was conserved among the ligands. We also asked whether or not this property is specific to PC12 cells and can be seen in other cell lines, such as human umbilical vein endothelial cells (HUVECs), Swiss 3T3, and HeLa cells. *E* of the EGF-dependent signaling pathways in HUVECs (15 sets of time courses in 4 pathways; Figure 15B, green points; Supplementary Data), Swiss 3T3 (39 sets of time courses in 12 pathways; Figure 15B, yellow points; Supplementary Data), and HeLa (34 sets of time courses in 14 pathways; Figure 15B, cyan points; Supplementary Data) similarly appeared along the theoretical line. This indicates that the attenuation property was conserved among the cell lines. Thus, the attenuation of signal transfer efficiency appeared as a general property for any signaling pathway that can be approximated by a consecutive first-order reaction and is not specific to signaling pathways, ligands, or cell lines.

## 3.3. Control of sensitivity to an activator

To explore the role of attenuation of signal transfer efficiency, we examined the effective dose of the activator for $Y_{peak}$ and $Z_{peak}$ (Figure 16). Note that $a$ can be regarded as the concentration of the activator (Figure 16A and B). $Y_{peak}$ increased as $a$ became larger (Figure 16C, upper panel). For example, $Y_{peak}$ was 0.5 at $a$ = 0.0577, which is the half-maximal effective concentration of the activator ($EC_{50}$) for $Y_{peak}$, and 1 at $a$ = 100 (when $d$ was 0.01). On the other hand, $t_{1/2}$ became smaller when $a$ became larger. Because we already found that the signal transfer efficiency attenuates as $t_{1/2}$ became smaller (Figure 15B), signal transfer efficiency attenuated as $a$ became larger. Therefore, $E$ at $a$ = 0.0577 should be larger than $E$ at $a$ = 100 (Figure 16C, middle panel). Because $Z_{peak}$ was relative to the product of $Y_{peak}$ and $E$, $Z_{peak}$ at $a$ = 0.0577 should be larger than the half of $Z_{peak}$ at $a$ = 100. Thus, the $EC_{50}$ for $Z_{peak}$ became smaller than that of $Y_{peak}$ (Figure 16C, lower panel). This indicates a left shift of the dose-response curve of $Z_{peak}$ compared to $Y_{peak}$ against $a$ (Figure 16D). This means that $Z_{peak}$ is more sensitive to an activator than $Y_{peak}$. Thus, attenuation of signal transfer efficiency increased downstream sensitivity to an activator under the experimental condition. Because attenuation of signal transfer efficiency is controlled by negative regulation, we examined the effect of negative regulation on increase in downstream sensitivity. We defined an index of increase in downstream sensitivity, $S_i$, as the ratio of the $EC_{50}$ for $Y_{peak}$ to that for $Z_{peak}$ (Figure 16E and Figure 17A-C). A larger $S_i$ represents an increase in the sensitivity of $Z_{peak}$, compared with that of $Y_{peak}$. $S_i$ decreased and became close to 1 but never became smaller than 1 when $d$ became larger, indicating that the $EC_{50}$ values for the upstream and downstream molecules became the same and that the upstream molecule never became more sensitive to the activator than the downstream molecule in the consecutive first-order reaction. $S_i$ became larger when $d$ became smaller, indicating that the increase in the downstream sensitivity became larger as the rate constant of negative regulation of the consecutive first-order reaction, $d$, became smaller. This

result indicates that the downstream molecule is generally more sensitive to an activator than the upstream molecule under these conditions and that the increase in the downstream sensitivity depends on the negative regulation. We confirmed these results by a mathematical analysis (Figure 17D-G and Supplementary Text 7.1.8).

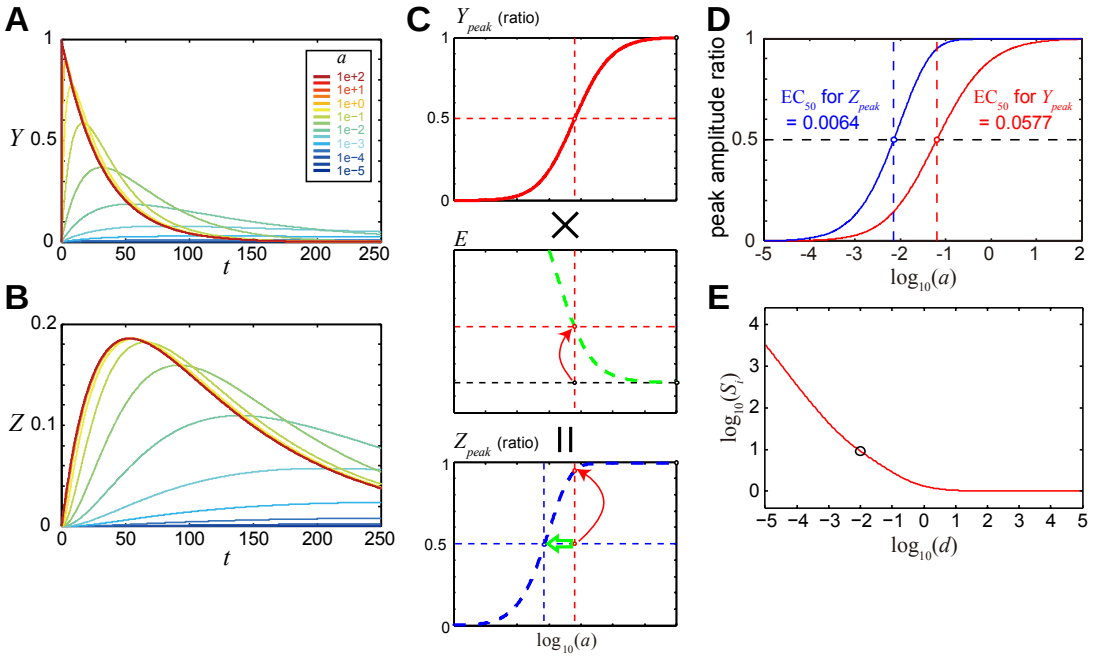


**Figure 16: The downstream molecule is more sensitive to an activator than the upstream molecule.**

(**A** and **B**) Time courses of *Y* and *Z*, respectively, in response to the indicated *a* (see inset; '1e+2' means $10^2$, for example). Note that *a* can be regarded as the concentration of the activator. The values of *b*, *c*, and *d* were 0.03, 0.01, and 0.01, respectively. (**C**) $Y_{peak}$, *E*, and $Z_{peak}$ against *a*. Attenuation of *E* was derived from panel **A** and Figure 15B, and results in the decrease of $EC_{50}$ for $Z_{peak}$. The maximal values of $Y_{peak}$ and $Z_{peak}$ were normalized to 1. (**D**) Dose-response curves of $Y_{peak}$ (red line) and $Z_{peak}$ (blue line) to the activator. The lines correspond to the white dotted lines in Figure 10B and C. The values of *b*, *c* and *d* were the same as those in panel **A**. The colored dashed lines indicate the $EC_{50}$ values for $Y_{peak}$ and $Z_{peak}$. (**E**) $S_i$ (= $EC_{50}$ for $Y_{peak}$/$EC_{50}$ for $Z_{peak}$) for the indicated *d* is shown. The circle indicates the parameters for **A**-**D**.

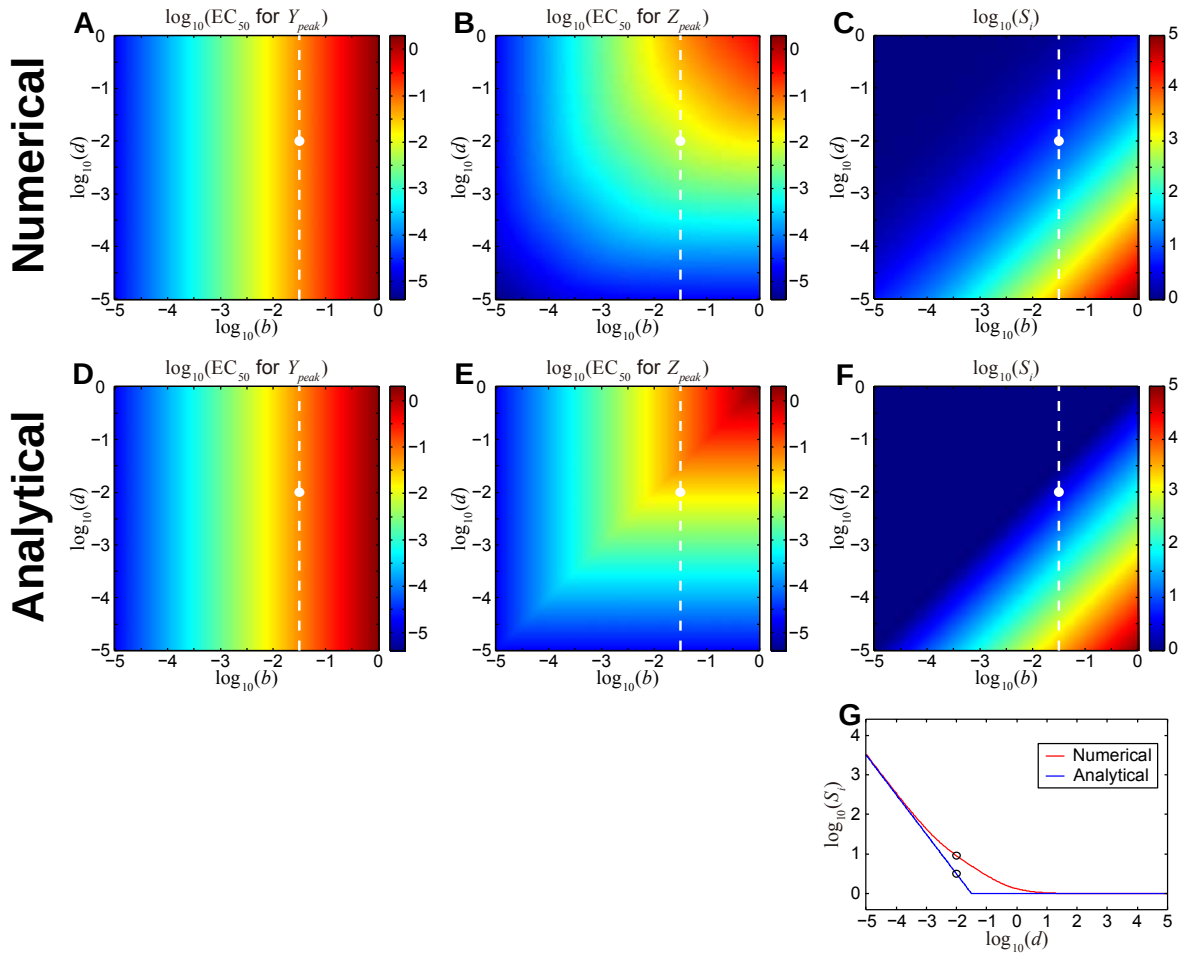


**Figure 17: Effect of the parameters on the $EC_{50}$ values and the increase in sensitivity.** (**A-C**) Numerical results of $EC_{50}$ for $Y_{peak}$, $EC_{50}$ for $Z_{peak}$, and $S_i$, respectively, against the indicated ranges of $b$ and $d$. The values are shown in color using a logarithmic scale. The white dot and dashed line indicate the parameters for Figure 16A-D and panel **G**, respectively. The diagonal pattern of the contour line in **c** indicates that $S_i$ is determined by $b/d$. (**D-F**) Analytical solution of $EC_{50}$ for $Y_{peak}$, approximated analytical solutions of $EC_{50}$ for $Z_{peak}$ and $S_i$, respectively. Please note that the approximation did not affect the qualitative characteristics of $EC_{50}$ for $Z_{peak}$ and $S_i$. (**G**) The red and blue line indicates numerical and analytical solutions of $S_i$ , respectively, for the indicated $d$. The black circles indicate the parameters for Figure 16A-D.

## 3.4. Control of sensitivity to an inhibitor

Next, we examined the sensitivity to an inhibitor. We created an inhibitor model by adding an inhibitor to the activator model, while maintaining the same relation between $Y$ and $Z$ (Figure 18A and Supplementary Text 7.1.9). The model can be described using the following ordinary differential equations:

$$\begin{cases} \dfrac{dW}{dt} &= -q \cdot W + p \cdot X, \\ \dfrac{dX}{dt} &= q \cdot W - (a + p) \cdot X, \\ \dfrac{dY}{dt} &= a \cdot X - b \cdot Y, \\ \dfrac{dZ}{dt} &= c \cdot Y - d \cdot Z. \end{cases} \tag{6}$$

We then examined the effect of the prior addition of the inhibitor on $Y_{peak}$ and $Z_{peak}$ in response to a fixed value of $a$ (fixed concentration of an activator). The model has two new rate constants, $p$ and $q$; these constants are the binding and dissociation rate constants of the inhibitor to $X$, respectively. The value of $p$ simultaneously means the concentration of the inhibitor. We assumed that the inhibitor was administered and reached an equilibrium before stimulation and set the initial conditions as follows:

$$\begin{cases} W(0) &= \dfrac{p}{p+q}, \\ X(0) &= \dfrac{q}{p+q}, \\ Y(0) &= 0, \\ Z(0) &= 0. \end{cases} \tag{7}$$

Hereafter, this model is referred to as the inhibitor model. Both $Y_{peak}$ and $Z_{peak}$ decreased as $p$ increased (Figure 18B and C). The half-maximal effective concentration of the inhibitor ($IC_{50}$) for $Y_{peak}$ was 1.61 and that for $Z_{peak}$ was 54.6 (Figure 18E). This indicates that $Z_{peak}$ was less sensitive to the inhibitor than $Y_{peak}$.

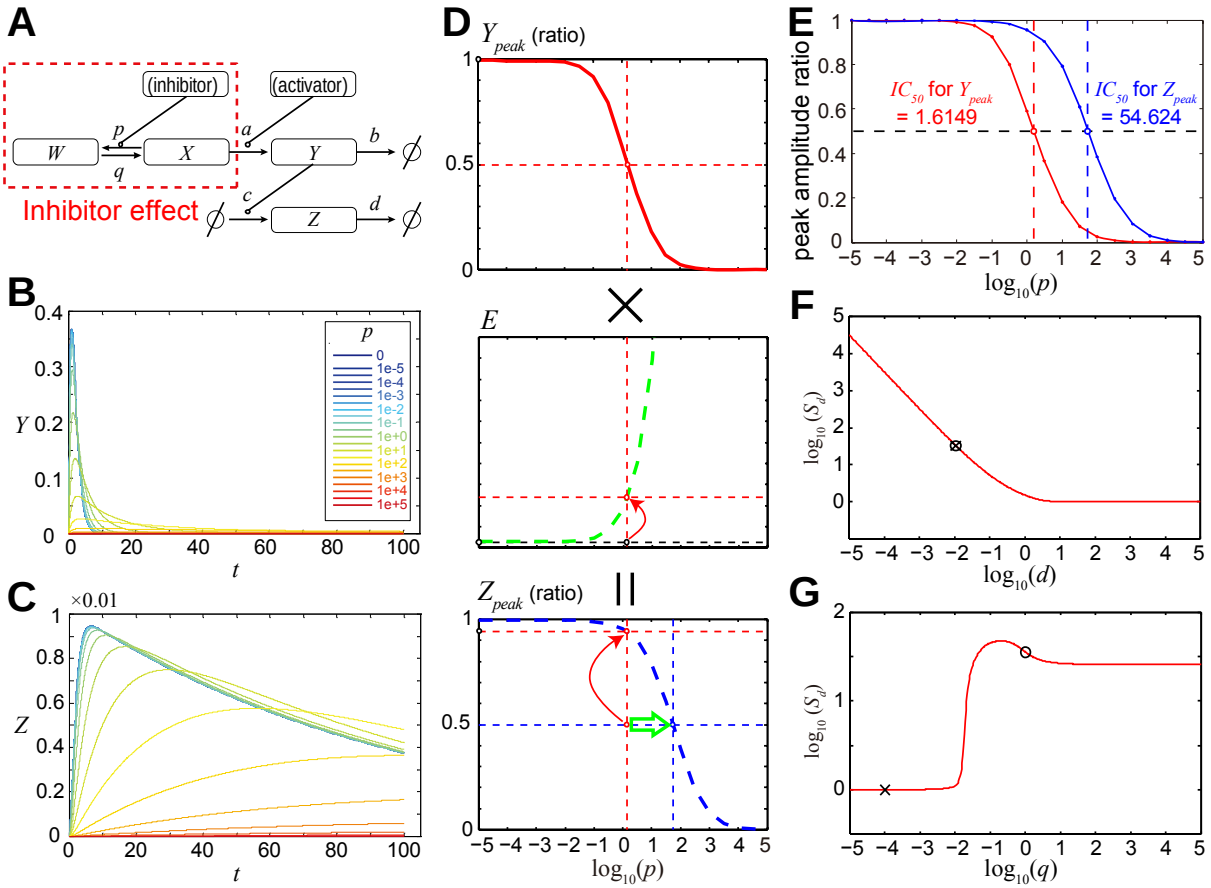


**Figure 18: The downstream molecule is less sensitive to an inhibitor than the upstream molecule.**

(**A**) Inhibitor model. The inhibitor acts on *X*, thereby inhibiting the activation of *Y*. The notations are the same as in Figure 1b. (**B** and **C**) Time courses of *Y* (**B**) and *Z* (**C**) in response to the indicated *p* (see inset). Note that *p* can be regarded as the concentration of the inhibitor. The values for *a*, *b*, *c, d*, and *q* were set at 1, 1, 0.01, 0.01, and 1, respectively. The inhibitor was administered and reached an equilibrium before stimulation. (**D**) $Y_{peak}$, *E*, and $Z_{peak}$ against *p*. Attenuation of *E* was derived from panel **B** and Figure 15B, and results in the increase of $IC_{50}$ for $Z_{peak}$. (**E**) Dose-response curves of $Y_{peak}$ (red line) and $Z_{peak}$ (blue line) for the inhibitor. The dashed lines indicate the $IC_{50}$ values for $Y_{peak}$ and $Z_{peak}$. The maximal values of $Y_{peak}$ and $Z_{peak}$ were normalized to 1. (**F** and **G**) $S_d$ (= $IC_{50}$ for $Z_{peak}$/$IC_{50}$ for $Y_{peak}$) for the indicated *d* and *q*, respectively, is shown. The remaining parameters were the same as those in panels **B**-**E**. The black circle and cross indicate the parameters used in panels **B**-**E** and in Figure 20, respectively.

Similar to the case of $EC_{50}$, $t_{1/2}$ became smaller when $p$ became smaller. Because we already found that the signal transfer efficiency attenuates as $t_{1/2}$ became smaller (Figure 15B), $E$ attenuated as $p$ became smaller. Therefore, $E$ at $p = 1.61$ should be larger than $E$ at $p = 10^{-5}$ (Figure 18D, middle panel). Because $Z_{peak}$ was relative to the product of $Y_{peak}$ and $E$, $Z_{peak}$ at $p = 1.61$ should be larger than the half of $Z_{peak}$ at $p = 10^{-5}$. Thus, the $IC_{50}$ for $Z_{peak}$ became larger than that of $Y_{peak}$ (Figure 18D, lower panel). This indicates that attenuation of signal transfer efficiency decreased downstream sensitivity to an inhibitor. Thus, attenuation of signal transfer efficiency is a core mechanism of the decrease in the downstream sensitivity to an inhibitor. We defined an index of decreasing sensitivity, $S_d$, as the ratio of the $IC_{50}$ for $Z_{peak}$ to that for $Y_{peak}$ (Figure 19), and examined the effect of negative regulation on the decrease in downstream sensitivity to an inhibitor. A larger $S_d$ represents a larger decrease in the sensitivity of $Z_{peak}$ compared with that of $Y_{peak}$. $S_d$ never became smaller than 1 under the indicated parameter space (Figure 19C), indicating that the downstream sensitivity to an inhibitor was always lower than the upstream sensitivity. $S_d$ became larger when $d$ became smaller (Figure 18F and Figure 19C), indicating that the decrease in the downstream sensitivity is regulated by negative regulation and that the downstream molecule is generally less sensitive to an inhibitor than the upstream molecule under the given conditions.

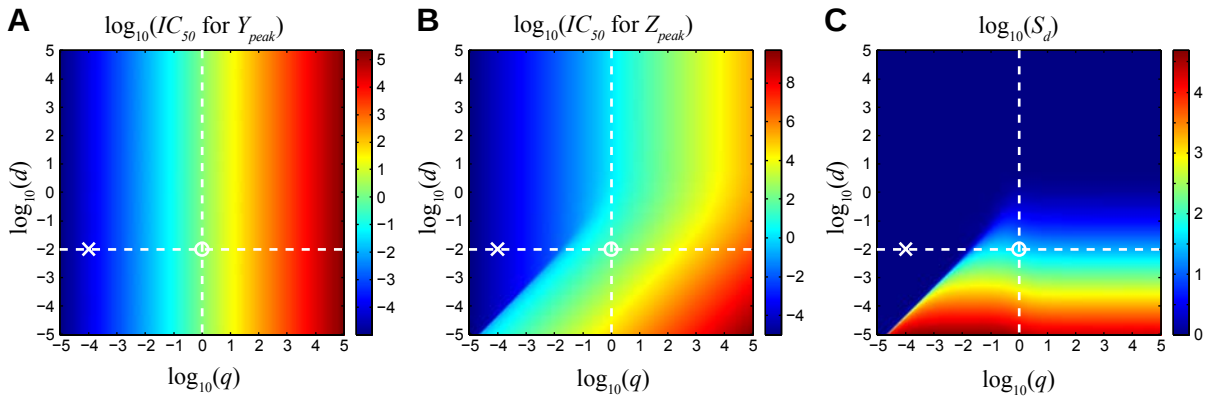


**Figure 19: Effect of the parameters *q* and *d* on the $IC_{50}$ values and the decrease in sensitivity.**

(**A** and **B**) $IC_{50}$ values for $Y_{peak}$ and $Z_{peak}$, respectively, against the indicated ranges of $q$ and $d$ are shown in color using a logarithmic scale. Both $a$ and $b$ were set at 1. The vertical and horizontal white dashed lines indicate the parameters for Figure 18F and G, respectively. The white circle and cross indicate the parameters for Figure 18B-E and Figure 20, respectively. (**C**) $S_d$ for the indicated ranges of $q$ and $d$ is shown in color using a logarithmic scale. The decrease in sensitivity was suppressed when $d$ was larger than $q$ and when these parameters were relatively small.

$S_d$ also became smaller when the dissociation rate constant of the inhibitor, $q$, became relatively small (Figure 18G and Figure 19C). Because an irreversible inhibitor can be regarded as a situation with a very small dissociation rate constant, this finding suggests that the decrease in downstream sensitivity would be suppressed if an irreversible inhibitor were to be used. Indeed, the $IC_{50}$ for $Z_{peak}$ was the same as that for $Y_{peak}$ when $q$ was smaller than that used in Figure 18B and C (Figure 18G and Figure 20). The suppression of the decrease in the downstream sensitivity occurred when $d$ was larger than $q$ and when these parameters were relatively small (Figure 19C). These conditions for the suppression of decrease in the downstream sensitivity were not affected by the other parameters, such as $a$ and $b$, although $S_d$ depended on these parameters (Figure 21), indicating that the relationship between $d$ and $q$ is an essential and robust index for the suppression of decrease in the downstream sensitivity. Thus, these results indicated that the downstream molecule was less sensitive to an inhibitor than the target molecule.

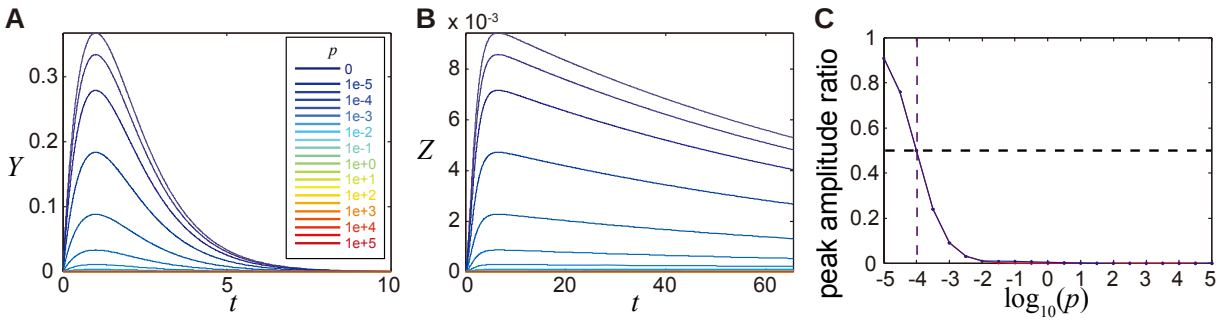


**Figure 20: The decrease in the sensitivity to an inhibitor was suppressed when *q* was small.**

(**A** and **B**) Time courses of *Y* and *Z*, respectively, for the indicated range of *p*. The inset in **A** indicates the value of *p*. *q* was changed to 0.0001 from Figure 18B and C. (**C**) Dose-response curve for $Y_{peak}$ (red line) and $Z_{peak}$ (blue line) for the inhibitor. Changing the value of *p* can be regarded as changing the concentration of the inhibitor. $Y_{peak}$ and $Z_{peak}$ were normalized according to the maximal responses.

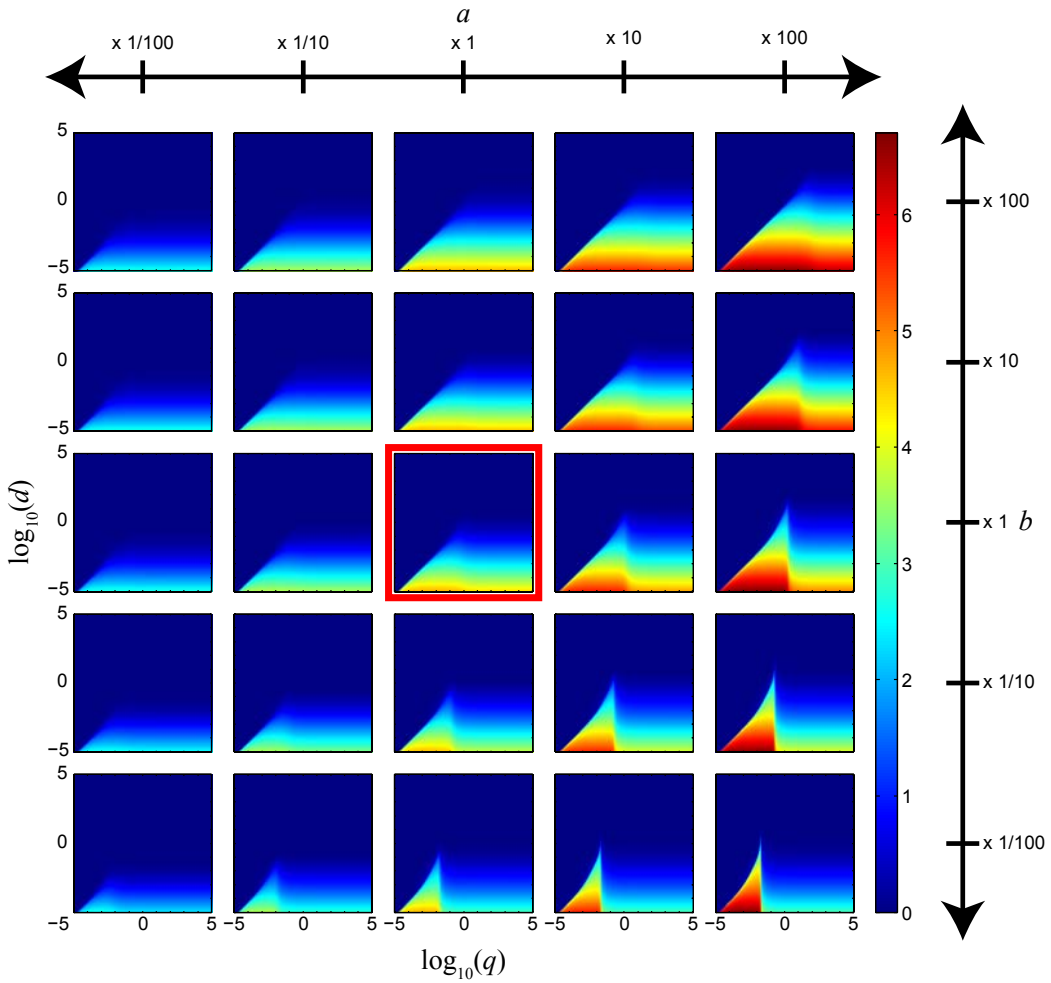


**Figure 21: Conditions for the suppression of the decrease in sensitivity.**

Each panel indicates the $S_d$ against the indicated range of $q$ and $d$ using logarithmic scales for the indicated parameters $a$ and $b$. The middle panel in the red box is the same as Figure 19C, although the color scale is different. The conditions for the suppression of the decrease in sensitivity (i.e. relationships of $d > q$) were not affected by the parameters $a$ and $b$, although $S_d$ depended on these parameters. This indicates that the relationship between $d$ and $q$ is an essential and robust index for the suppression of the decrease in sensitivity. When $q$ was relatively small, the dose of the inhibitor induced time courses of $Y$ that were almost proportional with each other (Figure 20). When the time courses of the upstream molecule of the consecutive first-order reaction were proportional with each other, that of the downstream molecule was also proportional with each other. Thus, the proportional relationship was conserved between the upstream and downstream molecules, resulting in the suppression of the decrease in sensitivity. The proportional relationship gradually disappeared with time, and the duration of the proportional relationship became shorter when $q$ became larger. When $d$ became smaller, the peak time of $Z$ became later and the non-proportional part of the time courses of $Y$ began to affect the $Z_{peak}$, resulting in a decrease in sensitivity. In this way, the balance between $d$ and $q$ determined the suppression of the decrease in sensitivity.

## 3.5. Experimental validation of the decrease in the downstream sensitivity to an inhibitor

Furthermore, we tried to verify experimentally that the downstream molecule was less sensitive to an inhibitor than the upstream molecule. We previously reported that the EGF-dependent Akt-S6 pathway can be represented as a consecutive first-order reaction (Fujita et al., 2010). We used lapatinib, an EGFR inhibitor (Rusnak et al., 2001), and measured the EGF-dependent phosphorylation of Akt and S6 in PC12 cells in the presence of the indicated concentrations of lapatinib (Figure 22A and B, respectively). Lapatinib inhibited the phosphorylation of both Akt and S6 in a dose-dependent manner. The $IC_{50}$ for the peak amplitude of the phosphorylation of Akt to lapatinib was about 112 nM and that of S6 was about 463 nM, which was about 4.1 times higher than that of Akt (Figure 22C and D). Thus, the downstream molecule, indeed, appeared to be less sensitive to the inhibitor than the upstream molecule in the consecutive first-order reaction. We confirmed that these experimental data were reasonably reproduced by the inhibitor model (Figure 23).

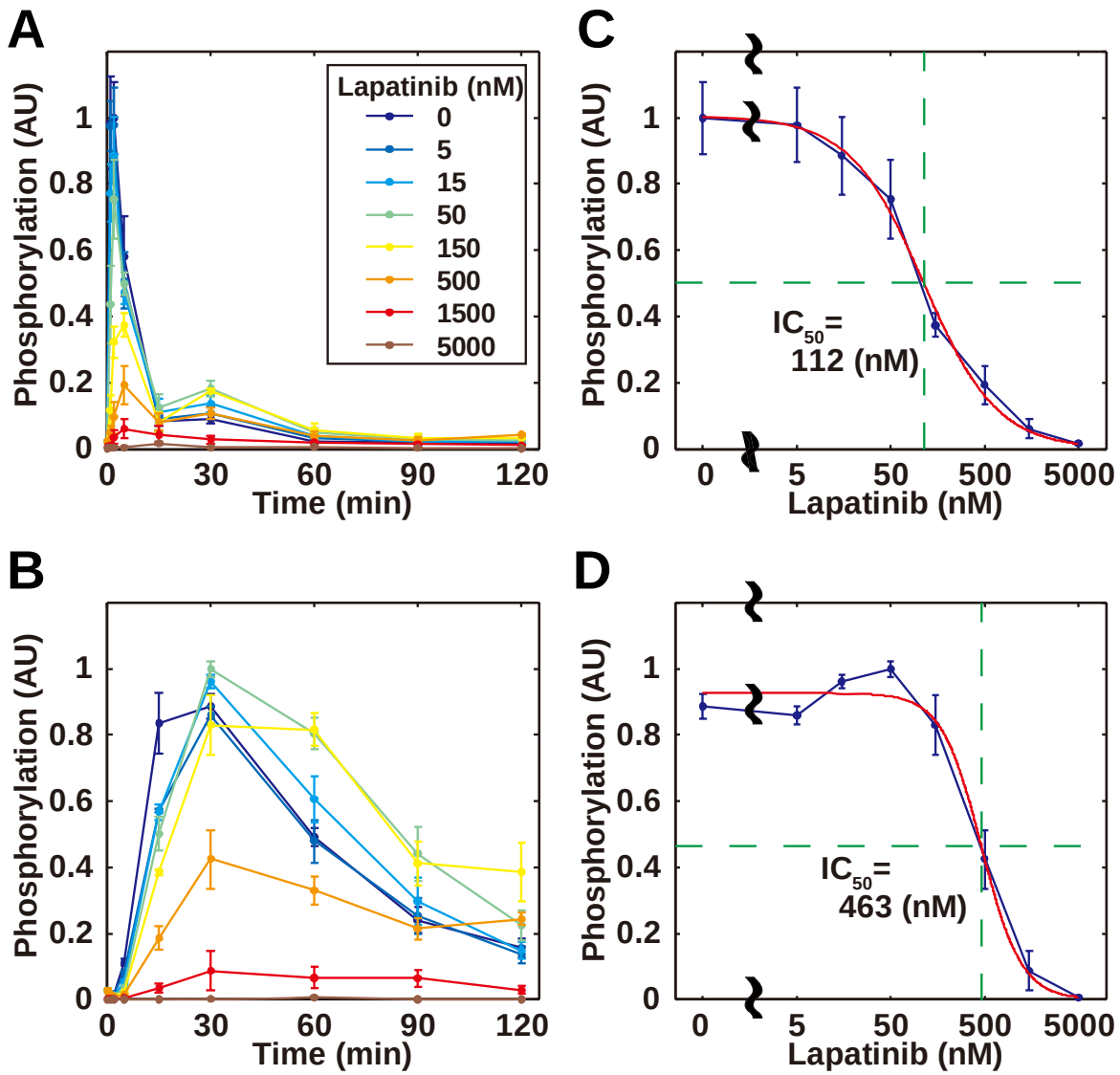


**Figure 22: Experimental validation of the decrease in the downstream sensitivity to an inhibitor.**

(**A** and **B**) After treatment with the indicated concentrations of lapatinib (an EGFR inhibitor) for 16 h, the PC12 cells were stimulated with EGF (30 ng/ml) and the phosphorylations of Akt and S6, respectively, were measured. The means and SEM of three independent experiments are shown. (**C** and **D**) Dose-response curves of the peak amplitudes of phosphorylated Akt and S6, respectively. The experimental data (blue line) was fitted using a sigmoid curve (red line). The green dashed lines indicate the $IC_{50}$ values for phosphorylated Akt and S6.

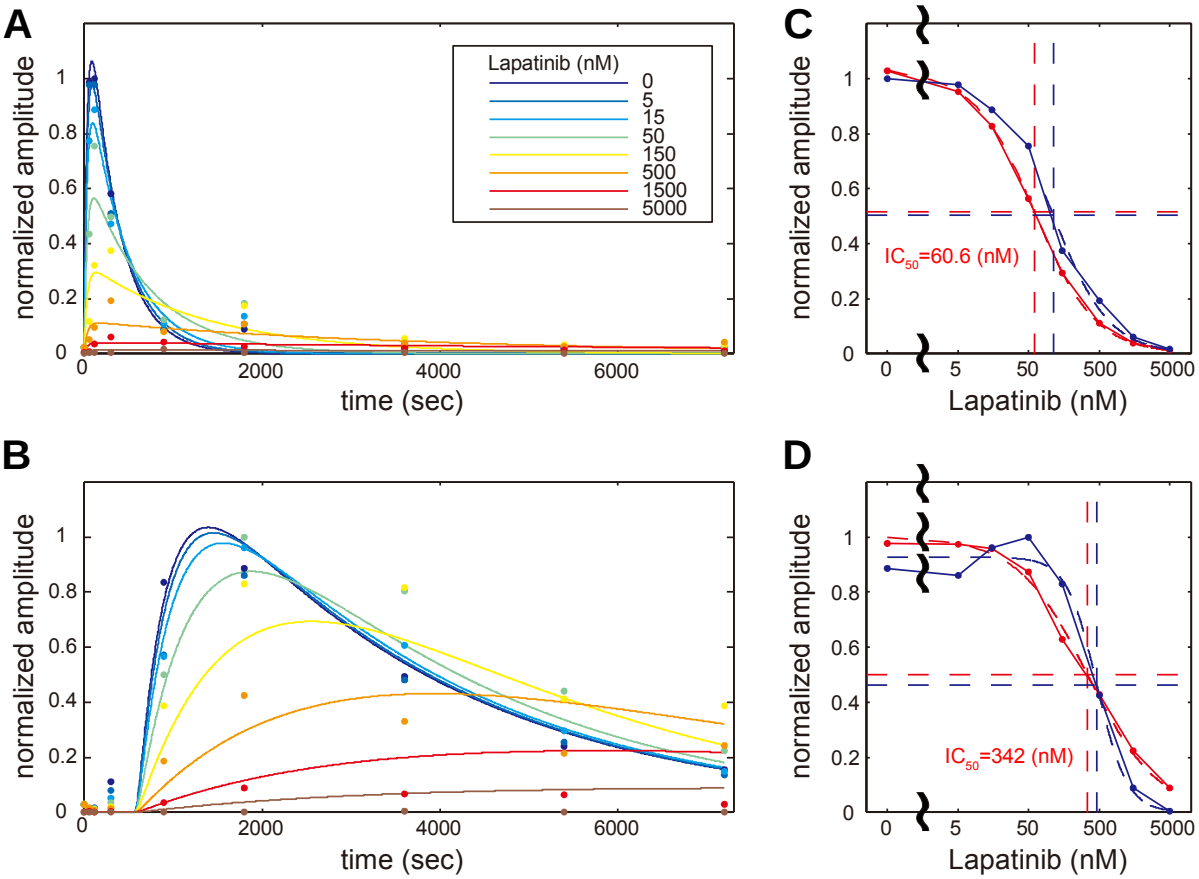


**Figure 23: The inhibitor model was capable of reproducing the experimental data.**
(**A** and **B**) Time courses of *Y* and *Z*, respectively, in the inhibitor model (lines) and in experiments (points). The inhibitor, *Y* and *Z* in the inhibitor model corresponded to lapatinib, phosphorylated Akt and S6, respectively, and the parameters for the inhibitor model were estimated using the experimental data (see Supplementary Text 7.1.10). The inhibitor concentrations are shown in the inset. The time courses of *Y* and *Z* successfully reproduced those of phosphorylated Akt and S6, respectively. (**C** and **D**) Dose-response curves of $Y_{peak}$ and $Z_{peak}$, respectively. $Y_{peak}$ and $Z_{peak}$ in the inhibitor model (red solid line) were fitted using a sigmoid curve (red dashed line). The blue lines show the peak amplitude of phosphorylated Akt (**C**) and S6 (**D**) in the experimental data. The $IC_{50}$ for $Y_{peak}$ was about 61 nM, and the $IC_{50}$ for $Z_{peak}$ was about 342 nM, which was 5.6 times higher than that of $Y_{peak}$. These values were very similar to the experimental data, suggesting that the decrease in the $IC_{50}$ observed in the experiment was caused by the consecutive first-order reaction.

## 3.6. Decrease in the downstream sensitivity to an inhibitor under physiological-like conditions

The addition of an inhibitor before stimulation with an activator (from Figure 18 to Figure 23) is the usual protocol for cell culture experiments in vitro; however, the addition of an inhibitor after constitutive activation by an activator reflects more physiological-like in vivo situations, such as the administration of an anticancer drug to cancer cells expressing a constitutively active oncogene product. It is known that a mutation of oncogene results in constitutive activation of a signaling pathway without a ligand, which leads to carcinogenesis. Therefore, we made an in vivo inhibitor model (Figure 24) that mimics the effect of an inhibitor on the constitutively activated signaling pathway and provides the frameworks to understand and evaluate the effect of anticancer drugs on tumor cells. Then we asked whether a similar decrease in sensitivity to an inhibitor can occur under such conditions. We found that $Z_{peak}$ was similarly less sensitive to the inhibitor than $Y_{peak}$ under physiological-like conditions (Figure 24). This finding raises the possibility that the downstream molecule may be less sensitive to an inhibitor than the target molecule in vivo.

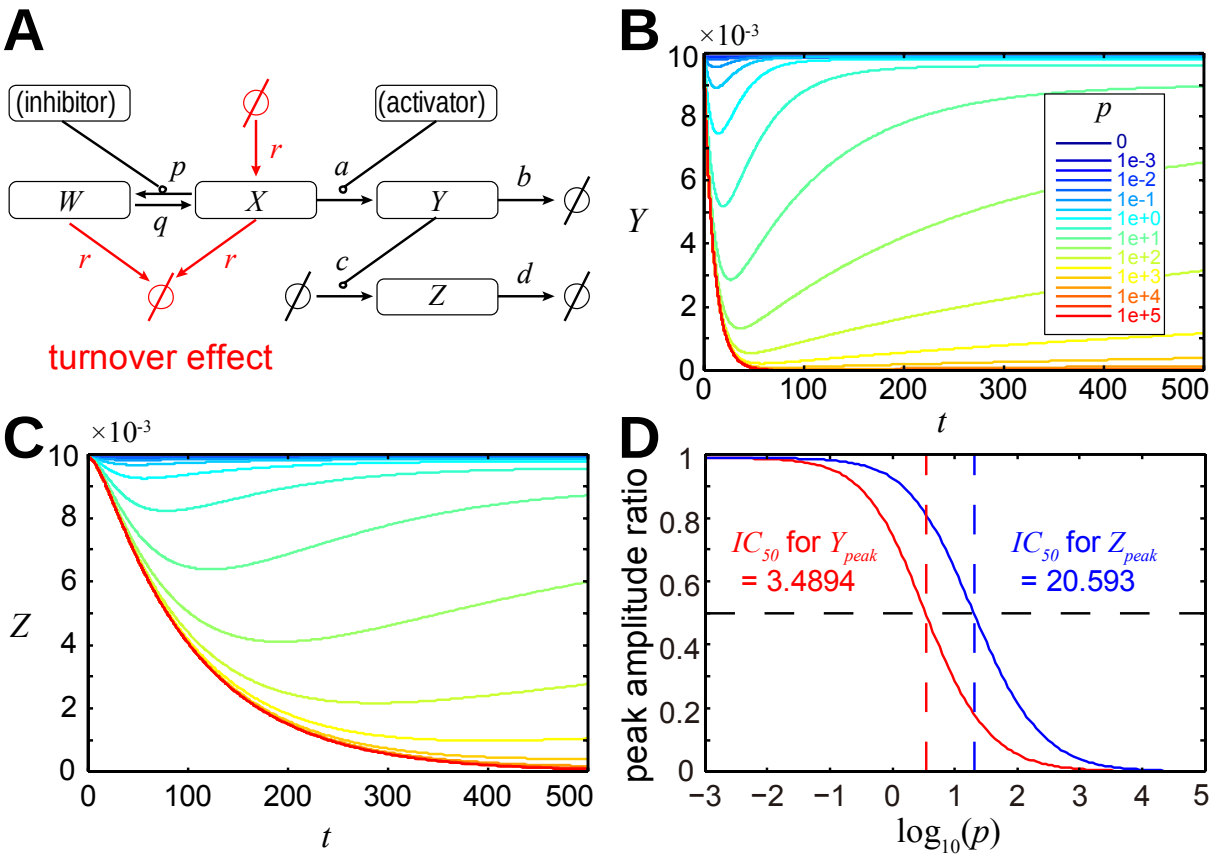


**Figure 24: The downstream molecule is less sensitive to an inhibitor than the upstream molecule under physiological-like conditions.**

(**A**) *In vivo* inhibitor model. The *in vivo* inhibitor model was created by adding turnover reactions to the inhibitor model, while the maintaining the same relation between *Y* and *Z* (see Supplementary Text 7.1.11). The *in vivo* inhibitor model had a new rate constant, *r*, corresponding to the synthesis and degradation rate constants of *X*. The turnover reactions for *X* are needed for constitutive activation. The notations are the same as in Figure 9B. (**B** and **C**) Time courses of *Y* (**B**) and *Z* (**C**) in response to the indicated *p* (see inset). Note that *p* can be regarded as the concentration of the inhibitor. The addition of the inhibitor resulted in a transient decrease in both *Y* and *Z*. Both $Y_{peak}$ and $Z_{peak}$ decreased as *p* increased. Note that here $Y_{peak}$ and $Z_{peak}$ denoted the decreased peak and the lowest value. The values for *a*, *b*, *c*, *d*, *q*, and *r* were set at 0.1, 0.1, 0.01, 0.01, 1 and 0.0001, respectively. The activator was administered and reached an equilibrium before inhibition. (**D**) Dose-response curves of $Y_{peak}$ (red line) and $Z_{peak}$ (blue line) for the inhibitor. The dashed lines indicate the $IC_{50}$ values for $Y_{peak}$ and $Z_{peak}$. The $IC_{50}$ for $Y_{peak}$ was 3.49 and that for $Z_{peak}$ was 20.6, indicating that $Z_{peak}$ was less sensitive to the inhibitor than $Y_{peak}$ under physiological-like conditions. The maximal values of $Y_{peak}$ and $Z_{peak}$ were normalized to 1.

# 4. DISCUSSION

## 4.1. Negative regulation

We examined the conditions for attenuation of signal transfer efficiency in the activator model and found that the signal transfer efficiency attenuates when the half-life of decay of the upstream molecule, $t_{1/2}$, is shorter than the time constant of negative regulation, $\tau$. Thus, the attenuation of signal transfer efficiency can be controlled by the negative regulations (Figure 25B). We experimentally found that attenuation of signal transfer efficiency is a conserved property of a linear signaling pathway regardless of the pathways, growth factors, and cell lines.

We also found that the downstream molecule was more sensitive to an activator than the upstream molecule. The increase in the downstream sensitivity to the activator can be controlled by the negative regulation via attenuation of signal transfer efficiency (Figure 25C). Similarly, the downstream molecule was less sensitive to an inhibitor than the upstream molecule, which can also be controlled by the negative regulation via attenuation of signal transfer efficiency (Figure 25D). The decrease in the sensitivity of the downstream molecule to an inhibitor was verified experimentally. We also found that the downstream molecule was less sensitive to the inhibitor than the upstream molecule under physiological-like conditions where upstream molecules are constitutively active. The sensitivities of the molecules to an activator or an inhibitor depended on the rate constant of negative regulation. Attenuation of signal transfer efficiency by negative regulation is one of the core mechanisms to control sensitivity to an activator and an inhibitor.

Negative regulation can be regarded as any type of reaction in a signaling pathway, such as degradation or dephosphorylation, and the rate constants of negative regulation can reflect the amount of an enzyme such as protease and phosphatase. Therefore, cells can control signal transfer efficiency and sensitivities to activators and inhibitors by changing the

expression levels of these enzymes. The different expression levels of these enzymes may account for the different sensitivities to activators or inhibitors among individual cells and cell lines. In addition, these enzymes reportedly have strong effects on the temporal patterns of signals and sensitivities to activators (Bhalla et al., 2002; Heinrich et al., 2002; O'Shaughnessy et al., 2011; Poritz et al., 2001).

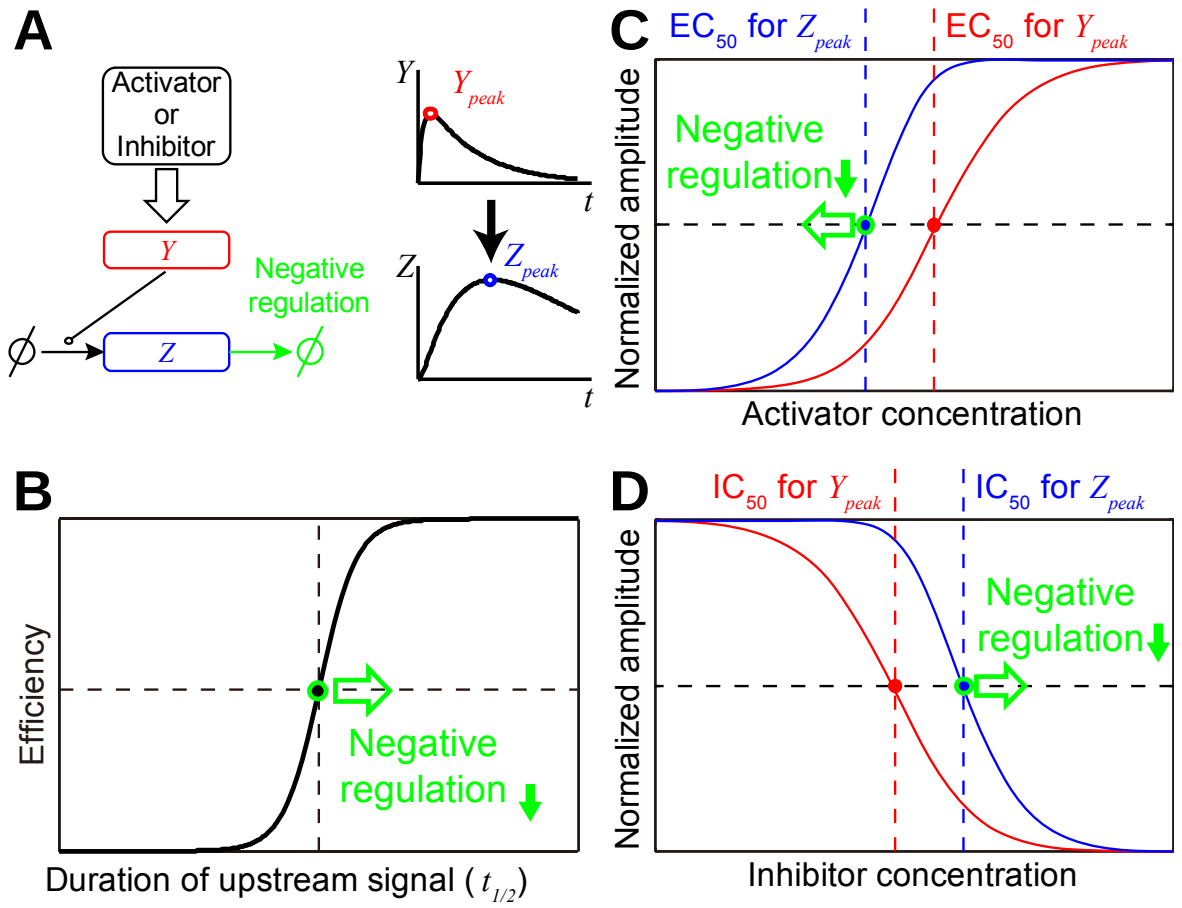


**Figure 25: Negative regulation controls signal transfer efficiency and sensitivity to an activator or an inhibitor.**

(**A**) Conceptual description of the activator and inhibitor model. The negative regulation of *Z* may correspond to degradation or dephosphorylation of a signaling pathway. (**B**) Attenuation of the signal transfer efficiency by the negative regulation. The weaker the negative regulation becomes, the stronger attenuation of efficiency becomes. (**C**) Sensitivity control to an activator by the negative regulation. The weaker the negative regulation becomes, the more sensitive the downstream molecule becomes. (**D**) Sensitivity control to an inhibitor by the negative regulation. The weaker the negative regulation becomes, the less sensitive the downstream molecule becomes.

## 4.2. Conditions about the analysis of sensitivity control

The analysis of sensitivity control to an activator and an inhibitor in this study requires the following three conditions: (i) the pathway of interest can be approximated by a consecutive first-order reaction, (ii) the time course of the upstream molecule can be expressed as the sum of two exponential curves, and (iii) the dose-dependent time courses of the upstream molecule can be expressed by changing $a$ as the doses of an activator or $p$ as the doses of an inhibitor while other parameters are fixed (for RESULTS 3.3 and below). On the other hand, the analysis of attenuation of signal transfer efficiency in this study (i.e. RESULTS 3.1 and 3.2) requires only the former two conditions. The sensitivity control reflects the relationship between an activator (or an inhibitor), $Y$ and $Z$. By contrast, the attenuation of the signal transfer efficiency depends on the relationship only between $Y$ and $Z$ but not between an activator (or an inhibitor) and $Y$. Therefore, the analysis of sensitivity control requires more stringent conditions. Condition (i) means that the elementary reactions in the pathways are not necessarily exact first-order reactions. For example, the Michaelis–Menten type of enzymatic reaction is not an exact first-order reaction, but it can be approximated by a first-order reaction when the substrate is abundant (Segel, 1993). Even a signaling pathway involving more complex multistep reactions can be approximated by consecutive first-order reactions (Figure 15) (Fujita et al., 2010). However, pathways including high-order reactions or feedback effects may not be able to be adequately approximated by a consecutive first-order reaction. Also, condition (ii) may not be satisfied in pathways including signaling molecules whose time courses are sustained or oscillated. Condition (iii) may not be satisfied when there are high-order reactions between $Y$ and the activator or the inhibitor.

## 4.3. Comparing to previous studies about sensitivity

In this study, we analyzed the sensitivity differences in the peak amplitudes in a consecutive first-order reaction. The sensitivity differences in the equilibrium amplitudes have also been analyzed, and the depletion of the substrate in a biochemical reaction has been shown to control the sensitivity (Huang and Ferrell, 1996; Kholodenko et al., 1997; Koshland et al., 1982). For example, consider the phosphorylation and dephosphorylation of a substrate in equilibrium. A kinase is activated by an activator and phosphorylates the substrate; the phosphorylated substrate (product) is then dephosphorylated and returns to being a substrate. The activated kinase and the product can be regarded as the upstream and downstream molecules of the biochemical reaction. Increasing the dose of the activator increases the amount of activated kinase. The substrate is phosphorylated by the activated kinase, and the substrate is consumed and eventually depleted in the presence of an excess of activated kinase. When the substrate is depleted, further increases in the amount of activator do not increase the amount of product, although the amount of activated kinase is increased. This means that the product reaches a plateau before the activated kinase reaches a plateau. Therefore, the $EC_{50}$ for the product is smaller than the $EC_{50}$ for the activated kinase when the substrate is depleted. Thus, the depletion of the substrate can induce an increase in sensitivity.

In contrast, when the amount of substrate is not changed, an enzymatic reaction can be approximated by a first-order reaction, as described above. In other words, the first-order reaction ignores the depletion of the substrate; therefore, the consecutive first-order reaction examined in this study is not influenced by the depletion effect. Thus, the mechanism responsible for the control of sensitivity in this study differs from that in previous studies (Huang and Ferrell, 1996; Kholodenko et al., 1997; Koshland et al., 1982). General biochemical reactions including the Michaelis–Menten type of enzymatic reaction possess the intrinsic characteristics of both the depletion effect and attenuation of signal transfer efficiency.

Therefore, both characteristics may generally contribute to the control of sensitivity. Reportedly, sensitivity can also be controlled by the characteristics of network motifs, such as a negative feedback loop and an incoherent feed-forward loop (Behar et al., 2007b, 2008; Entus et al., 2007; Yu et al., 2008).

Consecutive first-order reactions can control the sensitivity of downstream molecules to an inhibitor, indicating that the downstream molecule is not always inhibited as strongly as an upstream molecule even if the target molecule of the inhibitor is inhibited successfully and even if the downstream network of the target molecule is simple. The sensitivities of the downstream responses to several EGFR inhibitors are reportedly lower than those of the upstream molecules (Cheng et al., 2007; Moasser et al., 2001; Solca et al., 2004; Wakeling et al., 2002). The characteristics of the consecutive first-order reaction may contribute to these decreases in sensitivity, although the decreases in sensitivity may also be caused by other factors, such as the depletion effect in biochemical reactions and the characteristics of network motifs.

## 4.4. Extent of the attenuation of signal transfer efficiency

The attenuation of signal transfer efficiency may be involved in many cellular processes. For example, the process of gene expression is composed of both the synthesis and the degradation (i.e., negative regulation) of the gene product. The synthesis is induced by the activities of upstream signaling molecules, and the degradation of the gene product depends on the actual amount of gene product. This process may be approximated by a consecutive first-order reaction, where the activities of the upstream signaling molecule and the gene product can be regarded as *Y* and *Z* in the activator model, respectively (Alon, 2006b; Barenco et al., 2006; Entus et al., 2007; Tegner et al., 2003). In general, the synthesis and degradation rate constants for the time course of the cellular signaling pathway are larger than the degradation rate constant of the gene product (Alon, 2006b), suggesting that attenuation of signal transfer efficiency can be seen in signaling-dependent gene expression. Indeed, we found that the ERK-dependent c-FOS expression could be approximated by a consecutive first-order reaction and attenuation of signal transfer efficiency was seen (Figure 15). We could not examine downstream sensitivity to growth factors of the pathway because EGF-dependent ERK activation did not satisfy condition (iii). However, in a signaling pathway that satisfies conditions (i), (ii), and (iii), the gene product may be more sensitive to growth factors compared with the sensitivity of the upstream signaling molecule. The gene expression system may use this characteristic to increase its sensitivity to growth factors.

The attenuation of the signal transfer efficiency should be considered when interpreting experimental data. For example, a luciferase assay system is used as a reporter for promoter activity. Because luciferase expression is regulated by both synthesis and degradation, the process of luciferase expression can be approximated using a consecutive first-order reaction. Therefore, the luciferase activity may be more sensitive to stimulation than the promoter activity, and the increase of the sensitivity may depend on the degradation rate of the

luciferase. This suggests that a luciferase with enhanced sensitivity can be designed by decreasing the degradation rate. At the same time, this also means that the luciferase activity may potentially overestimate the promoter activity. To avoid such overestimations, the degradation rate of luciferase should be increased (compared with that of the signaling pathway) so that the luciferase activity begins to show a sensitivity similar to that of the promoter activity (Wang et al., 2008). However, as the degradation rate of luciferase increases, the amount of luciferase decreases and the lower detection limit of luciferase decreases. Therefore, a trade-off exists between the lower detection limit of luciferase and the decreased overestimation. Other probe systems, such as fluorescence resonance energy transfer probes and calcium ion indicators, with a similar synthesis and degradation framework, share the same problem.

## 4.5. Future directions

In this study, we uncovered an operating principle of one of the characteristics in biological dynamic systems. These characteristics including sensitivity control may not have interesting aspects in mathematics such as oscillations and chaos, and may not be a subject of mathematical study. However, these characteristics have interesting aspects in biology, and in order to uncover the operating principle of the characteristics, mathematical analyses are very important and essential. Furthermore, the uncovered principle should be verified experimentally. Such frequent interactions and integration between theory and experiment are also important and essential for uncovering the operating principle.

Using simple model may be one of the features of this study. Such simple models may seem strange for biologist, but are very powerful tool for uncovering the operating principle of the dynamics which can be reproduced by the model. Otherwise, many complex and detailed models have been made by many biological studies. These models may be able to reproduce experimental results more precisely than simple models. However, the detailed models have many parameters, and multiple sets of the parameters will reproduce the experimental results in same precision, and then, we will not be able to identify which part induces the dynamics focused on. Finally, in order to uncover the operating principle, the detailed models should be reduced into simple models in some way, but there are no general methods or procedures for the reduction.

By recent advancement of biology, new molecules are found, and knowledge about its functions and interactions are growing. These remarkable achievements seem to be brought by a paradigm of current biology that “molecules (or genes) are responsible for biological phenomena”. However, as seen in the example of the radio in section 1.1, it is clear that the molecules are just media of information transfer, and that the molecules themselves do not

have information for biological phenomena. There is the information in the spatiotemporal changes of the molecules, and they are responsible for biological phenomena that the signal processing systems or circuits composed of the molecules. In other words, we should investigate on the layer of the systems rather than that of the molecules for uncovering the operating principle of the phenomena. Thus, “system’s biology” is an inevitable way to truly understand the biological phenomena.

# 5. REFERENCES


Alon, U. (2006a). An Introduction to Systems Biology: Design Principles of Biological Circuits (New York: Chapman & Hall / CRC).

Alon, U. (2006b). Transcription Networks: Basic Concepts. In An introduction to systems biology: design principles of biological circuits (Chapman & Hall/CRC), pp. 5-26.

Ashall, L., Horton, C.A., Nelson, D.E., Paszek, P., Harper, C.V., Sillitoe, K., Ryan, S., Spiller, D.G., Unitt, J.F., Broomhead, D.S., *et al.* (2009). Pulsatile stimulation determines timing and specificity of NF-kappaB-dependent transcription. Science *324*, 242-246.

Barenco, M., Tomescu, D., Brewer, D., Callard, R., Stark, J., and Hubank, M. (2006). Ranked prediction of p53 targets using hidden variable dynamic modeling. Genome biology *7*, R25.

Becker, V., Schilling, M., Bachmann, J., Baumann, U., Raue, A., Maiwald, T., Timmer, J., and Klingmüller, U. (2010). Covering a broad dynamic range: information processing at the erythropoietin receptor. Science *328*, 1404-1408.

Behar, M., Dohlman, H.G., and Elston, T.C. (2007a). Kinetic insulation as an effective mechanism for achieving pathway specificity in intracellular signaling networks. Proceedings of the National Academy of Sciences of the United States of America *104*, 16146-16151.

Behar, M., Hao, N., Dohlman, H.G., and Elston, T.C. (2007b). Mathematical and computational analysis of adaptation via feedback inhibition in signal transduction pathways. Biophysical Journal *93*, 806-821.

Behar, M., Hao, N., Dohlman, H.G., and Elston, T.C. (2008). Dose-to-duration encoding and signaling beyond saturation in intracellular signaling networks. PLoS Computational Biology *4*, e1000197.

Behar, M., and Hoffmann, A. (2010). Understanding the temporal codes of intra-cellular signals. Current opinion in genetics & development *20*, 684-693.

Bennett, M.R., Pang, W.L., Ostroff, N.A., Baumgartner, B.L., Nayak, S., Tsimring, L.S., and Hasty, J. (2008). Metabolic gene regulation in a dynamically changing environment. Nature *454*, 1119-1122.

Bhalla, U.S., Ram, P.T., and Iyengar, R. (2002). MAP kinase phosphatase as a locus of flexibility in a mitogen-activated protein kinase signaling network. Science *297*, 1018-1023.

Bray, D. (1995). Protein molecules as computational elements in living cells. Nature *376*, 307-312.

Cheng, Z.-Y., Li, W.-J., He, F., Zhou, J.-M., and Zhu, X.-F. (2007). Synthesis and biological evaluation of 4-aryl-5-cyano-2H-1,2,3-triazoles as inhibitor of HER2 tyrosine kinase. Bioorganic and Medicinal Chemistry *15*, 1533-1538.

D'Errico, J. （2005） fminsearchbnd. MATLAB Central File Exchange. http://www.mathworks.com/matlabcentral/fileexchange/8277

De Koninck, P., and Schulman, H. (1998). Sensitivity of CaM kinase II to the frequency of

Ca2+ oscillations. Science *279*, 227-230.
Detwiler, P.B., Ramanathan, S., Sengupta, A., and Shraiman, B.I. (2000). Engineering aspects of enzymatic signal transduction: photoreceptors in the retina. Biophysical Journal *79*, 2801-2817.
Di Fiore, P.P., and Gill, G.N. (1999). Endocytosis and mitogenic signaling. Current opinion in cell biology *11*, 483-488.
Dolmetsch, R.E., Lewis, R.S., Goodnow, C.C., and Healy, J.I. (1997). Differential activation of transcription factors induced by Ca2+ response amplitude and duration. Nature *386*, 855-858.
Dolmetsch, R.E., Xu, K., and Lewis, R.S. (1998). Calcium oscillations increase the efficiency and specificity of gene expression. Nature *392*, 933-936.
Ebisuya, M., Kondoh, K., and Nishida, E. (2005). The duration, magnitude and compartmentalization of ERK MAP kinase activity: mechanisms for providing signaling specificity. Journal of cell science *118*, 2997-3002.
Entus, R., Aufderheide, B., and Sauro, H.M. (2007). Design and implementation of three incoherent feed-forward motif based biological concentration sensors. Systems and synthetic biology *1*, 119-128.
Fujita, K.A., Toyoshima, Y., Uda, S., Ozaki, Y.-i., Kubota, H., and Kuroda, S. (2010). Decoupling of receptor and downstream signals in the Akt pathway by its low-pass filter characteristics. Science signaling *3*, ra56.
Goentoro, L., Shoval, O., Kirschner, M.W., and Alon, U. (2009). The incoherent feedforward loop can provide fold-change detection in gene regulation. Molecular Cell *36*, 894-899.
Heinrich, R., Neel, B.G., and Rapoport, T.A. (2002). Mathematical models of protein kinase signal transduction. Molecular Cell *9*, 957-970.
Hersen, P., McClean, M.N., Mahadevan, L., and Ramanathan, S. (2008). Signal processing by the HOG MAP kinase pathway. Proceedings of the National Academy of Sciences of the United States of America *105*, 7165-7170.
Hoffmann, A., Levchenko, A., Scott, M.L., and Baltimore, D. (2002). The IkappaB-NF-kappaB signaling module: temporal control and selective gene activation. Science *298*, 1241-1245.
Hoops, S., Sahle, S., Gauges, R., Lee, C., Pahle, J., Simus, N., Singhal, M., Xu, L., Mendes, P., and Kummer, U. (2006). COPASI--a COmplex PAthway SImulator. Bioinformatics *22*, 3067-3074.
Huang, C.Y., and Ferrell, J.E. (1996). Ultrasensitivity in the mitogen-activated protein kinase cascade. Proceedings of the National Academy of Sciences of the United States of America *93*, 10078-10083.
Iino, Y., and Yoshida, K. (2009). Parallel use of two behavioral mechanisms for chemotaxis in Caenorhabditis elegans. The Journal of neuroscience : the official journal of the Society for Neuroscience *29*, 5370-5380.
Janes, K.A. (2005). A Systems Model of Signaling Identifies a Molecular Basis Set for

Cytokine-Induced Apoptosis. Science *310*, 1646-1653.
Kholodenko, B.N. (2006). Cell-signalling dynamics in time and space. Nature reviews. Molecular cell biology *7*, 165-176.
Kholodenko, B.N., Hancock, J.F., and Kolch, W. (2010). Signalling ballet in space and time. Nature reviews. Molecular cell biology *11*, 414-426.
Kholodenko, B.N., Hoek, J.B., Westerhoff, H.V., and Brown, G.C. (1997). Quantification of information transfer via cellular signal transduction pathways. FEBS Letters *414*, 430-434.
Korc, M., Haussler, C.A., and Trookman, N.S. (1987). Divergent effects of epidermal growth factor and transforming growth factors on a human endometrial carcinoma cell line. Cancer Research *47*, 4909-4914.
Koshland, D.E., Goldbeter, A., and Stock, J.B. (1982). Amplification and adaptation in regulatory and sensory systems. Science *217*, 220-225.
Lathi, B.P. (1998). Modern Digital and Analog Communication Systems, 3 edn (New York: Oxford Univ. Press).
Lazebnik, Y. (2002). Can a biologist fix a radio?--Or, what I learned while studying apoptosis. Cancer Cell *2*, 179-182.
Maeda, A., Ozaki, Y.-i., Sivakumaran, S., Akiyama, T., Urakubo, H., Usami, A., Sato, M., Kaibuchi, K., and Kuroda, S. (2006). Ca2+ -independent phospholipase A2-dependent sustained Rho-kinase activation exhibits all-or-none response. Genes to Cells *11*, 1071-1083.
Manning, B.D., and Cantley, L.C. (2007). AKT/PKB signaling: navigating downstream. Cell *129*, 1261-1274.
Marshall, C.J. (1995). Specificity of receptor tyrosine kinase signaling: transient versus sustained extracellular signal-regulated kinase activation. Cell *80*, 179-185.
Mathers, W.D., Sherman, M., Fryczkowski, A., and Jester, J.V. (1989). Dose-dependent effects of epidermal growth factor on corneal wound healing. Investigative ophthalmology & visual science *30*, 2403-2406.
Mettetal, J.T., Muzzey, D., Gomez-Uribe, C., and van Oudenaarden, A. (2008). The frequency dependence of osmo-adaptation in Saccharomyces cerevisiae. Science *319*, 482-484.
Meyuhas, O. (2008). Physiological roles of ribosomal protein S6: one of its kind. International review of cell and molecular biology *268*, 1-37.
Moasser, M.M., Basso, A., Averbuch, S.D., and Rosen, N. (2001). The tyrosine kinase inhibitor ZD1839 ("Iressa") inhibits HER2-driven signaling and suppresses the growth of HER2-overexpressing tumor cells. Cancer Research *61*, 7184-7188.
Moyer, J.D., Barbacci, E.G., Iwata, K.K., Arnold, L., Boman, B., Cunningham, A., DiOrio, C., Doty, J., Morin, M.J., Moyer, M.P*., et al.* (1997). Induction of apoptosis and cell cycle arrest by CP-358,774, an inhibitor of epidermal growth factor receptor tyrosine kinase. Cancer Research *57*, 4838-4848.
Muzzey, D., Gómez-Uribe, C.A., Mettetal, J.T., and van Oudenaarden, A. (2009). A

Systems-Level Analysis of Perfect Adaptation in Yeast Osmoregulation. Cell *138*, 160-171.
Nakakuki, T., Birtwistle, M.R., Saeki, Y., Yumoto, N., Ide, K., Nagashima, T., Brusch, L., Ogunnaike, B.A., Okada-Hatakeyama, M., and Kholodenko, B.N. (2010). Ligand-specific c-Fos expression emerges from the spatiotemporal control of ErbB network dynamics. Cell *141*, 884-896.
O'Rahilly, S., Turner, R.C., and Matthews, D.R. (1988). Impaired pulsatile secretion of insulin in relatives of patients with non-insulin-dependent diabetes. The New England journal of medicine *318*, 1225-1230.
O'Shaughnessy, E.C., Palani, S., Collins, J.J., and Sarkar, C.A. (2011). Tunable Signal Processing in Synthetic MAP Kinase Cascades. Cell *144*, 119-131.
Paolisso, G., Scheen, A.J., Giugliano, D., Sgambato, S., Albert, A., Varricchio, M., D'Onofrio, F., and Lefebvre, P.J. (1991). Pulsatile insulin delivery has greater metabolic effects than continuous hormone administration in man: importance of pulse frequency. The Journal of clinical endocrinology and metabolism *72*, 607-615.
Poritz, M.a., Malmstrom, S., Kim, M.K., Rossmeissl, P.J., and Kamb, A. (2001). Graded mode of transcriptional induction in yeast pheromone signalling revealed by single-cell analysis. Yeast *18*, 1331-1338.
Rusnak, D.W., Lackey, K., Affleck, K., Wood, E.R., Alligood, K.J., Rhodes, N., Keith, B.R., Murray, D.M., Knight, W.B., Mullin, R.J., and Gilmer, T.M. (2001). The effects of the novel, reversible epidermal growth factor receptor/ErbB-2 tyrosine kinase inhibitor, GW2016, on the growth of human normal and tumor-derived cell lines in vitro and in vivo. Molecular Cancer Therapeutics *1*, 85-94.
Samoilov, M., Arkin, A., and Ross, J. (2002). Signal Processing by Simple Chemical Systems. The journal of physical chemistry. A *106*, 10205-10221.
Sasagawa, S., Ozaki, Y., Fujita, K., and Kuroda, S. (2005). Prediction and validation of the distinct dynamics of transient and sustained ERK activation. Nature cell biology *7*, 365-373.
Schmidt, E.V. (1999). The role of c-myc in cellular growth control. Oncogene *18*, 2988-2996.
Schmidt, H., and Jirstrand, M. (2006). Systems Biology Toolbox for MATLAB: a computational platform for research in systems biology. Bioinformatics *22*, 514-515.
Segel, I.H. (1993). Zero-Order Kinetics. In Enzyme Kinetics : Behavior and Analysis of Rapid Equilibrium and Steady-State Enzyme Systems. (New York: Wiley-Interscience), pp. 43-44.
Shaw, M., and Cohen, P. (1999). Role of protein kinase B and the MAP kinase cascade in mediating the EGF-dependent inhibition of glycogen synthase kinase 3 in Swiss 3T3 cells. FEBS Letters *461*, 120-124.
Shoval, O., and Alon, U. (2010). SnapShot: network motifs. Cell *143*, 326-e321.
Sigismund, S., Argenzio, E., Tosoni, D., Cavallaro, E., Polo, S., and Di Fiore, P.P. (2008). Clathrin-mediated internalization is essential for sustained EGFR signaling but dispensable for degradation. Developmental Cell *15*, 209-219.

Solca, F.F., Baum, A., Langkopf, E., Dahmann, G., Heider, K.-h., Himmelsbach, F., and van Meel, J.C.A. (2004). Inhibition of epidermal growth factor receptor activity by two pyrimidopyrimidine derivatives. Journal of Pharmacology and Experimental Therapeutics *311*, 502-509.

Tegner, J., Yeung, M.K.S., Hasty, J., and Collins, J.J. (2003). Reverse engineering gene networks: integrating genetic perturbations with dynamical modeling. Proceedings of the National Academy of Sciences of the United States of America *100*, 5944-5949.

Tomida, T., Hirose, K., Takizawa, A., Shibasaki, F., and Iino, M. (2003). NFAT functions as a working memory of Ca2+ signals in decoding Ca2+ oscillation. Embo J *22*, 3825-3832.

Wakeling, A.E., Guy, S.P., Woodburn, J.R., Ashton, S.E., Curry, B.J., Barker, A.J., and Gibson, K.H. (2002). ZD1839 (Iressa): an orally active inhibitor of epidermal growth factor signaling with potential for cancer therapy. Cancer Research *62*, 5749-5754.

Wang, X., Errede, B., and Elston, T.C. (2008). Mathematical analysis and quantification of fluorescent proteins as transcriptional reporters. Biophysical Journal *94*, 2017-2026.

Woost, P.G., Brightwell, J., Eiferman, R.A., and Schultz, G.S. (1985). Effect of growth factors with dexamethasone on healing of rabbit corneal stromal incisions. Experimental eye research *40*, 47-60.

Yu, R.C., Pesce, C.G., Colman-Lerner, A., Lok, L., Pincus, D., Serra, E., Holl, M., Benjamin, K., Gordon, A., and Brent, R. (2008). Negative feedback that improves information transmission in yeast signalling. Nature *456*, 755-761.

Zingg, D., Riesterer, O., Fabbro, D., Glanzmann, C., Bodis, S., and Pruschy, M. (2004). Differential activation of the phosphatidylinositol 3'-kinase/Akt survival pathway by ionizing radiation in tumor and primary endothelial cells. Cancer Research *64*, 5398-5406.

# 6. ACKNOWLEDGEMENTS

I am extremely grateful to a lot of people. I thank Prof. Shinya Kuroda so much for teaching principles of scientific research. I received significant advices and technical assistance from Dr. Kazuhiro A. Fujita, Dr. Hiroyuki Kubota, Dr. Shinsuke Uda, Mr. Hiroaki Kakuda, Dr. Minoru Honda, Ms. Miharu Sato, Ms. Risa Kunihiro and other members of my laboratory. I also thank to my thesis committee members, Prof. Atsushi Mochizuki, Prof. Yuichi Iino, Assoc. Prof. Shunichi Sekine, Prof. Hideo Higuchi, and Prof. Kuroda for giving me several comments on the manuscript of this thesis. Finally, I gave great thanks to my family for their dedicated support.

This thesis is the result of the joint research of Mr. Kakuda, Dr. Fujita, Dr. Uda, Prof. Kuroda, and the author. Prof. Kuroda and the author designed the research. The author performed and analyzed the simulation. The author also performed and analyzed the experiment in RESULTS 3.2 with technical assistance of Ms. Sato. Mr. Kakuda, Dr. Fujita, and the author performed and analyzed the experiment in RESULTS 3.4. Dr. Uda supported the mathematical analysis in Supplementary Text 7.1.4.

In financial aspect, this work was partly supported by The Dynamic Mechanisms of and Fundamental Technology for Biological Systems, CREST, from the Japan Science and Technology (JST); by a KAKENHI Scientific Research grant (A) (#21240025) from the Ministry of Education, Culture, Sports, Science and Technology of Japan (MEXT); and by the Strategic International Cooperative Program (Research Exchange Type), JST. The author was also supported by research associate (RA) programs of the CREST program for my living expenses.

# 7. APPENDIX

## 7.1. Supplementary Text

### 7.1.1. Consecutive first-order reaction

A consecutive first-order reaction, which is called a low-pass filter in the field of engineering, can be represented as

$$F \xrightarrow{k/\tau} G \xrightarrow{1/\tau} (\phi),$$

where $k$ denotes the gain of the filter and $\tau$ denotes the time constant of the filter. The output of the reaction, $G(t)$, is dependent on the input, $F(t)$, and the temporal evolution of $G(t)$ is described by the ordinary differential equation as follows:

$$\tau \frac{dG(t)}{dt} = k \cdot F(t) - G(t). \tag{S1}$$

We obtained an analytical solution for $G(t)$ as follows:

$$G(t) = \frac{k}{\tau} \mathrm{e}^{-\frac{t}{\tau}} \int_{u=0}^{t} F(u) \mathrm{e}^{\frac{u}{\tau}} du. \tag{S2}$$

The gain $k$ scales the amplitude of $G(t)$ uniformly but does not affect the shape of the time course of $G(t)$. Therefore, the gain $k$ does not affect the results in the main text.

### 7.1.2. Activator model

The activator model can be described using the following ordinary differential equations:

$$\begin{cases} \dfrac{dX}{dt} &= -a \cdot X, \\ \dfrac{dY}{dt} &= a \cdot X - b \cdot Y, \\ \dfrac{dZ}{dt} &= c \cdot Y - d \cdot Z, \end{cases} \tag{S3}$$

where parameters $a, b, c$, and $d$ are the rate constants of the synthesis of $Y$, the degradation of $Y$, synthesis of Z, and the degradation of $Z$, respectively (see Figure 9B). Comparing the equation of $dZ/dt$ with equation (S1), following relationships were found:

$$\begin{cases} \tau = 1/d, \\ k = c/d. \end{cases} \tag{S4}$$

The initial conditions were given as follows:

$$\begin{cases} X(0) &= x, \\ Y(0) &= 0, \\ Z(0) &= 0, \end{cases} \tag{S5}$$

and the analytical solution of the equations is

$$\begin{cases} X(t) &= x\mathrm{e}^{-at}, \\ Y(t) &= \dfrac{ax}{b-a}\left(\mathrm{e}^{-at} - \mathrm{e}^{-bt}\right), \\ Z(t) &= \dfrac{-acx\mathrm{e}^{-at}}{(d-a)(a-b)} + \dfrac{-acx\mathrm{e}^{-bt}}{(a-b)(b-d)} + \dfrac{-acx\mathrm{e}^{-dt}}{(b-d)(d-a)}, \end{cases} \tag{S6}$$

where $(a \neq b \neq d)$.

Note that the parameter $x$ scales the amplitudes of all the time coureses uniformly but does not affect the shape of the time coureses. Therefore, the paramter $x$ does not affect the

results in the main text, and we set $x = 1$ unless otherwise specified.

Y and Z were regarded as amounts of activated upstream and downstream molecules of a signaling pathway, respectively. In this study, we focused on the relationships between Y and Z, and therefore the biological meaning of X was not specified. We changed the time course of Y by changing a and b, and examined the response of Zpeak in main text.

We can introduce more detailed expression of the activator model using $\hat{a}$,

$$\begin{cases} \dfrac{dX}{dt} &= -a \cdot X, \\ \dfrac{dY}{dt} &= \hat{a} \cdot X - b \cdot Y, \\ \dfrac{dZ}{dt} &= c \cdot Y - d \cdot Z, \end{cases} \tag{S7}$$

and then obtained the analytical solutions as

$$\begin{cases} X(t) &= x\mathrm{e}^{-at}, \\ Y(t) &= \dfrac{\hat{a}x}{b-a}\left(\mathrm{e}^{-at} - \mathrm{e}^{-bt}\right), \\ Z(t) &= \dfrac{-\hat{a}cx\mathrm{e}^{-at}}{(d-a)(a-b)} + \dfrac{-\hat{a}cx\mathrm{e}^{-bt}}{(a-b)(b-d)} + \dfrac{-\hat{a}cx\mathrm{e}^{-dt}}{(b-d)(d-a)}. \end{cases} \tag{S8}$$

Thus, the paramter $\hat{a}$ scales the amplitudes of time coureses of $Y$ and $Z$ uniformly but does not affect the shape of the time coureses. Therefore, the paramter $\hat{a}$ does not affect the results in the main text, and we set $\hat{a} = a$ in this study.

### 7.1.3. Peak time and peak amplitude of the activator model

The time course of $Y$ has a peak at the peak time $t_Y$, and $t_Y$ is given by the solution of the equation:

$$\begin{aligned}\frac{dY}{dt} &= \frac{a}{b-a}\left(-a\mathrm{e}^{-at_Y} + b\mathrm{e}^{-bt_Y}\right) \\ &= 0,\end{aligned} \tag{S9}$$

hence,

$$t_Y = \frac{\log\left(\frac{a}{b}\right)}{a-b} \tag{S10}$$

and from equation (S8), the peak amplitude $Y_{peak}$ can be obtained,

$$\begin{aligned}Y_{peak} &= Y(t_Y) \\ &= \frac{a}{b-a}\left\{\left(\frac{a}{b}\right)^{\frac{-a}{a-b}} - \left(\frac{a}{b}\right)^{\frac{-b}{a-b}}\right\} \\ &= \frac{a}{b-a}\left(\frac{a}{b}\right)^{\frac{-b}{a-b}}\left\{\left(\frac{a}{b}\right)^{\frac{b-a}{a-b}} - 1\right\} \\ &= \frac{a}{b-a}\left(\frac{a}{b}\right)^{\frac{-b}{a-b}}\left\{\frac{b}{a} - 1\right\} \\ &= \left(\frac{a}{b}\right)^{\frac{-b}{a-b}} \\ &= \left(\frac{a}{b}\right)^{\frac{1}{1-a/b}}.\end{aligned} \tag{S11}$$

Next, we assumed that the time course of $Z$ has a single peak ($Z_{peak}$) at $t = t_Z$. $t_Z$ is given by the solution of the equation $dZ(t_Z)/dt = 0$. But the equation $dZ/dt = 0$ is difficult to

solve for $t$. Therefore, we introduced an approximation of $Z$ using the symmetry and singularity of $Z$, and divided the parameter space as follows:

$$\begin{cases} \text{Area } I & : a < d \text{ and } b < d \\ \text{Area } II & : a > d \text{ and } a > b \\ \text{Area } III & : b > d \text{ and } a < b. \end{cases} \tag{S12}$$

In area I, we introduced a new parameter, $h$, as $d = a/h$. From equation (S12),

$$\begin{cases} a < d & \Rightarrow h < 1 \\ b < d & \Rightarrow \dfrac{bh}{a} < 1 \end{cases} \tag{S13}$$

and from equation (S8),

$$\begin{aligned} Z(t) &= \frac{-ace^{-at}}{(\frac{a}{h}-a)(a-b)} + \frac{-ace^{-bt}}{(a-b)(b-\frac{a}{h})} + \frac{-ace^{-\frac{a}{h}t}}{(b-\frac{a}{h})(\frac{a}{h}-a)} \\ &= \frac{h}{a}\left\{ \frac{-ace^{-at}}{(1-h)(a-b)} + \frac{ace^{-bt}}{(a-b)(1-\frac{bh}{a})} + \frac{che^{-\frac{a}{h}t}}{(1-\frac{bh}{a})(1-h)} \right\}. \end{aligned} \tag{S14}$$

Here, the Maclaurin series expansion of $e^x$ is

$$e^x = \sum_{n=0}^{\infty} \frac{x^n}{n!} \quad (\text{for all } x), \tag{S15}$$

and that of $\dfrac{1}{1-x}$ is

$$\frac{1}{1-x} = \sum_{n=1}^{\infty} x^n \quad (\text{for all } |x| < 1). \tag{S16}$$

Then the Maclaurin series expansion for the above equation under the conditions in (S13) is

given by,

$$
\begin{aligned}
Z(t) &= \frac{h}{a}\left\{\frac{-ace^{-at}}{(a-b)}\cdot\sum_{k=0}^{\infty}h^k+\frac{ace^{-bt}}{(a-b)}\cdot\sum_{k=0}^{\infty}\left(\frac{bh}{a}\right)^k\right. \\
&\quad \left.+ch\cdot\sum_{k=0}^{\infty}h^k\cdot\sum_{l=0}^{\infty}\left(\frac{bh}{a}\right)^l\cdot\sum_{m=0}^{\infty}\frac{1}{m!}\left(\frac{-at}{h}\right)^m\right\} \\
&= \frac{h}{a}\left\{\frac{-ace^{-at}}{(a-b)}+\frac{-ace^{-at}}{(a-b)}\cdot\sum_{k=1}^{\infty}h^k+\frac{ace^{-bt}}{(a-b)}+\frac{ace^{-bt}}{(a-b)}\cdot\sum_{k=1}^{\infty}\left(\frac{bh}{a}\right)^k\right. \\
&\quad \left.+c\cdot\sum_{k=1}^{\infty}h^k\cdot\sum_{l=0}^{\infty}\left(\frac{bh}{a}\right)^l\cdot\sum_{m=0}^{\infty}\frac{1}{m!}\left(\frac{-at}{h}\right)^m\right\} \\
&= \frac{h}{a}\left\{\frac{ac}{(b-a)}\left(e^{-at}-e^{-bt}\right)+O(h)\right\} \\
&\approx \frac{ac}{d(b-a)}\left(e^{-at}-e^{-bt}\right) \\
&= \frac{c}{d}\cdot\frac{a}{(b-a)}\left(e^{-at}-e^{-bt}\right).
\end{aligned}
\tag{S17}
$$

In Area I, the approximation of $Z$ using equation (S17) is equal to $Y$ (equation (S8)) without scaling factor $c/d$, hence,

$$
t_Z=\frac{\log\left(\frac{a}{b}\right)}{a-b} \tag{S18}
$$

$$
Z_{peak}=\frac{c}{d}\left(\frac{a}{b}\right)^{\frac{1}{1-a/b}}. \tag{S19}
$$

In area II , we set the parameter $h$ as $a = d/h$. From equation (S12),

$$
\begin{cases} a>d & \Rightarrow h<1 \\ a>b & \Rightarrow \dfrac{bh}{d}<1 \end{cases} \tag{S20}
$$

and from equation (S8),

$$
\begin{aligned}
Z(t) &= \frac{-\frac{d}{h}\cdot c\cdot \mathrm{e}^{-\frac{d}{h}t}}{(d-\frac{d}{h})(\frac{d}{h}-b)} + \frac{-\frac{d}{h}\cdot c\cdot \mathrm{e}^{-bt}}{(\frac{d}{h}-b)(b-d)} + \frac{-\frac{d}{h}\cdot c\cdot \mathrm{e}^{-dt}}{(b-d)(d-\frac{d}{h})} \\
&= \frac{\frac{h}{d}\cdot c\cdot \mathrm{e}^{-\frac{d}{h}t}}{(1-h)(1-\frac{bh}{d})} + \frac{-c\mathrm{e}^{-bt}}{(1-\frac{bh}{d})(b-d)} + \frac{c\mathrm{e}^{-dt}}{(b-d)(1-h)}.
\end{aligned} \tag{S21}
$$

From equations (S15) and (S16), the Maclaurin series expansion for the above equation under the conditions in equation (S20) is given by,

$$
\begin{aligned}
Z(t) &= \frac{ch}{d}\cdot\sum_{k=0}^{\infty}h^k\cdot\sum_{l=0}^{\infty}\left(\frac{bh}{d}\right)^l\cdot\sum_{m=0}^{\infty}\frac{1}{m!}\left(\frac{-dt}{h}\right)^m + \frac{-c\mathrm{e}^{-bt}}{(b-d)}\cdot\sum_{k=0}^{\infty}\left(\frac{bh}{d}\right)^k \\
&\quad + \frac{c\mathrm{e}^{-dt}}{(b-d)}\cdot\sum_{k=0}^{\infty}h^k \\
&= \frac{c}{d}\cdot\sum_{k=1}^{\infty}h^k\cdot\sum_{l=0}^{\infty}\left(\frac{bh}{d}\right)^l\cdot\sum_{m=0}^{\infty}\frac{1}{m!}\left(\frac{-dt}{h}\right)^m + \frac{-c\mathrm{e}^{-bt}}{(b-d)} + \frac{-c\mathrm{e}^{-bt}}{(b-d)}\cdot\sum_{k=1}^{\infty}\left(\frac{bh}{d}\right)^k \\
&\quad + \frac{c\mathrm{e}^{-dt}}{(b-d)} + \frac{c\mathrm{e}^{-dt}}{(b-d)}\cdot\sum_{k=1}^{\infty}h^k \\
&= \frac{c}{(b-d)}\left(\mathrm{e}^{-dt}-\mathrm{e}^{-bt}\right)+O(h) \\
&\approx \frac{c}{(b-d)}\left(\mathrm{e}^{-dt}-\mathrm{e}^{-bt}\right) \\
&= \frac{c}{d}\cdot\frac{d}{(b-d)}\left(\mathrm{e}^{-dt}-\mathrm{e}^{-bt}\right).
\end{aligned} \tag{S22}
$$

In Area II , we have

$$
t_Z = \frac{\log\left(\frac{d}{b}\right)}{d-b} \tag{S23}
$$

$$
Z_{peak} = \frac{c}{d}\left(\frac{d}{b}\right)^{\frac{1}{1-d/b}}. \tag{S24}
$$

In area III , we set the parameter $h$ as $b = d/h$ . From equation (S12),

$$\begin{cases} b > d & \Rightarrow h < 1 \\ a < b & \Rightarrow \dfrac{ah}{d} < 1 \end{cases} \tag{S25}$$

and from equation (S8),

$$\begin{aligned} Z(t) &= \frac{-ac\mathrm{e}^{-at}}{(d-a)(a-\frac{d}{h})} + \frac{-ac\mathrm{e}^{-\frac{d}{h}t}}{(a-\frac{d}{h})(\frac{d}{h}-d)} + \frac{-ac\mathrm{e}^{-dt}}{(\frac{d}{h}-d)(d-a)} \\ &= \frac{h}{d}\left\{ \frac{ac\mathrm{e}^{-at}}{(d-a)(1-\frac{ah}{d})} + \frac{\frac{h}{d}\cdot ac\mathrm{e}^{-\frac{d}{h}t}}{(1-\frac{ah}{d})(1-h)} + \frac{-ac\mathrm{e}^{-dt}}{(1-h)(d-a)} \right\}. \end{aligned} \tag{S26}$$

From equations (S15) and (S16), the Maclaurin series expansion for the above equation under the conditions in equation (S25) is given by,

$$\begin{aligned} Z(t) &= \frac{h}{d}\left\{ \frac{ac\mathrm{e}^{-at}}{(d-a)}\cdot\sum_{k=0}^{\infty}\left(\frac{ah}{d}\right)^k + \frac{ach}{d}\cdot\sum_{k=0}^{\infty}h^k\cdot\sum_{l=0}^{\infty}\left(\frac{ah}{d}\right)^l\cdot\sum_{m=0}^{\infty}\frac{1}{m!}\left(\frac{-dt}{h}\right)^m \right. \\ &\quad \left. + \frac{-ac\mathrm{e}^{-dt}}{(d-a)}\cdot\sum_{k=0}^{\infty}h^k \right\} \\ &= \frac{h}{d}\left\{ \frac{ac\mathrm{e}^{-at}}{(d-a)} + \frac{ac\mathrm{e}^{-at}}{(d-a)}\cdot\sum_{k=1}^{\infty}\left(\frac{ah}{d}\right)^k \right. \\ &\quad + \frac{ac}{d}\cdot\sum_{k=1}^{\infty}h^k\cdot\sum_{l=0}^{\infty}\left(\frac{ah}{d}\right)^l\cdot\sum_{m=0}^{\infty}\frac{1}{m!}\left(\frac{-dt}{h}\right)^m \\ &\quad \left. + \frac{-ac\mathrm{e}^{-dt}}{(d-a)} + \frac{-ac\mathrm{e}^{-dt}}{(d-a)}\cdot\sum_{k=1}^{\infty}h^k \right\} \\ &= \frac{h}{d}\left\{ \frac{ac}{(d-a)}\left(\mathrm{e}^{-at}-\mathrm{e}^{-dt}\right) + O(h) \right\} \\ &\approx \frac{1}{b}\cdot\frac{ac}{(a-d)}\left(\mathrm{e}^{-dt}-\mathrm{e}^{-at}\right) \\ &= \frac{ac}{bd}\cdot\frac{d}{(a-d)}\left(\mathrm{e}^{-dt}-\mathrm{e}^{-at}\right). \end{aligned} \tag{S27}$$

In Area III , we have

$$t_Z = \frac{\log\left(\frac{d}{a}\right)}{d-a} \tag{S28}$$

$$Z_{peak} = \frac{ac}{bd}\left(\frac{d}{a}\right)^{\frac{1}{1-d/a}}. \tag{S29}$$

In summary, the approximations for $Z(t), t_Z$, and $Z_{peak}$ in Areas I, II , and III are shown in Supplementary Table 1.

**Supplementary Table 1: Approximations for $Z(t), t_Z$, and $Z_{peak}$ in Areas I, II, and III.**

| Area | Conditions | Approximated $Z(t)$ | $t_Z$ | $Z_{peak}$ |
|---|---|---|---|---|
| I | $a < d, b < d$ | $\frac{c}{d} \cdot \frac{a}{(b-a)} \left( \mathrm{e}^{-at} - \mathrm{e}^{-bt} \right)$ | $\frac{\log\left(\frac{a}{b}\right)}{a-b}$ | $\frac{c}{d}\left(\frac{a}{b}\right)^{\frac{1}{1-a/b}}$ |
| II | $a > d, a > b$ | $\frac{c}{d} \cdot \frac{d}{(b-d)} \left( \mathrm{e}^{-dt} - \mathrm{e}^{-bt} \right)$ | $\frac{\log\left(\frac{d}{b}\right)}{d-b}$ | $\frac{c}{d}\left(\frac{d}{b}\right)^{\frac{1}{1-d/b}}$ |
| III | $b > d, a < b$ | $\frac{ac}{bd} \cdot \frac{d}{(a-d)} \left( \mathrm{e}^{-dt} - \mathrm{e}^{-at} \right)$ | $\frac{\log\left(\frac{d}{a}\right)}{d-a}$ | $\frac{ac}{bd}\left(\frac{d}{a}\right)^{\frac{1}{1-d/a}}$ |

It should be noted that these approximations become closer to the numerical value if the parameter $h$ becomes smaller than 1, where the parameter set is far from the boundaries of the areas. Each approximation of $t_Z$ and $Z_{peak}$ is equal to each other at the boundaries of the areas.

Note that the term $\frac{c}{d}$ $(=k)$ scales approximated $Z(t)$ and $Z_{peak}$ in all the three areas uniformly. Therefore, $E$ was defined in main text as

$$E = \frac{1}{k} \cdot \frac{Z_{peak}}{Y_{peak}}. \tag{S30}$$

### 7.1.4. A function included in the peak amplitudes increases strictly monotonically

$Y_{peak}$ and $Z_{peak}$ are represented by the form $A \cdot f(u)$, where

$$f(u) = u^{\frac{1}{1-u}}. \tag{S31}$$

For example, $Z_{peak}$ in area I, $A = c/d$ and $u = a/b$.

Here, we show that $f(u)$ is a strictly monotonically increaseing function where $u > 0$. The derivative of $f(u)$ is

$$\frac{df(u)}{du} = \frac{u\log(u) - (u-1)}{u(u-1)^2} \cdot u^{\frac{1}{1-u}}. \tag{S32}$$

Because $u(u-1)^2 > 0$ at $u \neq 1$ and $u^{\frac{1}{1-u}} > 0$, we show

$$g(u) = u\log(u) - (u-1) > 0, \tag{S33}$$

where $u \neq 1$.

The derivative of the function g(u) is

$$\frac{dg(u)}{du} = \log(u)$$
$$= \begin{cases} < 0 & (0 < u < 1), \\ = 0 & (u = 1), \\ > 0 & (u > 1), \end{cases} \tag{S34}$$

and,

$$g(1) = 1 \cdot \log(1) - (1-1)$$
$$= 0. \tag{S35}$$

Therefore, $g(u) > 0$ where $u > 0$ and $u \neq 1$. This result proves that the function $f(u)$ increases monotonically where for $u > 0$ and $u \neq 1$.

If $u = 1$, we have

$$\frac{df(1)}{du} = \frac{0}{0} \cdot 1^{\frac{1}{0}}, \tag{S36}$$

which includes two indeterminate forms. Applying L'Hospital's rule twice we have

$$\begin{aligned}
\lim_{u\to 1}\frac{df(u)}{du} &= \lim_{u\to 1}\frac{\frac{d}{du}\left(u\log(u)-(u-1)\right)}{\frac{d}{du}u(u-1)^2}\cdot\lim_{u\to 1}u^{\frac{1}{1-u}} \\
&= \lim_{u\to 1}\frac{\log(u)}{(3u-1)(u-1)}\cdot\frac{1}{e} \\
&= \lim_{u\to 1}\frac{\frac{d}{du}\log(u)}{\frac{d}{du}(3u-1)(u-1)}\cdot\frac{1}{e} \\
&= \lim_{u\to 1}\frac{\frac{1}{u}}{6u-4}\cdot\frac{1}{e} \\
&= \frac{1}{2e} \\
&> 0,
\end{aligned} \tag{S37}$$

where

$$\begin{aligned}
\lim_{u\to 1}u^{\frac{1}{1-u}} &= \lim_{v\to 0}\left(1-\frac{1}{v}\right)^{\frac{1}{1-\left(1-\frac{1}{v}\right)}} \\
&= \lim_{v\to 0}\left(1-\frac{1}{v}\right)^{-v} \\
&= \frac{1}{e}.
\end{aligned} \tag{S38}$$

This result proves that $f(u)$ is increasing function at $u = 1$.

In summary, we obtained

$$\frac{df(u)}{du} > 0 \tag{S39}$$

where $u > 0$, and we found that the function $f(u)$ increases strictly monotonically for $u > 0$. Consequently we have

$$\begin{cases} f(u_1) > f(u_2) \Leftrightarrow u_1 > u_2 \\ f(u_1) < f(u_2) \Leftrightarrow u_1 < u_2 \end{cases} \tag{S40}$$

The function $f$ is indicated in Figure 10D as $Y_{peak} = f(a/b)$.

### 7.1.5. Decoupling conditions

The time courses $Y_1$ and $Y_2$ have the parameters $(a_1, b_1)$ and $(a_2, b_2)$, respectively. The decoupling effect is defined as $Y_{peak}(1) > Y_{peak}(2)$ and $Z_{peak}(1) < Z_{peak}(2)$. The parameters are classified in Areas I to III, and the conditions for the decoupling effect are listed in Supplementary Table 2. Some conditions are written in simple form using equation (24). All the conditions have the relationship of $\frac{a_1}{b_1} > \frac{a_2}{b_2}$ [1], which comes from $Y_{peak}(1) > Y_{peak}(2)$.

A contradiction can be noted in the conditions (1), (2), (3), and (8) in Supplementary Table 2, indicating that the decoupling effect cannot occur under these conditions.

**Supplementary Table 2: Decoupling conditions.**

| Cond. No. | Parameter area | | $Z_{peak}(1) < Z_{peak}(2)$ | Parameters (1) | | Parameters (2) | |
|---|---|---|---|---|---|---|---|
| | $(a_1, b_1)$ | $(a_2, b_2)$ | [2] | [3] | [4] | [5] | [6] |
| (1) | Area I | Area I | $\frac{a_1}{b_1} < \frac{a_2}{b_2}$ | $a_1 < d$ | $b_1 < d$ | $a_2 < d$ | $b_2 < d$ |
| (2) | Area I | Area II | $\frac{a_1}{b_1} < \frac{d}{b_2}$ | $a_1 < d$ | $b_1 < d$ | $a_2 > d$ | $a_2 > b_2$ |
| (3) | Area I | Area III | $\left(\frac{a_1}{b_1}\right)^{\frac{1}{1-a_1/b_1}} < \frac{a_2}{b_2}\left(\frac{d}{a_2}\right)^{\frac{1}{1-d/a_2}}$ | $a_1 < d$ | $b_1 < d$ | $b_2 > d$ | $a_2 < b_2$ |
| (4) | Area II | Area I | $\frac{d}{b_1} < \frac{a_2}{b_2}$ | $a_1 > d$ | $a_1 > b_1$ | $a_2 < d$ | $b_2 < d$ |
| (5) | Area II | Area II | $\frac{d}{b_1} < \frac{d}{b_2}$ | $a_1 > d$ | $a_1 > b_1$ | $a_2 > d$ | $a_2 > b_2$ |
| (6) | Area II | Area III | $\left(\frac{d}{b_1}\right)^{\frac{1}{1-d/b_1}} < \frac{a_2}{b_2}\left(\frac{d}{a_2}\right)^{\frac{1}{1-d/a_2}}$ | $a_1 > d$ | $a_1 > b_1$ | $b_2 > d$ | $a_2 < b_2$ |
| (7) | Area III | Area I | $\frac{a_1}{b_1}\left(\frac{d}{a_1}\right)^{\frac{1}{1-d/a_1}} < \left(\frac{a_2}{b_2}\right)^{\frac{1}{1-a_2/b_2}}$ | $b_1 > d$ | $a_1 < b_1$ | $a_2 < d$ | $b_2 < d$ |
| (8) | Area III | Area II | $\frac{a_1}{b_1}\left(\frac{d}{a_1}\right)^{\frac{1}{1-d/a_1}} < \left(\frac{d}{b_2}\right)^{\frac{1}{1-d/b_2}}$ | $b_1 > d$ | $a_1 < b_1$ | $a_2 > d$ | $a_2 > b_2$ |
| (9) | Area III | Area III | $\frac{a_1}{b_1}\left(\frac{d}{a_1}\right)^{\frac{1}{1-d/a_1}} < \frac{a_2}{b_2}\left(\frac{d}{a_2}\right)^{\frac{1}{1-d/a_2}}$ | $b_1 > d$ | $a_1 < b_1$ | $b_2 > d$ | $a_2 < b_2$ |

### 7.1.6. Estimation of signal transfer efficiency from peak times

The signal transfer efficiency E was defined in main text as

$$E = \frac{1}{k} \cdot \frac{Z_{peak}}{Y_{peak}}, \tag{S41}$$

where $k = c / d$, which means the gain.

In area I, the signal transfer efficiency E is 1 because the approximation of $Z_{peak}$ is equal to $k \cdot Y_{peak}$.

In area II,

$$\begin{aligned} E &= \frac{\frac{c}{d}\left(\frac{d}{b}\right)^{\frac{b}{b-d}}}{k\left(\frac{a}{b}\right)^{\frac{b}{b-a}}} \\ &= \frac{\exp\left(\frac{-b}{d-b}\log\left(\frac{d}{b}\right)\right)}{\exp\left(\frac{-b}{a-b}\log\left(\frac{a}{b}\right)\right)} \\ &= \frac{\exp(-b \cdot t_Z)}{\exp(-b \cdot t_Y)} \\ &= \exp(-b(t_Z - t_Y)). \end{aligned} \tag{S42}$$

In area III,

$$
\begin{aligned}
E &= \frac{\frac{ac}{bd}\left(\frac{d}{a}\right)^{\frac{a}{a-d}}}{k\left(\frac{a}{b}\right)^{\frac{b}{b-a}}} \\
&= \frac{\left(\frac{d}{a}\right)^{\frac{a}{a-d}}}{\left(\frac{a}{b}\right)^{\frac{b}{b-a}-1}} \\
&= \frac{\left(\frac{d}{a}\right)^{\frac{a}{a-d}}}{\left(\frac{a}{b}\right)^{\frac{a}{b-a}}} \\
&= \frac{\exp\left(\frac{-a}{d-a}\log\left(\frac{d}{a}\right)\right)}{\exp\left(\frac{-a}{a-b}\log\left(\frac{a}{b}\right)\right)} \\
&= \frac{\exp(-a \cdot t_Z)}{\exp(-a \cdot t_Y)} \\
&= \exp(-a(t_Z - t_Y)).
\end{aligned}
\tag{S43}
$$

In summary,

$$
E = \begin{cases} 1 & (\mathrm{A}reaI) \\ \exp(-b\Delta t) & (\mathrm{A}reaII) \\ \exp(-a\Delta t) & (\mathrm{A}reaIII) \end{cases}
\tag{S44}
$$

where $\Delta t = t_Z - t_Y$.

We summarized these equations and found that the conditions for area II include $a > b$ and that the coefficient is the smaller value, $b$. In other words, the coefficient of $\Delta t$ is $a$ or $b$, whichever is smaller. The conditions for area III include $b > a$, and the coefficient is the

smaller value, $a$. Therefore we introduced a similar coefficient as follows:

$$E = \exp\left(\frac{-ab}{a+b}\Delta t\right). \tag{S45}$$

We estimated the value of $E$ from the equation in (S44) and the numerical value of $\Delta t$. We compared the estimated $E$ to the numerical value of $E$ and found that the difference in the estimation was more than 80% around the borders of areas II and III. We also found that using equation (S45) instead of (S44) improved the error near the border.

### 7.1.7. Parameter estimation of the activator model and selection of experimental data sets for validation of the attenuation property of signal transfer efficiency

The parameters of the activator model were estimated using experimental data (Supplementary Data) according to two methods in series. First, a meta-evolutionary programming method was used to approach the neighborhood of the local minimum. This method was originally implemented in COPASI (Hoops et al., 2006) and I translated it into a matlab function. Option settings are follows: number of generation = 2000, population size = 200, random number generator = Mersenne twister, number of seeds = 200. Second, the Nelder-Mead method was used to reach the local minimum. This method was implemented in matlab function (D'Errico, 2005). Option settings are follows: maximum number of function evaluations = $10^5$, tolerances = $10^{-4}$. Using these methods, the parameters were estimated to minimize the objective function value, which was defined as the sum of the square residuals between our measurements and the model trajectories.

We made two minor modifications to the activator model as follows. First, the output of the low-pass filter ($Z(t)$) was given a delay time $l$ because some downstream molecule of the pathway, the experimental counterpart of $Z(t)$, seemed to have a delay time. Accordingly, $Z(t)$ was modified to $Z(t-l)$, and $Z(t-l)$ was set as 0 at $t < l$. Second, the parameter $a$, $b$ and $x$ can have different and arbitrary values for respective time courses in a pathway. Please note that other parameters ($c$, $d$ and $l$) could have a common value for respective time courses in a pathway. In other words, if we have 6 sets of experimental time course from a single pathway, the 21 paramters ($a_1 \sim a_6$, $b_1 \sim b_6$, $c$, $d$, $l$, and $x_1 \sim x_6$) were estimated at once. These modification satisfyes the condtions i) and ii) but not for condition iii) shown in Disucussion.

There may be some interplay between the signaling dynamics and the ability to estimate parameters. However, our modeling framework is suitable for the analysis of transient time courses, and time courses of our experimental data are almost transient. Therefore, the parameters were correctly estimated by these data sets.

After 200 independent estimations, we selected the model with the minimum objective function value. The estimated parameters and the time courses of the estimated model are shown in Supplementary Data.

In the selected model, we calculated normalized RSS as follows and we excluded the set of the time course whose model does not satisfy any of the following inequations:

$$normalized\_RSS_i^{upstream} = \frac{\sum_{j=1}^{m}(Y(t_j|a_i,b_i,c,d,l,x_i) - measurement_i^{upstream}(t_j))^2}{\sum_{j=1}^{m}(measurement_i^{upstream}(t_j))^2} < 0.1,$$

$$normalized\_RSS_i^{downstream} = \frac{\sum_{j=1}^{m}Z(t_j|a_i,b_i,c,d,l,x_i) - measurement_i^{downstream}(t_j))^2}{\sum_{j=1}^{m}(measurement_i^{downstream}(t_j))^2} < 0.1,$$

$$normalized\_RSS_{all}^{upstream} = \frac{\sum_{i=1}^{n}\sum_{j=1}^{m}(Y(t_j|a_i,b_i,c,d,l,x_i) - measurement_i^{upstream}(t_j))^2}{\sum_{i=1}^{n}\sum_{j=1}^{m}(measurement_i^{upstream}(t_j))^2} < 0.3,$$

$$normalized\_RSS_{all}^{downstream} = \frac{\sum_{i=1}^{n}\sum_{j=1}^{m}Z(t_j|a_i,b_i,c,d,l,x_i) - measurement_i^{downstream}(t_j))^2}{\sum_{i=1}^{n}\sum_{j=1}^{m}(measurement_i^{downstream}(t_j))^2} < 0.3,$$

where $i$ and $j$ represents the doses and the time points, respectively. We confirmed that

choice of the cutoff values for normalized RSS has little effect on our results. We also excluded the inhbitor experiments and the set of the time courses whose half-life time ($t_{1/2}$) or peak amplitudes coud not be obtained by experiment because of sustained response or nonresponsive to the stimuli. We selected the rest of the time courses which satisfy the conditions i) and ii), and analyzed their experimental data for Figure 15. $t_{1/2}$ was obtained by linear interpolation of the experimental time course of the upstream molecule. The time constant of the pathway $\tau$ was obtained as $1/d$ of the model. The signal transfer efficiency ($E$) was obtained from the ratio of the peak amplitudes of the experimenatl time courses and then divided by $k = c/d$ of the model. Then $E$ was plotted against $\frac{t_{1/2}}{\tau}$ with the theoretical line in Figure 15 (for derivation of the theoretical line, see Figure 14).

### 7.1.8. $EC_{50}$ decrease in the activator model

In section 7.1.4, we found that $f(u) = u^{\frac{1}{1-u}}$ for $u > 0$ is strictly monotonically increasing function (equation (S39)). In this section, we show other three characteristics of $f(u)$ and then proof of $EC_{50}$ decrease in the activator model. We also show the relationships between sensitivity increase index ( $S_i$ ) and the negative regulation of the pathway ( $d$ ).

First, we show $0 < f(u) < 1$. For limit on $u \to 0$, we have

$$\begin{aligned} \lim_{u\to 0} f(u) &= (0)^{\frac{1}{1-0}} \\ &= 0. \end{aligned} \tag{S46}$$

For limit on $u \to \infty$, applying L'Hospital's rule we have

$$\begin{aligned} \lim_{u\to \infty} f(u) &= \lim_{u\to \infty} u^{\frac{1}{1-u}} \\ &= \exp\left( \lim_{u\to \infty} \frac{\log u}{1-u} \right) \\ &= \exp\left( \lim_{u\to \infty} \frac{\frac{d}{du}\log u}{\frac{d}{du}(1-u)} \right) \\ &= \exp\left( \lim_{u\to \infty} \frac{\frac{1}{u}}{-1} \right) \\ &= \exp(0) \\ &= 1 \end{aligned} \tag{S47}$$

From these results and equation (S39), we found

$$0 < f(u) < 1 \tag{S48}$$

Second, we show $\frac{1}{u}\cdot f(u) = f(1/u)$. We have

$$\begin{aligned}\frac{1}{u}\cdot f(u) &= \frac{1}{u}\cdot u^{\frac{1}{1-u}} \\ &= u^{\frac{1}{1-u}-1} \\ &= u^{\frac{u}{1-u}} \\ &= \left(\frac{1}{u}\right)^{\frac{u}{u-1}} \\ &= \left(\frac{1}{u}\right)^{\frac{1}{1-1/u}} \\ &= f(1/u).\end{aligned} \tag{S49}$$

Then we found

$$\frac{1}{u}\cdot f(u) = f(1/u). \tag{S50}$$

Third, we show that the solution of $f(u) = \frac{1}{2}$ is $u = 2$. We have

$$\begin{aligned}f(2) &= (2)^{\frac{1}{1-2}} \\ &= (2)^{-1} \\ &= \frac{1}{2}.\end{aligned} \tag{S51}$$

Together with strictly monotonically increasing characteristics of $f(u)$ (equation (S39)), we found

$$f(u) = \frac{1}{2} \Leftrightarrow u = 2. \tag{S52}$$

Finally, we prove the decrease of $EC_{50}$ in the downstream molecule of the activator model. $EC_{50}$ was defined as the concentration of the activator which induce the 50% of maximum response. In this section, $a$ is regarded as the concentration of the activator.

Consider the $EC_{50}$ of $Y_{peak}$ using analytical solution. From equations (S11) and (S31),

$$\begin{aligned} Y_{peak} &= \left(\frac{a}{b}\right)^{\frac{1}{1-a/b}} \\ &= f\left(\frac{a}{b}\right), \end{aligned} \tag{S53}$$

and from equation (S48), we found that maximum response of $Y_{peak}$ is 1. Therefore, at the $EC_{50}$

$$Y_{peak} = \frac{1}{2}. \tag{S54}$$

From equation (S52), we have

$$f\left(\frac{a}{b}\right) = \frac{1}{2} \Rightarrow a = 2b. \tag{S55}$$

Thus, the $EC_{50}$ of $Y_{peak}$ is obtained as $2b$.

Consider the $EC_{50}$ of $Z_{peak}$ using approximated analytical solution.

In Area II, from equation (S24), $Z_{peak}$ should not be affected by $a$.

In Area I, from equations (S19) and (S31),

$$Z_{peak} = \frac{c}{d}\left(\frac{a}{b}\right)^{\frac{1}{1-a/b}} = \frac{c}{d}\cdot f\left(\frac{a}{b}\right). \quad \text{(S56)}$$

From equation (S39), $Z_{peak}$ monotonically increases for $a$, and from equation (S12), expression of $Z_{peak}$ is switched to that for Area II where $a \geq d$. Therefore, the maximum response of $Z_{peak}$ is same as the $Z_{peak}$ in Area II, and

$$\max\left(Z_{peak}\right) = \frac{c}{d}\left(\frac{d}{b}\right)^{\frac{1}{1-d/b}} = \frac{c}{d}\cdot f\left(\frac{d}{b}\right), \quad \text{(S57)}$$

and at the $EC_{50}$ of $Z_{peak}$, $a$ should satisfy following equation

$$\frac{c}{d}\cdot f\left(\frac{a}{b}\right) = \frac{1}{2}\cdot\frac{c}{d}\cdot f\left(\frac{d}{b}\right)$$

$$\Rightarrow f\left(\frac{a}{b}\right) = \frac{1}{2}\cdot f\left(\frac{d}{b}\right). \quad \text{(S58)}$$

Because $Z_{peak}$ monotonically increases for $a$ (from equation (S39)), the $EC_{50}$ of $Z_{peak}$ reaches the maximum when the right hand side of equation (S58) reaches the maximum. From equation (S48), the maximum of the right hand side is

$$\lim_{\frac{d}{b}\to\infty}\frac{1}{2}\cdot f\left(\frac{d}{b}\right) = \frac{1}{2}. \quad \text{(S59)}$$

Therefore, the maximum of the $EC_{50}$ of $Z_{peak}$ is

$$f\left(\frac{a}{b}\right)=\frac{1}{2}\Rightarrow a=2b, \tag{S60}$$

and is the same as $EC_{50}$ of $Y_{peak}$ (equation (S55)). Thus, it is proved that the $EC_{50}$ of $Z_{peak}$ should be equal or smaller than that of $Y_{peak}$ in Area I.

In Area III, from equations (S29) and (S31),

$$\begin{aligned} Z_{peak} &= \frac{ac}{bd}\left(\frac{d}{a}\right)^{\frac{1}{1-d/a}} \\ &= \frac{ac}{bd}\cdot f\left(\frac{d}{a}\right). \end{aligned} \tag{S61}$$

From equation (S50),

$$\begin{aligned} Z_{peak} &= \frac{c}{b}\cdot\frac{a}{d}\cdot f\left(\frac{d}{a}\right) \\ &= \frac{c}{b}\cdot f\left(\frac{a}{d}\right). \end{aligned} \tag{S62}$$

From equation (S39), $Z_{peak}$ monotonically increases for $a$, and from equation (S12), expression of $Z_{peak}$ is switched to that for Area II where $a \geq b$. Therefore, the maximum response of $Z_{peak}$ is same as the $Z_{peak}$ in Area II, and

$$\max\left(Z_{peak}\right)=\frac{c}{d}\cdot f\left(\frac{d}{b}\right), \tag{S63}$$

and at the $EC_{50}$ of $Z_{peak}$, $a$ should satisfy following equation

$$\frac{c}{b}\cdot f\left(\frac{a}{d}\right)=\frac{1}{2}\cdot\frac{c}{d}\cdot f\left(\frac{d}{b}\right)$$

$$\Rightarrow f\left(\frac{a}{d}\right)=\frac{1}{2}\cdot\frac{b}{d}\cdot f\left(\frac{d}{b}\right). \tag{S64}$$

Using equation (S50), we have

$$f\left(\frac{a}{d}\right)=\frac{1}{2}\cdot f\left(\frac{b}{d}\right). \tag{S65}$$

Because $Z_{peak}$ monotonically increases for $a$ (from equation (S39)), the $EC_{50}$ of $Z_{peak}$ reaches the maximum when the right hand side of equation (S55) reaches the maximum. From equation (S48), the maximum of the right hand side is

$$\lim_{\frac{b}{d}\to\infty}\frac{1}{2}\cdot f\left(\frac{b}{d}\right)=\frac{1}{2}. \tag{S66}$$

Therefore, the maximum of the $EC_{50}$ of $Z_{peak}$ is

$$f\left(\frac{a}{d}\right)=\frac{1}{2}\Rightarrow a=2d. \tag{S67}$$

From equation (S12), $d<b$ in Area III. Therefore, it is proved that the $EC_{50}$ of $Z_{peak}$ should be smaller than the $EC_{50}$ of $Y_{peak}$ (equation (S52)).

Thus, it is proved that the $EC_{50}$ of $Z_{peak}$ should be equal or smaller than that of $Y_{peak}$.

Additionally, we show the relationships between sensitivity increase index ($S_i$) and the negative regulation of the pathway ($d$). In the main text, $S_i$ was defined as

$$S_i = \frac{\mathrm{EC}_{50} \text{ of } Y_{peak}}{\mathrm{EC}_{50} \text{ of } Z_{peak}}. \tag{S68}$$

From Figure 10D, we found that $f(u)$ is almost same to its maximum value in $u >> 1$. Therefore, the $\mathrm{EC}_{50}$ of $Z_{peak}$ can be approximated by its maximum value,

$$\mathrm{EC}_{50} \text{ of } Z_{peak} \approx \begin{cases} 2b & (d > b), \\ 2d & (d < b). \end{cases} \tag{S69}$$

Together with equations (S52) and (S68), we have

$$S_i \approx \begin{cases} 1 & (d > b), \\ \dfrac{b}{d} & (d < b). \end{cases} \tag{S70}$$

This result means that $S_i$ reaches 1 when $d$ became larger than $b$, and $S_i$ increases as the inverse of $d$ when $d$ became larger than $b$. This description is equivalent to the descriptions for Figure 16E. Equations (S52), (S69), and (S70) are shown in Figure 17D, E, and F, respectively. In Figure 17G, equation (S70) are compared with numerical results (Figure 16E). We confirmed that the approximation used in equations (S69), and (S70) does not affect the qualitative characteristics of the $\mathrm{EC}_{50}$ for $Z_{peak}$ and $S_i$.

### 7.1.9. Inhibitor model

The inhibitor model can be described by the ordinary differential equations as follows:

$$\begin{cases} \dfrac{dW}{dt} &= -q \cdot W + p \cdot X \\ \dfrac{dX}{dt} &= q \cdot W - (a+p) \cdot X \\ \dfrac{dY}{dt} &= a \cdot X - b \cdot Y \\ \dfrac{dZ}{dt} &= c \cdot Y - d \cdot Z \end{cases} \tag{S71}$$

where the parameters $p$ and $q$ denote the forward and reverse rate constants of the inhibitor reactions, respectively (see Figure 18A). The initial conditions were given as follows:

$$\begin{cases} W(0) &= \dfrac{p \cdot x}{p+q} \\ X(0) &= \dfrac{q \cdot x}{p+q} \\ Y(0) &= 0 \\ Z(0) &= 0 \end{cases} \tag{S72}$$

where the parameter $x$ denotes the total initial amount of the sum of $X$ and $W$.

The analytical solution of the equations is as follows:

$$\begin{cases} W(t) &= \dfrac{px}{(p+q)(\beta-\alpha)}\left(\beta \mathrm{e}^{\alpha t} - \alpha \mathrm{e}^{\beta t}\right) \\ X(t) &= \dfrac{qx}{(p+q)(\beta-\alpha)}\left\{(\beta+a)\mathrm{e}^{\alpha t} - (\alpha+a)\mathrm{e}^{\beta t}\right\} \\ Y(t) &= \dfrac{aqx}{p+q}\left\{\dfrac{(\beta+a)\mathrm{e}^{\alpha t}}{(\beta-\alpha)(\alpha+b)} - \dfrac{(\alpha+a)\mathrm{e}^{\beta t}}{(\beta-\alpha)(\beta+b)} - \dfrac{(\alpha+\beta+a+b)\mathrm{e}^{-bt}}{(\alpha+b)(\beta+b)}\right\} \\ Z(t) &= \dfrac{acqx}{p+q}\left\{\dfrac{(\beta+a)\mathrm{e}^{\alpha t}}{(\beta-\alpha)(\alpha+b)(\alpha+d)} - \dfrac{(\alpha+a)\mathrm{e}^{\beta t}}{(\beta-\alpha)(\beta+b)(\beta+d)}\right. \\ & \quad \left. - \dfrac{(\alpha+\beta+a+b)\mathrm{e}^{-bt}}{(\alpha+b)(\beta+b)(d-b)} + \dfrac{(\alpha+\beta+a+d)\mathrm{e}^{-dt}}{(\alpha+d)(\beta+d)(d-b)}\right\} \end{cases} \tag{S73}$$

where

$$\begin{cases} \alpha &= \frac{1}{2}\left(-(p+q+a)+\sqrt{(p+q+a)^2-4aq}\right) \\ \beta &= \frac{1}{2}\left(-(p+q+a)-\sqrt{(p+q+a)^2-4aq}\right) \end{cases} \tag{S74}$$

and $\alpha \neq \beta \neq -b \neq -d$ .

In the analysis of the inhibitor model (i.e. RESULTS 3.4), the parameter $x$ was set as 1 for convenience and simplicity without a loss of generality.

### 7.1.10. Parameter estimation of the inhibitor model

The parameters of the inhibitor model were estimated using experimental data (Figure 22) according to two methods in series as described above (Supplementary Text 7.1.7).

We made two minor modifications to the inhibitor model as follows. First, the parameter $p$ was scaled according to the inhibitor concentration. Second, the output of the low-pass filter $(Z(t))$ was given a delay time $l$ because pS6, the experimental counterpart of $Z(t)$, seemed to have a delay time. Accordingly, $Z(t)$ was modified to $Z(t-l)$, and $Z(t-l)$ was set as 0 at $t < l$.

After 20 independent estimations, we selected the model with the minimum objective function value. The estimated parameters are shown in Supplementary Table 3, and the time courses of the estimated model are shown in Figure 23.

**Supplementary Table 3: Estimated parameters of the inhibitor model.**

| Parameter name | Value | Unit |
|---|---|---|
| $a$ | $3.126\times10^{-3}$ | $sec^{-1}$ |
| $b$ | $2.794\times10^{-2}$ | $sec^{-1}$ |
| $c$ | $3.041\times10^{-3}$ | $(-)$ |
| $d$ | $3.466\times10^{-4}$ | $sec^{-1}$ |
| $p$ | $3.952\times10^{+1}$ | $sec^{-1}\cdot nM^{-1}$ |
| $q$ | $1.791\times10^{+3}$ | $sec^{-1}$ |
| $x$ | $1.252\times10^{+1}$ | $(-)$ |
| $l$ | $5.683\times10^{+2}$ | $sec$ |
| $(inhibitor)$ | 0,5,15,50,150,500,1500,5000 | $nM$ |

### 7.1.11. *In vivo* inhibitor model

The *in vivo* inhibitor model can be described using ordinary differential equations as follows:

$$\begin{cases} \dfrac{dW}{dt} &= -(q+r)\cdot W + p\cdot X \\ \dfrac{dX}{dt} &= q\cdot W - (a+p+r)\cdot X + r \\ \dfrac{dY}{dt} &= a\cdot X - b\cdot Y \\ \dfrac{dZ}{dt} &= c\cdot Y - d\cdot Z \end{cases} \tag{S75}$$

where the parameter $r$ denotes the synthesis and degradation rate constants of the turnover reactions of $X$ (see Figure 24A). We assumed that the activator was administered and reached an equilibrium before inhibition and set the initial conditions as follows:

$$\begin{cases} W(0) &= 0 \\ X(0) &= \dfrac{r}{a+r} \\ Y(0) &= \dfrac{a}{b}\cdot\dfrac{r}{(a+r)} \\ Z(0) &= \dfrac{ac}{bd}\cdot\dfrac{r}{(a+r)}. \end{cases} \tag{S76}$$

### 7.1.12. Convex and monotonic dose responses in receptor dynamics

The receptor dynamics can be described using the following ordinary differential equations:

$$\begin{cases} \dfrac{dR}{dt} &= d-(a+c)\cdot R, \\ \dfrac{dP}{dt} &= a\cdot R-b\cdot P. \end{cases} \tag{S77}$$

$R$ and $P$ denote nonphsphorylated (inactive) and phosphorylated (active) receptors, respectively (Figure 6). The paramter $a$ is the rate constants of the stimulation of $R$ and simulatneously means a concentration of the activator. The paramter $b$ is the degradation rate constants of $P$. The parameter $c$ and $d$ are the degradation and synthesis rate constants of the turnover reactions of $R$, respectively. Both the amounts of activator and pool of inactivated receptors were fixed as 1. The initial conditions were given as follows:

$$\begin{cases} R(0) &= r, \\ P(0) &= 0, \end{cases} \tag{S78}$$

and analytic solution of the equations is

$$\begin{cases} R(t) &= r\mathrm{e}^{-(a+c)t}+\dfrac{d}{a+c}\left(1-\mathrm{e}^{-(a+c)t}\right), \\ P(t) &= \dfrac{ar}{a-b+c}\left(\mathrm{e}^{-bt}-\mathrm{e}^{-(a+c)t}\right) \\ &\quad +\dfrac{ad}{b(a+c)(a-b+c)}\left\{(a+c)\left(1-\mathrm{e}^{-bt}\right)-b\left(1-\mathrm{e}^{-(a+c)t}\right)\right\} \\ &= P_r(t)+P_d(t), \end{cases} \tag{S79}$$

where

$$\begin{cases} P_r(t) &= \dfrac{ar}{a-b+c}\left(\mathrm{e}^{-bt}-\mathrm{e}^{-(a+c)t}\right), \\ P_d(t) &= \dfrac{ad}{b(a+c)(a-b+c)}\left\{(a+c)\left(1-\mathrm{e}^{-bt}\right)-b\left(1-\mathrm{e}^{-(a+c)t}\right)\right\}. \end{cases} \tag{S80}$$

We show that $P_r(t)$ can induce convex dose response under a certain condition and that $P_d(t)$ always induce monotonically increase dose response. Obviously, $P_r(t)$ and $P_d(t)$ equal to 0 when $a=0$ and should not have negative values,

$$\begin{cases} \left.\dfrac{\partial P_r(t)}{\partial a}\right|_{a=0} > 0, \\ \left.\dfrac{\partial P_d(t)}{\partial a}\right|_{a=0} > 0. \end{cases} \tag{S81}$$

Therefore,

$$\frac{\partial P_r(t)}{\partial a} < 0 \tag{S82}$$

means convex dose response of $P_r(t)$, and

$$\frac{\partial P_d(t)}{\partial a} > 0 \tag{S83}$$

means monotonically increasing dose response of $P_d(t)$.

First, we show convex dose response of $P_r(t)$. From equation (S80), we have

$$\begin{aligned} \frac{\partial P_r(t)}{\partial a} &= \left(\frac{ar}{a-b+c}\right)' \cdot \left(\mathrm{e}^{-bt} - \mathrm{e}^{-(a+c)t}\right) + \frac{ar}{a-b+c} \cdot \left(\mathrm{e}^{-bt} - \mathrm{e}^{-(a+c)t}\right)' \\ &= \frac{r\left(a-b+c-a\right)}{\left(a-b+c\right)^2} \cdot \left(\mathrm{e}^{-bt} - \mathrm{e}^{-(a+c)t}\right) + \frac{ar}{a-b+c} \cdot t \cdot \mathrm{e}^{-(a+c)t} \\ &= \frac{r \cdot \left(c-b\right)}{\left(a-b+c\right)^2} \cdot \left(\mathrm{e}^{-bt} - \mathrm{e}^{-(a+c)t}\right) + \frac{r \cdot at\left(a-b+c\right)}{\left(a-b+c\right)^2} \cdot \mathrm{e}^{-(a+c)t} \\ &= \frac{r}{\left(a-b+c\right)^2} \left\{\left(c-b\right)\left(\mathrm{e}^{-bt} - \mathrm{e}^{-(a+c)t}\right) + at\left(a-b+c\right) \cdot \mathrm{e}^{-(a+c)t}\right\} \\ &= \frac{r \cdot \mathrm{e}^{-(a+c)t}}{\left(a-b+c\right)^2} \left\{\left(c-b\right)\left(\mathrm{e}^{(a-b+c)t} - 1\right) + at\left(a-b+c\right)\right\}. \end{aligned} \tag{S84}$$

Here, the term $\frac{r \cdot \mathrm{e}^{-(a+c)t}}{(a-b+c)^2}$ should be positive, and we show

$$\begin{aligned} Q_r &\equiv (c-b)\left(\mathrm{e}^{(a-b+c)t}-1\right)+at(a-b+c) \\ &< 0, \end{aligned} \tag{S85}$$

under a certain condition. From equation (S85), we have

$$(c-b)\cdot \mathrm{e}^{(a-b+c)t} < -at(a-b+c)+(c-b),$$

$$\Rightarrow c-b < \left\{-at(a-b+c)+(c-b)\right\}\cdot \mathrm{e}^{-(a-b+c)t}, \tag{S86}$$

Then we multiply $\frac{1}{a}\cdot \mathrm{e}^{\frac{c-b}{a}} > 0$ to the both sides of the equation (S86),

$$\begin{aligned} \frac{c-b}{a}\cdot \mathrm{e}^{\frac{c-b}{a}} &< \frac{-at(a-b+c)+(c-b)}{a}\cdot \mathrm{e}^{\frac{c-b}{a}-t(a-b+c)} \\ &= \left\{-at\left(1+\frac{c-b}{a}\right)+\frac{c-b}{a}\right\}\cdot \mathrm{e}^{\frac{c-b}{a}-at\left(1+\frac{c-b}{a}\right)}, \end{aligned}$$

$$\Rightarrow x\mathrm{e}^{x} < \left\{x-at(1+x)\right\}\cdot \mathrm{e}^{x-at(1+x)}, \tag{S87}$$

where

$$x = \frac{c-b}{a}. \tag{S88}$$

Here, we define $f(u)$ as

$$f(u) = u\mathrm{e}^{u}, \tag{S89}$$

and then the equation (S87) is

$$f(x) < f\left(x-at(1+x)\right). \tag{S90}$$

Thus, the equation (S82) equals to (S90), which includes function $f(u)$.

Then we examine the characteristics of $f(u)$ (see Figure S1). From equation (S89),

$$\frac{\partial f(u)}{\partial u} = (u+1)\mathrm{e}^{u}, \tag{S91}$$

and we have

$$\frac{\partial f(u)}{\partial u} = \begin{cases} < 0 & (u < -1), \\ > 0 & (u > -1). \end{cases} \tag{S92}$$

This means that $f(u)$ is monotonically decreasing function under $u < -1$ and is monotonically increasing function under $u > -1$. Therefore, $f(u)$ takes minimum value at $u = -1$ and

$$f(-1) = -\frac{1}{e}. \tag{S93}$$

Additionally, we have

$$f(0) = 0, \tag{S94}$$

and

$$\lim_{u \to -\infty} f(u) = -0, \tag{S95}$$

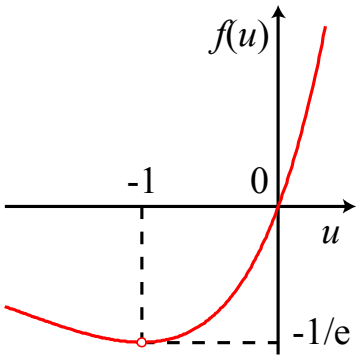


**Figure S1: Characteristics of the function $f(u) = u\mathrm{e}^{u}$.**

From equations (S92), (S94), and (S95), we have

$$f(u)\big|_{u>0} > 0 > f(u)\big|_{u<0}. \tag{S96}$$

When $x < -1$, we have

$$at(x+1) < 0, \tag{S97}$$

and then

$$x < x - at(x+1). \tag{S98}$$

From equations (S92) and (S96), if the condition

$$x - at(x+1) > 0 \tag{S99}$$

would be satisfied, the equation (S90) should be satisfied. Here, the term $at$ can take any positive value. Therefore, there should be appropriate $t$ that satisfy the equation (S99) for any value of $x < -1$. Thus, when $x < -1$, the equation (S90) and (S82) should be satisfied.

When $x > -1$, we have

$$at(x+1) > 0, \tag{S100}$$

and then

$$x > x - at(x+1).$$

From equations (S92) and (S96), the condition

$$\begin{cases} x < 0 \\ x - at(x+1) < -1 \end{cases} \tag{S101}$$

is necessary to be satisfied the equation (S90). The term $at$ can take any positive value and the term $x - at(1+x)$ can take any value which is smaller than -1. From equation (S95), the term $f(x - at(1+x))$ can take larger value than $f(x) < 0$ for any $x$ under the condition of appropriate $t$. In other words, there should be $t$ that satisfy the equations (S101) and (S90) for any value of $-1 < x < 0$. Thus, when $-1 < x < 0$, the equations (S90) and (S82) should be satisfied.

Thus, we proved that the equation (S82) should be satisfied (i.e. $P_r(t)$ shows convex dose response) when $x < 0$. From equation (S88), this condition $x < 0$ equals to

$$b > c\,. \tag{S102}$$

It should be noted that the equation (S82) is satisfied for any value of $a$. It means that, the convex dose response of $P_r(t)$ should be observed regardless of the value of $a$ when $b > c$. Additionally, it is also noteworthy that the equation $Q_r = 0$ seems to have a unique nontrivial solution of t,

$$t = \frac{x - \cdot W_n\left(x\mathrm{e}^{x}\right)}{a(x+1)}, \tag{S103}$$

where the function $W_n(x)$ denotes the Lambert's W function.

Next, we show monotonically increasing dose response of $P_d(t)$. From equation (S80), we have

$$P_d(t) = \frac{ad}{by(y-b)}\left\{y\left(1-\mathrm{e}^{-bt}\right)-b\left(1-\mathrm{e}^{-yt}\right)\right\}, \tag{S104}$$

where

$$y = a + c. \tag{S105}$$

Then,

$$\begin{aligned}
\frac{\partial P_d(t)}{\partial a} &= \left(\frac{ad}{by(y-b)}\right)'\left\{y\left(1-\mathrm{e}^{-bt}\right)-b\left(1-\mathrm{e}^{-yt}\right)\right\} \\
&\quad + \frac{ad}{by(y-b)}\left\{y\left(1-\mathrm{e}^{-bt}\right)-b\left(1-\mathrm{e}^{-yt}\right)\right\}' \\
&= \frac{d}{b}\cdot\frac{y(y-b)-a\{(y-b)+y\}}{y^2(y-b)^2}\left\{y\left(1-\mathrm{e}^{-bt}\right)-b\left(1-\mathrm{e}^{-yt}\right)\right\} \\
&\quad + \frac{d}{b}\cdot\frac{a}{y(y-b)}\left(1-\mathrm{e}^{-bt}-bt\cdot\mathrm{e}^{-yt}\right) \\
&= \frac{d}{b}\cdot\frac{(y-a)(y-b)}{y^2(y-b)^2}\left\{y\left(1-\mathrm{e}^{-bt}\right)-b\left(1-\mathrm{e}^{-yt}\right)\right\} \\
&\quad - \frac{d}{b}\cdot\frac{ay}{y^2(y-b)^2}\left\{y\left(1-\mathrm{e}^{-bt}\right)-b\left(1-\mathrm{e}^{-yt}\right)\right\} \\
&\quad + \frac{d}{b}\cdot\frac{ay(y-b)}{y^2(y-b)^2}\left(1-\mathrm{e}^{-bt}-bt\cdot\mathrm{e}^{-yt}\right) \\
&= \frac{cd}{by^2(y-b)^2}\cdot(y-b)\left\{y\left(1-\mathrm{e}^{-bt}\right)-b\left(1-\mathrm{e}^{-yt}\right)\right\} \\
&\quad + \frac{ady}{by^2(y-b)^2}\left\{(y-b)\left(1-\mathrm{e}^{-bt}-bt\cdot\mathrm{e}^{-yt}\right)-y\left(1-\mathrm{e}^{-bt}\right)+b\left(1-\mathrm{e}^{-yt}\right)\right\} \\
&= \frac{cd\cdot\mathrm{e}^{-(b+y)t}}{by^2(y-b)^2}\cdot(y-b)\left\{y\left(\mathrm{e}^{(b+y)t}-\mathrm{e}^{yt}\right)-b\left(\mathrm{e}^{(b+y)t}-\mathrm{e}^{bt}\right)\right\} \\
&\quad + \frac{ady}{by^2(y-b)^2}\cdot\left[b\cdot\mathrm{e}^{-bt}+b\{(b-y)t-1\}\cdot\mathrm{e}^{-yt}\right] \\
&= \frac{cd\cdot\mathrm{e}^{-(b+y)t}}{by^2(y-b)^2}\cdot(y-b)\left\{(y-b)\cdot\mathrm{e}^{(b+y)t}-y\cdot\mathrm{e}^{yt}+b\cdot\mathrm{e}^{bt}\right\} \\
&\quad + \frac{ady\cdot\mathrm{e}^{-yt}}{y^2(y-b)^2}\cdot\left[\mathrm{e}^{(y-b)t}+\{(b-y)t-1\}\right]
\end{aligned} \tag{S106}$$

Here, both the terms $\frac{cd\cdot\mathrm{e}^{-(b+y)t}}{by^2(y-b)^2}$ and $\frac{ady\cdot\mathrm{e}^{-yt}}{y^2(y-b)^2}$ should be positive. Then we show both the terms

$$(y-b)\left\{(y-b)\cdot \mathrm{e}^{(b+y)t} - y\cdot \mathrm{e}^{yt} + b\cdot \mathrm{e}^{bt}\right\} \quad (\equiv Q_{d\_1}) \tag{S107}$$

and

$$\mathrm{e}^{(y-b)t} + \{(b-y)t - 1\} \quad (\equiv Q_{d\_2}) \tag{S108}$$

are positive.

From equation (S15), the Maclaurin series expansion of $Q_{d\_1}$ is given by,

$$\begin{aligned} Q_{d\_1} &= (y-b)\left\{(y-b)\sum_{n=0}^{\infty}\frac{(b+y)^n t^n}{n!} - y\sum_{n=0}^{\infty}\frac{y^n t^n}{n!} + b\sum_{n=0}^{\infty}\frac{b^n t^n}{n!}\right\} \\ &= (y-b)\sum_{n=0}^{\infty}\frac{t^n}{n!}\left\{(y-b)(b+y)^n - y^{n+1} + b^{n+1}\right\} \\ &= (y-b)\sum_{n=0}^{\infty}\frac{t^n}{n!}\left\{(y-b)\sum_{k=0}^{n}{}_nC_k\, b^{n-k}y^k - (y-b)\sum_{k=0}^{n}b^{n-k}y^k\right\} \\ &= (y-b)^2\sum_{n=0}^{\infty}\frac{t^n}{n!}\cdot\sum_{k=0}^{n}({}_nC_k - 1)b^{n-k}y^k, \end{aligned} \tag{S109}$$

where ${}_nC_k$ means the number of combinations of $n$ elements taken $k$ at a time, and

$${}_nC_k > 1 \quad \text{for any} \quad n \geq 0 \quad \text{and} \quad k \geq 0. \tag{S110}$$

Therefore, all the term in the equation (S109) are positive, and we obtain

$$Q_{d\_1} > 0. \tag{S111}$$

For the term $Q_{d\_2}$, from equation (S108) we have

$$\frac{\partial Q_{d\_2}}{\partial t} = \left(\mathrm{e}^{(y-b)t}\right)' + \left\{(b-y)t - 1\right\}'$$
$$= (y-b)\mathrm{e}^{(y-b)t} + (b-y)$$
$$= (y-b)\cdot\left(\mathrm{e}^{(y-b)t} - 1\right). \tag{S112}$$

Here, for $t > 0$,

$$\mathrm{e}^{(y-b)t} = \begin{cases} > 1 & (y-b > 0), \\ < 1 & (y-b < 0). \end{cases} \tag{S113}$$

From equations (S112) and (S113),

$$\frac{\partial Q_{d\_2}}{\partial t} = \begin{cases} (>0)\cdot(>0) & \text{for } (y-b>0) \\ (<0)\cdot(<0) & \text{for } (y-b<0) \end{cases}$$
$$> 0, \tag{S114}$$

where $t > 0$. From equation (S108), we have

$$Q_{d\_2}\Big|_{t=0} = \mathrm{e}^{(y-b)0} + \left\{(b-y)\cdot 0 - 1\right\}$$
$$= 1 - 1$$
$$= 0. \tag{S115}$$

Therefore, from equations (S114) and (S115),

$$Q_{d\_2} > Q_{d\_2}\Big|_{t=0}$$
$$= 0. \tag{S116}$$

Thus, we obtain

$$Q_{d\_2} > 0. \tag{S117}$$

Thus, as equations (S111) and (S117), we proved that both $Q_{d\_1}$ and $Q_{d\_2}$ are

positive. This means that $\frac{\partial P_d(t)}{\partial a} > 0$ (equation (S83)) is satisfied, and that the term $P_d(t)$ always induces monotonically increasing dose response.

Thus, we proved that $P_r(t)$ can induce convex dose response when $b > c$, and that $P_d(t)$ always induces monotonically increasing dose response.

In order to satisfy the equilibrium condition of $R$ for $a = 0$ under any condition, the supplying and degradation reactions of the inactive receptors are often expressed as following; the amount of pool of inactivated receptors was fixed to the same as the initial amount of inactivated receptors ($r$), and the rate constant of supplying and the degradation reactions of the inactive receptors are the same (i.e. $c = d$). Under such expression, when $c$ and $d$ become large, the intensity of the monotonically increasing dose response from $P_d(t)$ become large (because $d$ scales $P_d(t)$), and simultaneously the intensity of the convex dose response from $P_r(t)$ become small, and resulting in the monotonic dose response of $P(t)$. Therefore, it may hard to distinguish these two effects of the rate constants in a model using such expressions.

## 7.2. Supplementary Data

**Data 1: Experimental data used in Figure 15 and Figure 22.**

Horizontal label of each table indicates doses (ng/ml) of stimuli. Vertical label of each table indicates time (min) after stimulation. Following table is a part of the full table. The full table is too large to be included in this Thesis and can be obtained as the supplementary materials of the publication of this study.

PC12 cells
EGF step

pEGFR

| | 0.1 | 0.3 | 1 | 3 | 10 | 30 |
|---|---|---|---|---|---|---|
| 0 | 0.004134 | 0.004134 | 0.004134 | 0.004134 | 0.004134 | 0.004134 |
| 1 | 0.008284 | 0.023428 | 0.132333 | 0.493679 | 1 | 0.96128 |
| 2 | 0.006457 | 0.023609 | 0.134463 | 0.289085 | 0.397819 | 0.265905 |
| 5 | 0.011265 | 0.03402 | 0.124668 | 0.243832 | 0.303853 | 0.347539 |
| 10 | 0.012574 | 0.032787 | 0.09392 | 0.142813 | 0.113664 | 0.105775 |
| 15 | 0.012211 | 0.037879 | 0.122039 | 0.109944 | 0.10783 | 0.099619 |
| 30 | 0.012386 | 0.023724 | 0.053005 | 0.04977 | 0.039624 | 0.028877 |
| 60 | 0.009258 | 0.017562 | 0.017962 | 0.009978 | 0.002531 | 0.003742 |
| 120 | | | | | | |
| 180 | | | | | | |
| 240 | | | | | | |

pAkt

| | 0.1 | 0.3 | 1 | 3 | 10 | 30 |
|---|---|---|---|---|---|---|
| 0 | 0.016011 | 0.016011 | 0.016011 | 0.016011 | 0.016011 | 0.016011 |
| 1 | 0.020147 | 0.06639 | 0.362501 | 0.721726 | 0.870719 | 1 |
| 2 | 0.09927 | 0.416555 | 0.834236 | 0.921125 | 0.960403 | 0.880567 |
| 5 | 0.239849 | 0.349482 | 0.492532 | 0.503531 | 0.377642 | 0.276313 |
| 10 | 0.151968 | 0.20379 | 0.258214 | 0.241987 | 0.155186 | 0.115747 |
| 15 | 0.093929 | 0.14863 | 0.199677 | 0.185524 | 0.121104 | 0.077362 |
| 30 | 0.070475 | 0.125107 | 0.134001 | 0.090577 | 0.066353 | 0.05692 |
| 60 | 0.048823 | 0.067029 | 0.05942 | 0.045423 | 0.038635 | 0.042657 |
| 120 | | | | | | |
| 180 | | | | | | |
| 240 | | | | | | |

pS6

| | 0.1 | 0.3 | 1 | 3 | 10 | 30 |
|---|---|---|---|---|---|---|
| 0 | 0.007779 | 0.007779 | 0.007779 | 0.007779 | 0.007779 | 0.007779 |
| 1 | 0.005922 | 0.005958 | 0.006639 | 0.006895 | 0.007171 | 0.006958 |
| 2 | 0.004629 | 0.005676 | 0.007939 | 0.011278 | 0.012481 | 0.012898 |
| 5 | 0.008686 | 0.019667 | 0.046312 | 0.064565 | 0.075493 | 0.07891 |
| 10 | 0.078518 | 0.221606 | 0.391491 | 0.434493 | 0.459431 | 0.430364 |
| 15 | 0.256017 | 0.525002 | 0.680638 | 0.717271 | 0.653994 | 0.605451 |
| 30 | 0.448116 | 0.861826 | 1 | 0.929892 | 0.754136 | 0.622781 |
| 60 | 0.295432 | 0.661 | 0.750949 | 0.549031 | 0.374957 | 0.32016 |
| 120 | | | | | | |
| 180 | | | | | | |
| 240 | | | | | | |

⋮

HeLa
EGF step

pEGFR

| | 0 | 1 |
|---|---|---|
| 0 | 0.002693 | 0.002693 |
| 1 | 0.00949 | 0.283574 |
| 2 | 0.010071 | 0.2866 |
| 5 | 0.006478 | 0.285075 |
| 15 | 0.009017 | 0.247621 |
| 30 | 0.007949 | 0.273662 |
| 60 | 0.004336 | 0.172755 |
| 90 | 0.006713 | 0.123114 |
| 120 | 0.00364 | 0.06328 |
| 180 | 0.001519 | 0.024936 |
| 240 | 0.001453 | 0.012461 |
| 360 | 0.001145 | 0.002189 |
| 480 | 0.001306 | 0.001223 |
| 600 | 0.003328 | 0.001712 |
| 720 | 0.002915 | 0.001094 |

pAkt

| | 0 | 1 |
|---|---|---|
| 0 | 0.041762 | 0.041762 |
| 1 | 0.0489 | 0.201275 |
| 2 | 0.098072 | 0.74099 |
| 5 | 0.052871 | 0.705573 |
| 15 | 0.039235 | 0.231475 |
| 30 | 0.049335 | 0.336529 |
| 60 | 0.014265 | 0.177647 |
| 90 | 0.005924 | 0.025345 |
| 120 | 0.00216 | 0.016273 |
| 180 | 0 | 0.053629 |
| 240 | 0.015426 | 0.05931 |
| 360 | 0.01936 | 0.065283 |
| 480 | 0.044321 | 0.081018 |
| 600 | 0.045492 | 0.095992 |
| 720 | 0.057698 | 0.082263 |

pS6

| | 0 | 1 |
|---|---|---|
| 0 | 0.547275 | 0.547275 |
| 1 | 0.682594 | 0.653942 |
| 2 | 0.716696 | 0.607209 |
| 5 | 0.728917 | 0.667762 |
| 15 | 0.913298 | 0.705779 |
| 30 | 0.924357 | 0.748727 |
| 60 | 0.805917 | 0.885404 |
| 90 | 0.827608 | 0.760051 |
| 120 | 0.688852 | 0.832575 |
| 180 | 0.703904 | 1.073944 |
| 240 | 0.66432 | 0.99487 |

⋮

**Data 2: RSS and estimated parameters used in Figure 15 and Figure 22.**

Following table is a part of the full table. The full table is too large to be included in this Thesis and can be obtained as the supplementary materials of the publication of this study.

| field name | No. | cells & stimulation | upstream molecule | downstream molecule | dose (ng/ml) | normalized_RSS_of_upstream_for_each_dose | normalized_RSS_of_downstream_for_each | normalized_RSS_of_upstream_for_all_d | normalized_RSS_of_downstream_for_all | t1of2_exp |
|---|---|---|---|---|---|---|---|---|---|---|
| filter cond. | | w/o 'PC12_EGF_inh' | | | | <0.3 | <0.3 | <0.1 | <0.1 | w/o NaN |
| | 1 | 'PC12_EGF_step | 'pEGFR' | 'pAkt' | 0.1 | 1.81E+01 | 1.10E-01 | 1.57E-01 | 3.89E-02 | NaN |
| | 2 | 'PC12_EGF_step | 'pEGFR' | 'pAkt' | 0.3 | 8.19E+00 | 1.33E-01 | 1.57E-01 | 3.89E-02 | 3.20E+03 |
| | 3 | 'PC12_EGF_step | 'pEGFR' | 'pAkt' | 1 | 9.73E-01 | 9.42E-02 | 1.57E-01 | 3.89E-02 | 1.38E+03 |
| | 4 | 'PC12_EGF_step | 'pEGFR' | 'pAkt' | 3 | 6.17E-02 | 1.70E-02 | 1.57E-01 | 3.89E-02 | 2.88E+02 |
| | 5 | 'PC12_EGF_step | 'pEGFR' | 'pAkt' | 10 | 9.83E-02 | 2.12E-02 | 1.57E-01 | 3.89E-02 | 1.10E+02 |
| | 6 | 'PC12_EGF_step | 'pEGFR' | 'pAkt' | 30 | 1.50E-01 | 1.81E-02 | 1.57E-01 | 3.89E-02 | 2.48E+02 |
| | 7 | 'PC12_EGF_step | 'pEGFR' | 'pERK1' | 0.1 | 3.43E+00 | 2.20E-01 | 1.74E-01 | 3.14E-02 | NaN |
| | 8 | 'PC12_EGF_step | 'pEGFR' | 'pERK1' | 0.3 | 4.38E+00 | 1.33E-01 | 1.74E-01 | 3.14E-02 | 3.20E+03 |
| | 9 | 'PC12_EGF_step | 'pEGFR' | 'pERK1' | 1 | 1.40E+00 | 7.63E-02 | 1.74E-01 | 3.14E-02 | 1.38E+03 |
| | 10 | 'PC12_EGF_step | 'pEGFR' | 'pERK1' | 3 | 1.54E-01 | 2.28E-02 | 1.74E-01 | 3.14E-02 | 2.88E+02 |
| | 11 | 'PC12_EGF_step | 'pEGFR' | 'pERK1' | 10 | 1.03E-01 | 1.06E-02 | 1.74E-01 | 3.14E-02 | 1.10E+02 |
| | 12 | 'PC12_EGF_step | 'pEGFR' | 'pERK1' | 30 | 1.52E-01 | 1.84E-02 | 1.74E-01 | 3.14E-02 | 2.48E+02 |
| | 13 | 'PC12_EGF_step | 'pEGFR' | 'pERK2' | 0.1 | 4.25E+00 | 2.74E-01 | 1.85E-01 | 3.28E-02 | NaN |
| | 14 | 'PC12_EGF_step | 'pEGFR' | 'pERK2' | 0.3 | 5.46E+00 | 1.26E-01 | 1.85E-01 | 3.28E-02 | 3.20E+03 |
| | 15 | 'PC12_EGF_step | 'pEGFR' | 'pERK2' | 1 | 1.55E+00 | 8.43E-02 | 1.85E-01 | 3.28E-02 | 1.38E+03 |
| | 16 | 'PC12_EGF_step | 'pEGFR' | 'pERK2' | 3 | 1.65E-01 | 1.68E-02 | 1.85E-01 | 3.28E-02 | 2.88E+02 |
| | 17 | 'PC12_EGF_step | 'pEGFR' | 'pERK2' | 10 | 1.12E-01 | 1.39E-02 | 1.85E-01 | 3.28E-02 | 1.10E+02 |
| | 18 | 'PC12_EGF_step | 'pEGFR' | 'pERK2' | 30 | 1.51E-01 | 1.70E-02 | 1.85E-01 | 3.28E-02 | 2.48E+02 |
| | 19 | 'PC12_EGF_step | 'pAkt' | 'pS6' | 0.1 | 1.14E-01 | 3.57E-03 | 2.99E-02 | 7.59E-03 | 7.66E+02 |
| | 20 | 'PC12_EGF_step | 'pAkt' | 'pS6' | 0.3 | 1.35E-01 | 4.93E-03 | 2.99E-02 | 7.59E-03 | 5.91E+02 |
| | 21 | 'PC12_EGF_step | 'pAkt' | 'pS6' | 1 | 6.76E-02 | 2.99E-03 | 2.99E-02 | 7.59E-03 | 3.97E+02 |
| | 22 | 'PC12_EGF_step | 'pAkt' | 'pS6' | 3 | 1.61E-02 | 6.44E-03 | 2.99E-02 | 7.59E-03 | 3.49E+02 |
| | 23 | 'PC12_EGF_step | 'pAkt' | 'pS6' | 10 | 1.34E-02 | 1.53E-02 | 2.99E-02 | 7.59E-03 | 2.68E+02 |
| | 24 | 'PC12_EGF_step | 'pAkt' | 'pS6' | 30 | 8.68E-03 | 1.44E-02 | 2.99E-02 | 7.59E-03 | 2.33E+02 |
| | 25 | 'PC12_EGF_step | 'pAkt' | 'pS6K' | 0.1 | 2.47E-01 | 7.87E-02 | 3.28E-02 | 4.33E-02 | 7.66E+02 |
| | 26 | 'PC12_EGF_step | 'pAkt' | 'pS6K' | 0.3 | 1.26E-01 | 6.64E-02 | 3.28E-02 | 4.33E-02 | 5.91E+02 |
| | 27 | 'PC12_EGF_step | 'pAkt' | 'pS6K' | 1 | 6.46E-02 | 5.47E-02 | 3.28E-02 | 4.33E-02 | 3.97E+02 |
| | 28 | 'PC12_EGF_step | 'pAkt' | 'pS6K' | 3 | 1.81E-02 | 2.09E-02 | 3.28E-02 | 4.33E-02 | 3.49E+02 |
| | 29 | 'PC12_EGF_step | 'pAkt' | 'pS6K' | 10 | 1.54E-02 | 1.98E-02 | 3.28E-02 | 4.33E-02 | 2.68E+02 |
| | 30 | 'PC12_EGF_step | 'pAkt' | 'pS6K' | 30 | 1.22E-02 | 4.32E-02 | 3.28E-02 | 4.33E-02 | 2.33E+02 |
| | 31 | 'PC12_EGF_step | 'pAkt' | 'peIF4B' | 0.1 | 2.66E-01 | 5.46E-02 | 4.03E-02 | 3.75E-02 | 7.66E+02 |
| | 32 | 'PC12_EGF_step | 'pAkt' | 'peIF4B' | 0.3 | 1.78E-01 | 3.36E-02 | 4.03E-02 | 3.75E-02 | 5.91E+02 |
| | 33 | 'PC12_EGF_step | 'pAkt' | 'peIF4B' | 1 | 7.41E-02 | 1.26E-02 | 4.03E-02 | 3.75E-02 | 3.97E+02 |
| | 34 | 'PC12_EGF_step | 'pAkt' | 'peIF4B' | 3 | 2.57E-02 | 2.53E-02 | 4.03E-02 | 3.75E-02 | 3.49E+02 |
| | 35 | 'PC12_EGF_step | 'pAkt' | 'peIF4B' | 10 | 1.64E-02 | 5.53E-02 | 4.03E-02 | 3.75E-02 | 2.68E+02 |
| | 36 | 'PC12_EGF_step | 'pAkt' | 'peIF4B' | 30 | 1.48E-02 | 5.99E-02 | 4.03E-02 | 3.75E-02 | 2.33E+02 |
| | 37 | 'PC12_EGF_step | 'pAkt' | 'pGSK3b' | 0.1 | 8.86E-01 | 7.15E-02 | 1.20E-01 | 4.78E-02 | 7.66E+02 |
| | 38 | 'PC12_EGF_step | 'pAkt' | 'pGSK3b' | 0.3 | 3.59E-01 | 4.72E-02 | 1.20E-01 | 4.78E-02 | 5.91E+02 |
| | 39 | 'PC12_EGF_step | 'pAkt' | 'pGSK3b' | 1 | 1.49E-01 | 2.91E-02 | 1.20E-01 | 4.78E-02 | 3.97E+02 |
| | 40 | 'PC12_EGF_step | 'pAkt' | 'pGSK3b' | 3 | 6.87E-02 | 6.20E-02 | 1.20E-01 | 4.78E-02 | 3.49E+02 |
| | 41 | 'PC12_EGF_step | 'pAkt' | 'pGSK3b' | 10 | 8.69E-02 | 4.05E-02 | 1.20E-01 | 4.78E-02 | 2.68E+02 |
| | 42 | 'PC12_EGF_step | 'pAkt' | 'pGSK3b' | 30 | 8.87E-02 | 4.90E-02 | 1.20E-01 | 4.78E-02 | 2.33E+02 |
| | 43 | 'PC12_EGF_step | 'pAkt' | 'pTSC2' | 0.1 | 6.57E-01 | 1.85E-01 | 4.78E-02 | 1.23E-01 | 7.66E+02 |
| | 44 | 'PC12_EGF_step | 'pAkt' | 'pTSC2' | 0.3 | 1.55E-01 | 2.38E-01 | 4.78E-02 | 1.23E-01 | 5.91E+02 |
| | 45 | 'PC12_EGF_step | 'pAkt' | 'pTSC2' | 1 | 6.96E-02 | 5.79E-02 | 4.78E-02 | 1.23E-01 | 3.97E+02 |
| | 46 | 'PC12_EGF_step | 'pAkt' | 'pTSC2' | 3 | 2.17E-02 | 7.02E-02 | 4.78E-02 | 1.23E-01 | 3.49E+02 |
| | 47 | 'PC12_EGF_step | 'pAkt' | 'pTSC2' | 10 | 3.41E-02 | 1.46E-01 | 4.78E-02 | 1.23E-01 | 2.68E+02 |
| | 48 | 'PC12_EGF_step | 'pAkt' | 'pTSC2' | 30 | 1.48E-02 | 1.26E-01 | 4.78E-02 | 1.23E-01 | 2.33E+02 |

**Data 3: Time courses in experiment and simulation of Figure 15.**

Following two pages are a part of the full data set. The data set is too large (110 pages in total) to be included in this Thesis and can be obtained as the supplementary materials of the publication of this study.

Each page includes an experimental data set of an upstream and a downstream molecule.
Left upper two panels; experimental data.
Right upper two panels; simulation data.

The sets of the time courses satisfied both the conditions (i) and (ii) (see DISCUSSION 4.2) were indicated by solid lines, otherwise indicated by dashed lines. The sets of the experimental time courses satisfied both the conditions (i) and (ii) were indicated by closed circles, otherwise indicated by open circles. The doses of the stimuli were shown as colors. The hotter color means the larger dose.

Lower four panels; the half life time ($t_{1/2}$), peak intensity of an upstream molecule, and peak intensity of an downstream molecule in experiment (horizontal axis) and in simulation (vertical axis), and signal transfer efficiency obtained from experiment (horizontal axis) and from estimation ($E'''$ in Figure 14, vertical axis).

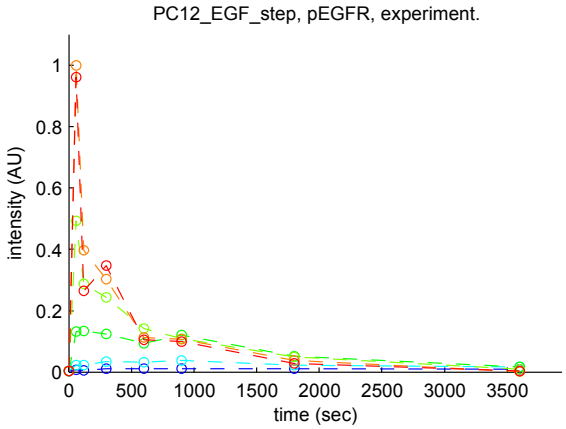
PC12_EGF_step, pEGFR, experiment.
intensity (AU)
time (sec)

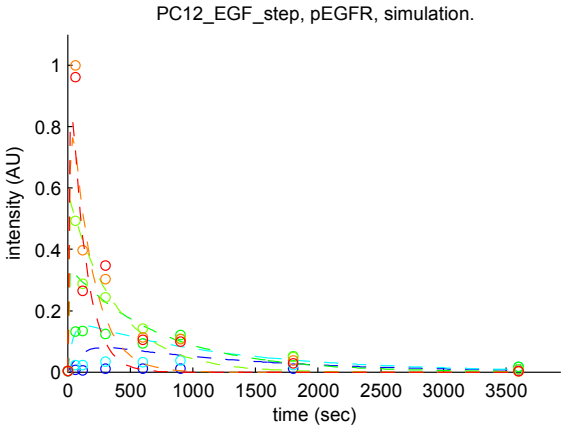
PC12_EGF_step, pEGFR, simulation.
intensity (AU)
time (sec)

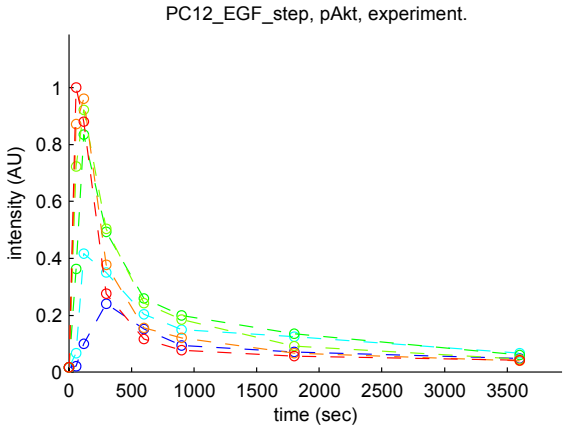
PC12_EGF_step, pAkt, experiment.
intensity (AU)
time (sec)

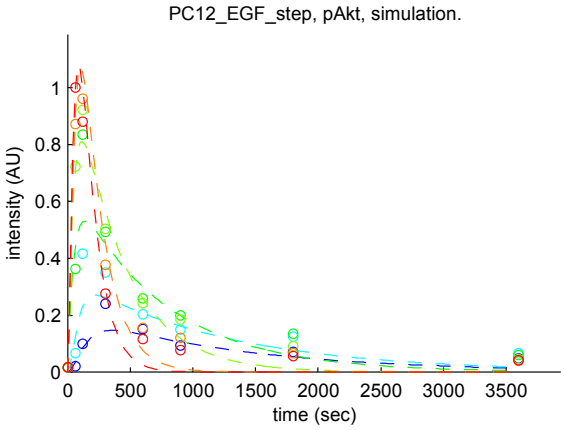
PC12_EGF_step, pAkt, simulation.
intensity (AU)
time (sec)

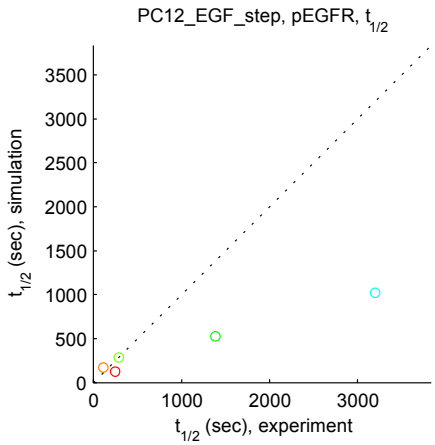
PC12_EGF_step, pEGFR, t1/2
t1/2 (sec), simulation
t1/2 (sec), experiment

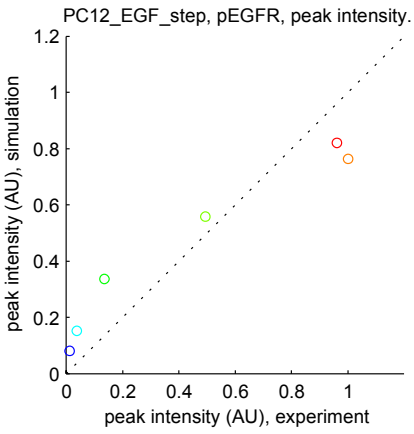
PC12_EGF_step, pEGFR, peak intensity.
peak intensity (AU), simulation
peak intensity (AU), experiment

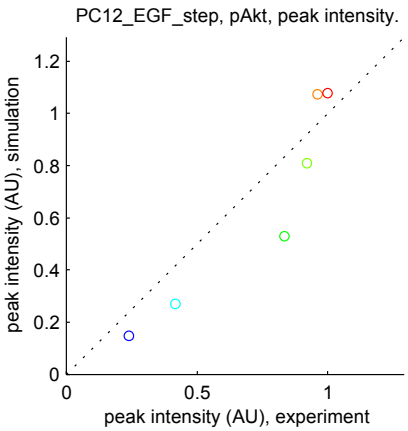
PC12_EGF_step, pAkt, peak intensity.
peak intensity (AU), simulation
peak intensity (AU), experiment

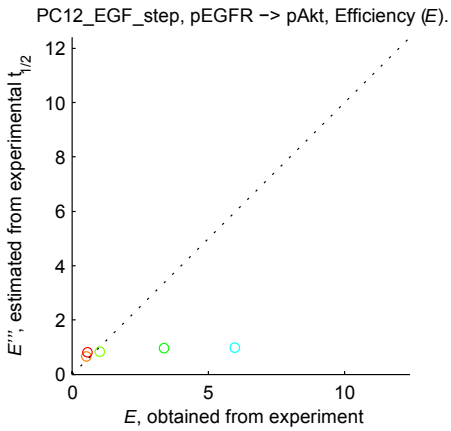
PC12_EGF_step, pEGFR -> pAkt, Efficiency (E).
E''', estimated from experimental t1/2
E, obtained from experiment

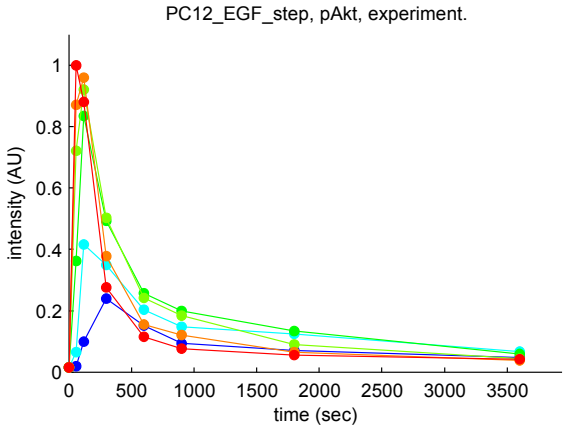
PC12_EGF_step, pAkt, experiment.
intensity (AU)
time (sec)

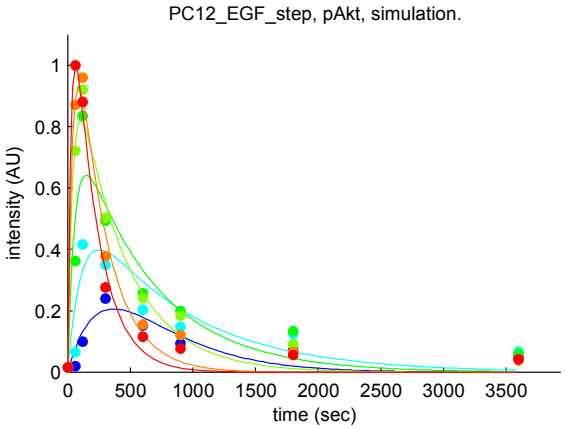
PC12_EGF_step, pAkt, simulation.
intensity (AU)
time (sec)

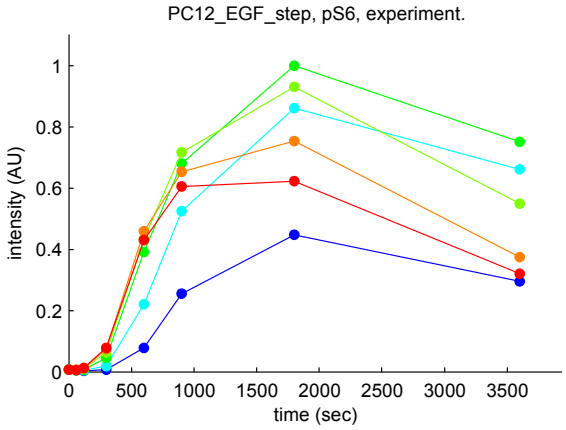
PC12_EGF_step, pS6, experiment.
intensity (AU)
time (sec)

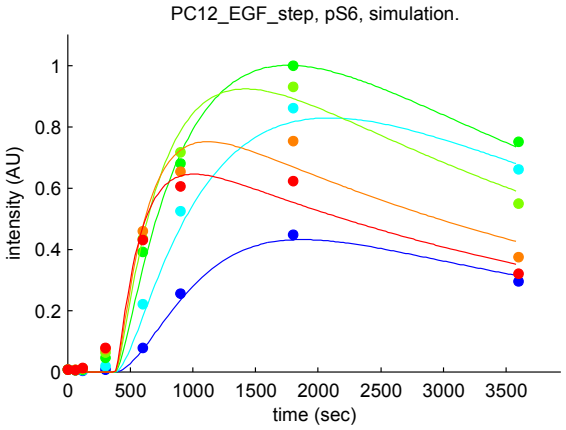
PC12_EGF_step, pS6, simulation.
intensity (AU)
time (sec)

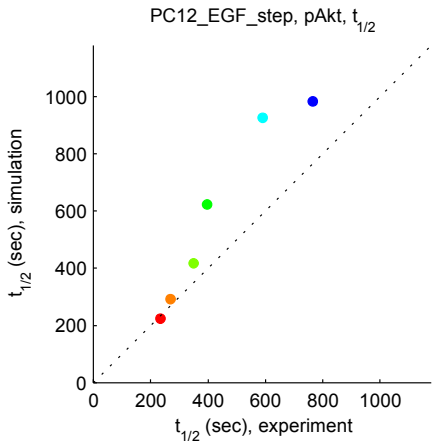
PC12_EGF_step, pAkt, t1/2
t1/2 (sec), simulation
t1/2 (sec), experiment

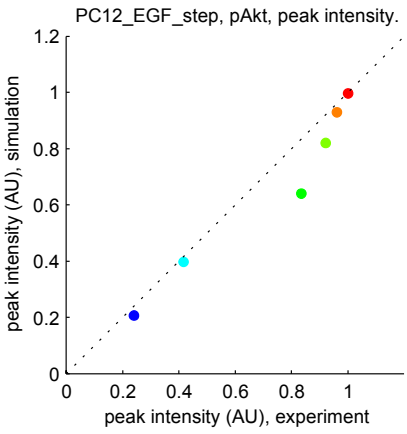
PC12_EGF_step, pAkt, peak intensity.
peak intensity (AU), simulation
peak intensity (AU), experiment

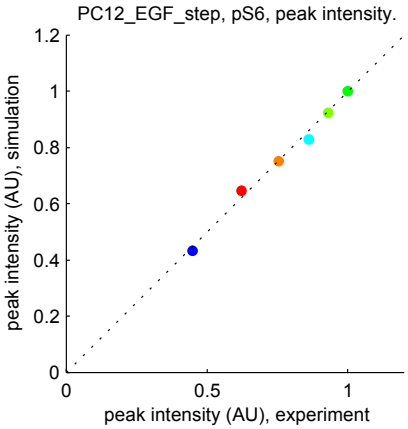
PC12_EGF_step, pS6, peak intensity.
peak intensity (AU), simulation
peak intensity (AU), experiment

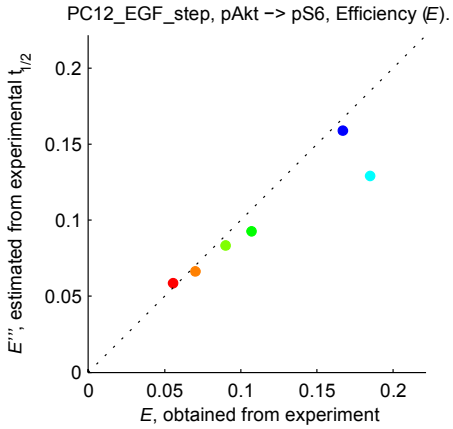
PC12_EGF_step, pAkt -> pS6, Efficiency (E).
E''', estimated from experimental t1/2
E, obtained from experiment